

**Regional climate modelling:
The Eastern European "summer drying" problem
and the representation of coastal surface wind speed
in a multi model ensemble**

Dissertation
zur Erlangung des Doktorgrades
der Naturwissenschaften im Fachbereich
Geowissenschaften
der Universität Hamburg

vorgelegt von
Ivonne Anders
aus Görlitz

Hamburg
2015

Als Dissertation angenommen vom Fachbereich Geowissenschaften
der Universität Hamburg
auf Grund der Gutachten von Prof. Dr. Hans von Storch
und Dr. Burkhardt Rockel

Hamburg, den 12.06.2015

Prof. Dr. Cristian Betzler
Leiter des Fachbereiches Geowissenschaften

Abstract

An ensemble of regional climate models (RCM) can provide a robust view on the climate and related uncertainties. In the last decade, large projects, e.g., PRUDENCE, ENSEMBLES and CORDEX, have been set up to organise and coordinate multi model ensemble simulations with respect to the researchers and public needs.

In some of the RCM results, from the projects mentioned before, an overestimation of summer air temperature in south-eastern Europe had been identified, which coincides with a strong underestimation of precipitation in this season, the "summer drying" problem of climate models.

One application of climate models is to assess future wind climate, which is particularly relevant for the assessment of energy potential, risk management and engineering. As observations for wind speed and direction are rare, models can close this gap and provide homogenous wind fields for further investigations. Several studies investigated RCM performance over open ocean and in near coastal regions and found a good agreement of simulated wind speed distribution and wind speed percentiles. Within the PRUDENCE project the deficiency has been identified, that the models using no gust parameterisation are not able to simulate wind speeds above 8Bft.

According to the first issue – the "summer drying" – the hypothesis that the biases are related to a false representation of soil properties in this region, based on divergences between the soil maps of Haase et al. (2007) and Stremme (1937) and that of FAO, which is commonly used in climate models, is investigated in more detail. Therefore, two simulations with the RCM CLM have been carried out using default sandy loam and silt loam over an area north of the Black Sea. As a consequence of the different soil characteristics, the results indicate increased soil moisture by up to 60% in the modified simulation compared to the control simulation. In addition to local changes in near surface parameters (e.g. temperature decrease by up to 1.5 K), large-scale changes involving temperature, precipitation and surface pressure are observed.

Regarding wind climate assessment, the second focus of the present study is to investigate the ability of RCMs to simulate surface wind speed in coastal regions of the North Sea. The analysis was based on the ENSEMBLES project results, due they give the opportunity to analyse the model performance for the wind characteristics among a large multi model hindcast ensemble for the time period 1961 – 2000. The observational data for 10 m wind speed was provided by the German and the Dutch meteorological services, DWD and KNMI. From most of the contributing RCMs simulation results of two spatial resolutions, 50 km and 25 km, are available.

Several measures and skill scores were applied to analyse the RCMs performance compared to the driving field and to evaluate accuracy gain by including higher spatial resolution of the model grid. At inland stations RCMs overestimate the mean wind speed, whereas maximum wind speed percentiles are captured very well. The higher resolved 25 km are often closer to the observations than the 50 km. The RCM ensemble mean performs good and adds value to the driving GCM ERA40. Additionally, a weather regime classification has been carried out and investigated, together with a second classification provided by ENSEMBLES, to be able to reflect the North Sea wind climate. Findings from the regime dependent evaluation of the RCMs wind climate can only be addressed to local effects of the near environment of the measuring sites.

Contents

1	Introduction	1
1.1	Motivation	1
1.2	Thesis Objective	3
1.3	Thesis Outline	4
2	Description of underlying data sets	6
2.1	Wind Observation Data and Data Quality	6
2.2	Reanalysis Data	9
2.3	Multi Regional Climate Model Ensemble	10
3	Analysis of the possible influence of prescribed soil type distribution on the representation of present climate in the Regional Climate Model CLM	14
3.1	Introduction	14
3.2	CLM Regional Climate Model and Experimental Model Setup	15
3.3	RCM response on changing soil conditions	18
3.4	Summary	24
4	Main circulation pattern for Europe and the North Sea	27
4.1	Introduction	27
4.2	Large Scale circulation pattern for Europe	28
4.3	Weather regime classification for the North Sea	34
4.4	Summary	45
5	Representation of Surface Wind Speed in the Multi Model Ensemble	47
5.1	Introduction	47
5.2	The mean wind conditions in the Southern North Sea and the German Bight	49
5.3	Methods and Measures	58
5.4	Near surface wind performance of the multi model ensemble	61
5.5	Regime-dependent validation of simulated surface wind speeds	75
5.6	Discussion and summary	82
6	Conclusion and Outlook	88
6.1	Conclusion	88
6.2	Outlook	92
	List of Abbreviations	95

References	97
Appendix	109
Acknowledgement	124

1 Introduction

1.1 Motivation

Regional climate models (RCMs) play an essential role in climate and climate change assessment for all regions of the world. Forced by General Circulation Models (GCM) they are used in a range of different applications related to past, present and future climate. Compared to the coarsely resolved global models, with the higher spatial resolution and with the more complex physics described in the models, the RCMs can better resolve small scale processes and increase the information gain, especially in complex terrain (Prein et al. (2013), Heikkilä et al. (2011), Prömmel et al. (2010)). Forced by perfect boundary conditions coming from reanalysis data, e.g. NCEP (Kalnay et al. (1996)) and ERA40 (Uppala et al. (2005)), the regional climate models can give additional information in areas, where observational data are rarely available. These RCM hindcast simulations are very important, as on one hand they help to close observational gaps, on the other hand it is possible to evaluate the RCMs ability to simulate the present climate. This information helps to identify deficiencies in the models, which need to be reduced and forces further model development. Additionally, the knowledge of model uncertainties supports the understanding and interpretation of future climate simulations.

However, single model output is not sufficient to comply with the demands from impact researchers and end users. A more robust view on the climate and related uncertainties can be provided only by an ensemble of RCMs. In the last decade, large projects have been set up to organise and coordinate multi model ensemble simulations with respect to the researchers and public needs. These simulations are a strong base to support the regularly published Intergovernmental Panel on Climate Change (IPCC) Assessment reports with results from state-of-the-art global and regional climate models. From the numerical weather forecast, the same as from large climate model projects, it is known, that the mean from a large ensemble is closer to the real state of the atmosphere than any single model run (Tebaldi and Knutti (2007)). The first large European project combining state-of-the-art regional climate models to a multi model ensemble, was the EU-funded PRUDENCE project (Christensen and Christensen (2007), Christensen et al. (2007)). The present study is partly funded by the PRUDENCE-following EU-funded project ENSEMBLES (<http://ensembles-eu.metoffice.com/>) and it is based on the ENSEMBLES project results. Within this framework RCM runs have been carried out to simulate the climate of the second half of the last century forced by ERA40 reanalysis data, a hindcast simulation, as mentioned before. For simulations of the future climate until the end of this century

the SRES A1B scenario IPCC-SRES (2000) has been applied. In the project a large number of RCMs combined with different GCMs spanned a matrix of simulations, in order to cover the spread of uncertainties originating from the individual models. Results from ENSEMBLES have been used in many climate change and impact studies across Europe within the last years. The results are still in use, but are actually supplemented by higher spatially resolved regional climate simulations provided from the CORDEX initiative (e.g. CORDEX Europe; <http://www.euro-cordex.net/>).

Within the PRUDENCE project, for some of the RCM simulations an overestimation of summer air temperature in south-eastern Europe had been identified, which coincides with a strong underestimation of precipitation in this season (Christensen and Christensen (2007)). This issue has been called the "summer drying"-problem and does not only occur in RCMs, but can also be found in GCM results. In several studies, possible reasons for this feature have been investigated (Hagemann et al. (2001), Seneviratne et al. (2006b), Rowell and Jones (2006)). Most of the simulation results from the different models in the ENSEMBLES - project show the same overestimation of near surface temperature in the region North and West of the Black Sea Kjellström et al. (2010). Kotlarski et al. (2014) published recently an evaluation of the CORDEX hindcast simulations for the time period 1989 – 2008 for Europe. Again, 6 out of 9 regional climate model simulations showed the drying-out already found in earlier simulation results.

One application of climate models is to assess future wind climate, which is particularly relevant for the assessment of energy potential, risk management and engineering. Observations for wind speed and direction are rare and often only short time series are available, which are additionally inhomogenous over time, due to changes in the measurements and changes in the near environment of the observational site. Thus, again, models can close this gap and provide homogeneous wind field data. Investigating regional or local wind climate differs in many aspects. For the energy sector, it is important to identify larger regions where the wind speed has a certain range and main direction in a predefined height above the ground (Landberg et al. (2003), Kiss and Janosi (2008)). Additionally, the correct simulation of the daily cycle of the wind speed is the base for European energy trading. For risk management, high wind speeds and storms are most interesting. For engineering, the knowledge of very local wind characteristics is essential.

Another deficiency of the regional climate models has been identified in the PRUDENCE results. Rockel and Woth (2007) focused on near-surface wind speed over Europe and identified that most of the RCMs have not been able to simulate wind velocities above

8 Bft over land. Related to the different applications mentioned before, wind speed distribution, and wind speed percentiles from regional climate models have been evaluated by Winterfeldt and Weisse (2009), Kunne (2012), Barthelmie and Palutikof (1996), Herrmann et al. (2011), and Winterfeldt et al. (2011). Several studies investigated wind conditions under a changing climate using RCM simulations (Najac et al. (2009), Leckebusch and Ulbrich (2004), Pryor and Schoof (2010), Pryor et al. (2012)). Furthermore Suselj et al. (2010) and Donat et al. (2010) analysed storm activities in relation to weather pattern and North Atlantic Oscillation (NAO). Cavicchia et al. (2014) investigated storm trends in the Mediterranean; Krueger et al. (2013) in the North-Atlantic.

1.2 Thesis Objective

The present study is based on simulation results from the ENSEMBLES framework.

The existing overestimation of the south-eastern European summer temperature in the ENSEMBLES results raised up the question whether there could be a simple way, to at least reduce the positive temperature bias in summer. In this thesis, the hypothesis is that the biases could be related to a false representation of soil properties in this region. This theory is based on divergences between the soil maps of Haase et al. (2007) and Stremme (1937) and that provided by Food and Agriculture Organization (FAO), which is commonly used in (regional and global) climate models. Therefore, two simulations are performed with the regional climate model CLM with the ENSEMBLES model setup, one using default sandy loam and the other using silt loam over an area north of the Black Sea. According to this investigation the following research questions are addressed:

- Is there an influence of the underlying soil type distribution on the results from a regional climate model?
- Can the summer drying in south-eastern Europe be reduced in the models?

A the second focus of this work is the wind climate. Several studies investigated RCM performance over open ocean and in near coastal regions and found a good agreement of simulated wind speed distribution and wind speed percentiles (Winterfeldt and Weisse (2009), Kunne (2012)). Within the PRUDENCE project the deficiency has been identified that the models using no gust parameterisation are not able to simulate wind speeds above 8Bft.

The overall aim of the present study is to investigate the ability of RCMs to simulate surface wind speed. Hereby, coastal regions are in special focus, since the simulation of

the narrow transition zone between water and land is a challenging task for models. The difference in surface properties at the coastline leads to a strong disturbance in the general flow. The ENSEMBLES project results give the opportunity to analyse the model performance for the wind characteristics among a large multi model hindcast ensemble for the time period 1961 – 2000. The investigation is focused on the North Sea coastal areas of Germany and the Netherlands. The observational data is provided by the German weather service - Deutscher Wetterdienst (DWD)- and by the meteorological service from the Netherlands (KNMI). From most of the included RCMs two spatial resolutions, 50 km and 25 km, are available.

Dealing with these issues brings up the following research questions, which are investigated in this thesis:

- What is a suitable weather regime classification to describe the wind climate in the Southern North Sea?
- Are the regional climate models able to reproduce the observed large scale atmospheric pattern?
- Is the RCM ensemble able to represent the temporal and statistical characteristics of the wind field at different locations over the German and Dutch coast of the North Sea?
- How do atmospheric patterns relate to the representation of the wind climate in the climate model simulations?
- What are the benefits and shortcomings of using regional climate models for wind speed analysis compared to the coarse resolution reanalysis fields?
- Is there an added value of the regional climate models results for wind climate by increasing the spatial resolution from 50 km to 25 km?

1.3 Thesis Outline

The thesis is structured as follows. An overview of the used data is given in **Chapter 2**, starting with the locations of observed wind speed data provided by the DWD and KNMI, including an objective detection of breaks within the time series to identify suitable, mostly undisturbed, time slices. Furthermore, two reanalysis data sets are introduced, the same as the multi regional climate model ensemble, which is later used for wind climate evaluation. Related to the topic of the so called "summer drying"-problem in most of the

regional climate models, in **Chapter 3** the influence of prescribed soil type distribution on the representation of present climate in the regional climate model CLM is investigated. According to the investigation of the simulated wind climate in the southern and eastern part of the North Sea, in **Chapter 4** two objective regime classifications have been investigated on being representative for the area of interest. The agreement between RCM-based and observed regimes is calculated. At the beginning of **Chapter 5** an overview of the mean wind condition in the North Sea coastal area and the role of the North Atlantic Oscillation (NAO) is given. A variety of statistical tools is described and applied to analyse the RCMs ability to reproduce the regional wind climate. Further, an added value assessment is presented using RCMs for surface wind speed simulation compared to the driving reanalysis data from ERA40. The derived daily weather regimes for the North Sea are finally applied to analyse the model performance depending on different wind directions. The thesis is concluded in **Chapter 6** by summarising the main results from the different studies. A brief discussion and outlook on open issues is given suggesting further investigations.

2 Description of underlying data sets

2.1 Wind Observation Data and Data Quality

Wind measurements at the German Coast The German meteorological service DWD provided measurements for 31 stations across the German coastal area. The data used here is the mean speed (FF) and the mean direction (DD) of the surface wind as a mean over the preceding hour. Beside these values the daily maximum of the wind speed (FX) is available. Until the end of the year 1974 the wind direction measured in degree was transformed into the 32-scale wind classes. From 1975 onwards, the classes have been changed to 36. For the following analyses of the data for the wind direction, the values have been transformed back to the mean degree in each class.

Wind measurements across the Netherlands The wind measurements network of the Royal Netherlands Meteorological Institute (KNMI) contains about 50 stations across the Netherlands. For these stations hourly values are available for the mean speed (FF) and the mean direction (DD) of the wind over the last 10 minute period in the preceding hour, the hourly mean of the wind speed (FH) and the maximum wind speed (FX) in the preceding hour. Each data set is labeled with a quality flag giving additional information about the data. The precision of measurements was +/- 0.5 m/s until June 1996. From July 1996 onwards the wind speeds are measured in integer values of m/s.

The problem of homogeneity of the observation data and the definition of suitable data sets to compare with Wind measurements are very strongly influenced by changes in, for example, surface roughness and by shadowing effects from trees and buildings. Also changes in the instrument, the measuring height or the location are reasons for inhomogeneities of the data. A homogenisation of wind measurements is critical as the measurements are influenced by local wind effects. Stations history is often incomplete and changes in the station surrounding (growing trees, new buildings in the neighbourhood) are rarely documented.

The wind speed data U has been corrected for differences in the measuring height by using the documented heights from the station histories and applying the logarithmic wind profile (cf. equation 2.1). U_r is the measured wind speed at height z_r , z is the reference height of 10 m. Without any knowledge about the measuring site and its surrounding per definition z_0 is 0.03 m for all land stations and 0.002 m for stations on water.

$$U(z) = U_r \frac{\ln(z/z_0)}{\ln(z_r/z_0)}, z = 10 m \quad (2.1)$$

To find an optimal set of observational data to compare to the simulated wind speeds from the models all station histories have been analysed. The most important criterion was no change in the location of the station, the second a small difference in the measuring height (mainly corrected, see above), the third one no change in the instrumentation.

Additional to this information an algorithm for detecting breaks in the observed time series based was used on annual, but also monthly mean wind speeds. For detecting breaks in a time series at least one homogenous reference series is necessary for comparison. In reality no such time series exists. The first idea is to compare this series with all other series within the same climatic area by making a series of differences. By definition, the series were compared to all other observations. These difference series are then tested for discontinuities by the technique of Caussinus and Lyazrhi (1997). At this stage, it is not known which individual series is the cause of a shift that is detected in a difference series. But, if a detected change-point remains constant throughout the set of comparisons of a candidate station with its neighbours, it can be attributed to this candidate station.

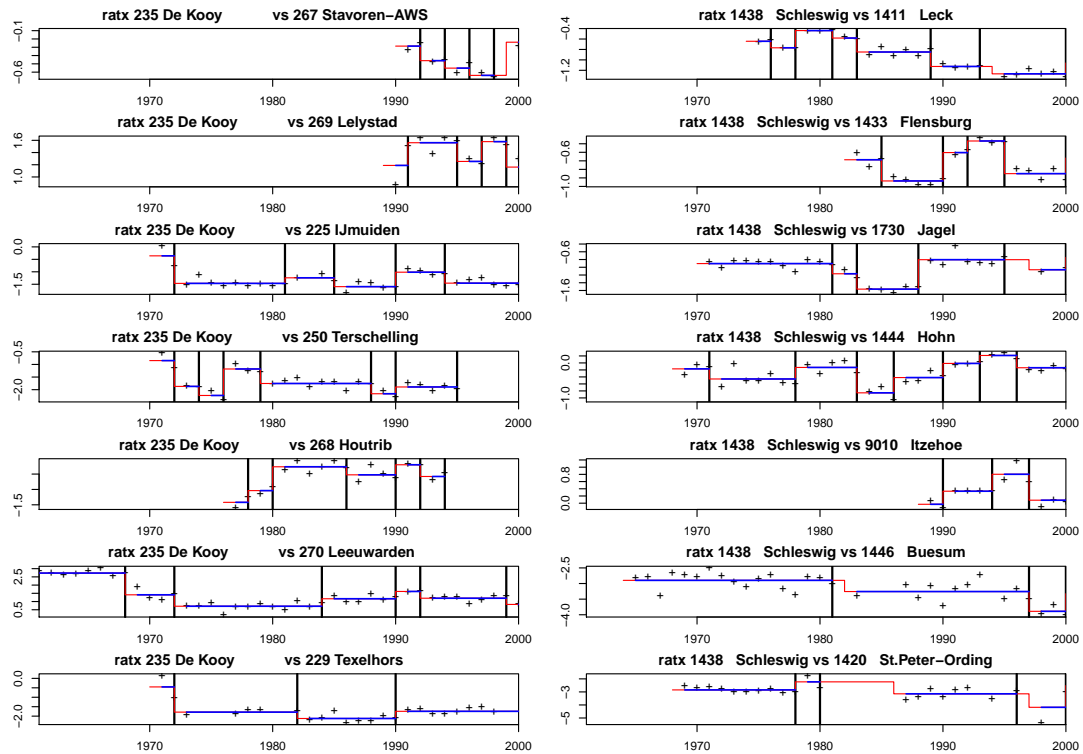


Figure 2.1: Jumps (black vertical lines) detected in series of annual mean differences (+) in relation to the surrounding stations of De Kooy (ID235) (left) and Schleswig (ID1438) (right). Red horizontal lines are the mean over all values between breaks.

Figure 2.1 shows, exemplarily, the breaks in the difference series the from stations De Kooy (ID 235) (cf. left panel) and Schleswig (ID 1438) (cf. right panel) compared to the closest

stations around. For comparison, only the neighbouring stations within the same measuring network have been taken into account. The original time series have been corrected for changes in the measuring height (see above). The location of the station De Kooy has been changed three times, 25.09.1972, 26.08.1980 and 02.05.1989. The changes in 1972 and 1989 can be identified very well as jumps quite in the time series of the differences. The change in 1980 can not be identified clearly. The stations location of Schleswig has not been changed over time, just the measuring height changed on 01.04.1991. No clear jump can be seen. For the jump detection, several methods have been applied described in Caussinus and Mestre (2004) and Picard et al. (2005). None of the methods seems to be appropriate to lead to good results for all stations. This shows that the knowledge about the stations history is indispensable.

Table 2.1: Wind speed observations from the DWD network and the KNMI network, their location, height above sea level z_{asl} , measuring height above the ground z_{ag} and availability for $t1$: 1971 - 1983 and $t2$: 1971 - 2000

ID	Name	lon °E	lat °N	z_{asl} (m)	z_{ag} (m)	in t1	in t2
DWD							
1529	Soltau	9.8	52.96	76	15.6	x	x
1402	List	8.41	55.01	26	12	x	x
1468	Bremerhaven	8.58	53.53	6	12	x	-
1474	Bremen	8.8	53.05	4	10	x	x
1040	Helgoland	7.91	54.19	16	10	x	-
1438	Schleswig	9.55	54.53	43	16.6	x	x
1444	Hohn	9.54	54.31	17	10	x	x
1497	Oldenburg	8.18	53.18	11	9.6	x	x
1132	Lingen	7.31	52.52	22	15	x	-
9007	Wittmundhafen	7.67	53.55	8	10	x	x
1730	Jagel	9.52	54.46	22	10	x	x
KNMI							
260	De Bilt	5.18	52.1	2	20	x	x
270	Leeuwarden	5.75	53.22	1.5	10	x	x
280	Eelde	6.59	53.12	3.5	10	x	-
370	Eindhoven	5.41	51.45	20.3	10	x	-
375	Volkel	5.71	51.66	21.1	10	x	x
380	Beek	5.78	50.92	125.6	10	x	-
344	Zestienhoven	4.44	51.95	-4.8	10	x	-
290	Twenthe	6.9	52.27	34.5	10	x	-
350	Gilze-Rijen	4.94	51.57	11.1	10	x	x
225	IJmuiden	4.56	52.46	4.4	13.5	x	x

Together with the provided station histories two time windows were defined, where as many as possible of the measurements are less disturbed. For the Netherlands observation data of 10 stations for the time period 1971-1983 and 5 stations from 1971 to 2000 were chosen. For the German coast it is 11 and 8 stations respectively. In Table 2.1 the basic information about these stations is listed. Figure 2.2 indicates their locations in a

geographical map. Within the stated time periods none of the measurements is disturbed by any changes in the stations location.

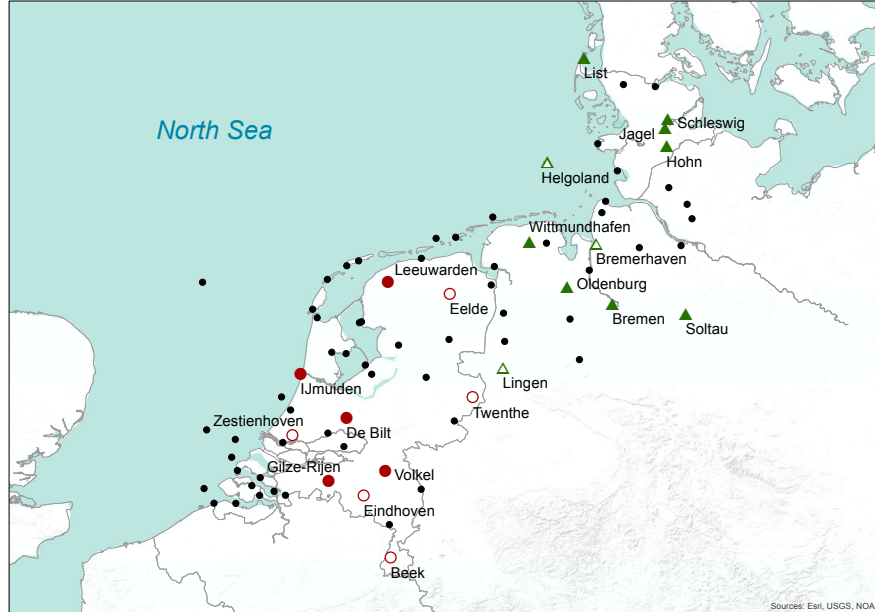


Figure 2.2: Observation data available for the area of investigation (all symbols), covering the time period 1971 to 1983 (coloured solid and open symbols) and the time period 1971 to 2000 (solid symbols only) from the DWD measuring network (triangles) and the KNMI network (circles).

2.2 Reanalysis Data

ERA40 Reanalysis Data The re-analysis product from European Centre for Medium-Range Weather Forecasts (ECMWF) ERA40 is a global gridded dataset (Uppala et al. (2005)), which has a horizontal spectral resolution of T159 (about 1.125°), 60 vertical hybrid levels and a 6-hourly output covering the time period from 1958 to August 2002. In this study it is not only used for the lateral and upper boundary driving, but also for the validation of surface wind speed and of the mid-troposphere circulation patterns.

UKMO Mean Sea Level Pressure This dataset holds gridded Northern Hemisphere (north of 15° N) monthly and daily series of Mean Sea Level Pressure (MSLP) fields. The horizontal resolution is 5° latitude by 10° longitude. The monthly series data are available for the period 1873 to 2005; the daily series data are available for the period 1881 to 2005 (MetOffice (2001)). Based on this data set a weather regime classification for the North Sea has been carried out (cf. Section 4.3).

2.3 Multi Regional Climate Model Ensemble

Within the ENSEMBLES project 14 participating European institutions and two Canadian research institutes ran their regional climate models for the same European domain (cf. Figure 2.3; including the Mediterranean and Island) with the same grid size of 0.44° and in a second simulation 0.22° . The hindcast simulations use 6-hourly ERA40 reanalysis as forcing data and cover at least the time period from 1961 to 2000. All partners had to provide output data according to a pre-defined list. With the help of such ensemble simulations of the period covered by ERA40 it is possible to detect and attribute regional climate change and to assess regional model performance on inter annual and shorter time scales over several decades.



Figure 2.3: Orography of the ENSEMBLES model domain (roughly) covered by most of the simulations, with the horizontal grid resolution 50 km.

From the regional climate models daily mean wind speed, daily maximum wind speed without gusts and daily mean sea level pressure has been used in this study. From few models also daily maximum wind speed including gust parameterisation is available. In 3 out of the 16 RCMs the time series for daily wind speed are incomplete or the simulation area does not cover the area of interest. Therefore, not all models have been taken into account for further wind climate analysis.

For the sake of completeness all contributing institutions in the ENSEMBLES project and the RCMs are introduced shortly:

1. The Community Climate Change Consortium for Ireland (C4I) carried out regional climate model simulations with the Rossby Centre Regional Climate Model Version 3 (RCA3) developed from the High Resolution Limited Area Model (HIRLAM). The former model version RCA2 is described in detail by Jones et al. (2004) and Kjellström et al. (2005).
2. The Czech Hydrometeorological Institute (CHMI) used a climate version of the french model ALADIN-CLIMATE/CZ (Farda et al. (2007)). The model is originally used operational as forecast model by several of European weather services (e.g., Czech Republic and Austria).
3. The Centre National de Recherche Météorologiques (CNRM) in France used their own climate version of the limited area model ALADIN (Radu et al. (2008)).
4. The Danish Meteorological Institute (DMI) used the HIRHAM regional climate model. It has been developed by the DMI in cooperation with the Max-Planck Institute for Meteorology in Hamburg and includes the ECHAM4 physics (Christensen et al. (1996)).
5. The Eidgenössische Technische Hochschule Zürich (ETHZ) applied the Climate Local Model (CLM) (now called COSMO-CLM). This is the climate version of the weather forecast model of the german weather service DWD, (Böhm et al. (2006)).
6. Within the ENSEMBLES Project the GKSS Research Center (GKSS) (now Helmholtz-Zentrum Geesthacht) also applied the regional climate model CLM like the ETHZ. The simulations used different fixed fields, like soil and vegetation description, and GKSS applied the spectral nudging approach described by von Storch et al. (2000). Although the research center has been renamed by the end of year 2010, in this study the abbreviation GKSS is used, as it was in the ENSEMBLES project.
7. The HadRM (Jones et al. (2004)) is the Hadley Centre (HC) RCM. It is a limited-area and high-resolution model based on the HadAM3H the atmospheric component of the atmosphere-ocean coupled general circulation model (HadCM3) (cf. Collins et al. (2006)). HadRM3Q0, HadRM3Q3 and HadRM3Q16 are three versions of the HadRM3 model, differing by the numeric values of some model parameters that substantially impact the simulated climate response to anthropogenic radiative forcing.

8. The International Center for Theoretical Physics (ICTP) applied the regional climate model system RegCM, originally developed at the National Center for Atmospheric Research (NCAR). Later, it was mainly developed and supported by the ICTP. The most recent version is RegCM4, published in 2010. The simulations evaluated in this work refer to the former model version RegCM3 (Giorgi and Mearns (1999)).
9. Like the C4I also the Spanish Instituto Nacional de Meteorologia (INM) applied the Rossby Centre Regional Climate Model Version 3 (RCA3) (cf. first item in this list). In their model version no sea ice is included (Jones et al. (2004) and Kjellström et al. (2005)).
10. The Royal Netherlands Meteorological Institute (KNMI) applied the 2nd version of the Regional Atmospheric Climate Model (RACMO). In this model version the ECMWF CY 23r4 physics (the same as in the ERA40 reanalysis) is included. The model version is described in detail by Lenderik et al. (2003).
11. The Norwegian Meteorological Institute (METNO) applied the HIRHAM regional climate model in this project. The model versions at METNO and the DMI are similar with some modifications (Haugen and Haakenstad (2006)).
12. The RCM REMO is applied at the Max-Planck-Institute (MPI) for Meteorology in Hamburg (Jacob (2001)). REMO has two different parameterization schemes - the original implemented physics from the DWD and, additionally, the physics from the global climate model ECHAM4.
13. The Swedish Meteorological and Hydrological Institute (SMHI) also run the Rossby Centre model RCA3 (Kjellström et al. (2005)). Differences in the model simulations are, for example, a different number of vertical layers and the model internal time step.
14. The Universidad de Castilla La Mancha (UCLM) applied the Mesoscale Prognosis model (PROMES) described by Sanchez et al. (2004).
15. The Consortium on Regional Climatology and Adaptation to Climate Change (OURA-NOS) applied the Canadian Regional Climate Model (CRCM) (Plummer et al. (2006)), which has been developed at the Université du Québec à Montréal (UQAM). The equations in CRCM, configured for climate simulations, are described by Caya and Laprise (1999) and Caya et al. (1995).
16. The RCM used by Environment Canada (EC) is the Global Environment Multiscale - Limited Area Model (GEM-LAM) This is a one-way nested version of GEM. The core

of GEM-LAM is identical to the global version of GEM, which is used operationally. In this project the GEM-LAM is used in climate mode.

For a detailed list of the participating RCM and their main features (grid type, grid size etc.), see the Appendix A.2.

3 Analysis of the possible influence of prescribed soil type distribution on the representation of present climate in the Regional Climate Model CLM

3.1 Introduction

Previous simulations over Europe carried out with different regional climate models (RCMs) carried out within the PRUDENCE project show a dry and warm bias during summer north and east of the Black Sea (Jacob et al. (2007), Hagemann et al. (2004), Moberg and Jones (2004), Räisänen et al. (2004), Vidale et al. (2003), Noguer et al. (1998), Christensen et al. (1997)). As the results from RCM climate simulations are not only used by regional climate modellers, but also by scientists in other disciplines, this so called "summer drying" presents a major issue affecting a larger scientific community.

Approaches to explain the phenomena of summer drying have been undertaken by, for example, Machenhauer et al. (1998) putting forward systematic dynamical errors of the driving model and the RCM. But also deficiencies in physical parameterization and in land surface parameter fields could be possible reasons (Hagemann et al. (2001)). Seneviratne et al. (2006b) investigated the influence of soil moisture-coupling for recent and future climate conditions in a regional climate model. They showed that the coupling can strongly affect the temperature variability e.g. in the Mediterranean for the present climate and Central and Eastern Europe for the future climate. In another study Rowell and Jones (2006) defined the causes and assessed the uncertainty of the future European summer drying. Fischer et al. (2007a,b) presented an analysis of the 2003 European summer heat wave including the associated land-atmosphere interactions involved. They pointed out that the available soil moisture content during spring is very important for a realistic simulation of the observed climate during the subsequent summer in this region. The models sensitivity of initial soil moisture conditions on the European heatwave 2003 has been also investigated by Ferranti and Viterbo (2006).

Soil moisture plays an important role within the climate system because it has a long memory that influences the atmospheric processes at the land surface (Seneviratne et al. (2006a), Pan et al. (2001), Koster and Suarez (2001), Seneviratne et al. (2006a), Wu and Dickinson (2004)). Varying soil moisture has a direct influence on soil temperature, evaporation and surface albedo (Eltahir (1998)). Thereby radiation and humidity conditions at surface level change. Findell and Eltahir (2003a,b) investigated the interaction between soil moisture and the boundary layer. They showed that the variability of soil moisture conditions over large regions has a direct influence on important processes associated with rainfall in the boundary layer. The positive feedback between soil moisture and precipita-

tion rate is supported by studies from Schär et al. (1999), Eltahir (1998) and Betts et al. (1996). Koster and Suarez (2003) pointed out that a significant impact on precipitation strongly depends on the initial soil moisture and the sensitivity of evaporation on the soil moisture state. Betts (2004) found the strong evaporation-precipitation feedback over the continents of the Northern Hemisphere during summer in the ERA40-model. This is supported by Koster et al. (2004) and Koster et al. (2006) identifying different regions on the continent with a strong coupling between soil moisture and precipitation. The influence of changing soil moisture conditions on the surface albedo can be masked by the strong response of the vegetation to water stress (Teuling and Seneviratne (2008)).

The natural soil moisture field is characterized by small-scale spatial and temporal variability affected by a complex orography and spatially variable vegetation and soil type distribution. These components can only be schematically implemented in RCMs. Several investigations have been carried out focusing on the sensitivity of RCMs to changes in vegetation and/or land use (e.g. Sánchez et al. (2007), Marshall et al. (2004), Pielke (2001), Pielke et al. (1999)). The soil types in RCMs have different fixed definitions for soil characteristics such as porosity, heat capacity and water conductivity. Such parameters strongly influence the soil moisture conditions and also surface fluxes. Block (2007) identified the uncertainty for simulated surface variables by varying the values of these soil characteristics in the CLM within a reasonable range. A strong response was seen in the Mediterranean and Southeast Europe in latent and sensible heat fluxes but also in the air temperature. Fennessy and Shukla (1999) identified the impact of initial soil moisture as mainly local and being largest on the near-surface fields.

The majority of RCMs use a soil type distribution derived from a global dataset provided by the Food and Agriculture Organization (FAO) (see chapter 3.2). In Southeast Europe - the region of the summer drying phenomena seen in RCMs - from FAO soil map sandy loam is derived. However, the International Soil Map of Europe published by Stremme (1937) identifies silt loam. The occurrence of silt loam in this area is supported by a dataset recently published by Haase et al. (2007).

In this study the influence of the two different prescribed soil type distributions on a RCMs representation of present climate have been investigated. Our main focus has been on changes due to different soil characteristics in Southeast Europe.

3.2 CLM Regional Climate Model and Experimental Model Setup

Model Details

The Climate Local Model (CLM) is the climate version of the weather forecast model of the German Weather Service (DWD) (Böhm et al. (2006)). It is a non-hydrostatic

Table 3.1: Selection of hydraulic and thermal parameters of sandy loam (Doms et al. (2002)) and silt loam (estimated from Driessen (1986), Doms et al. (2002)).

	sandy loam	silt loam
volume of voids [-]	0.445	0.485
field capacity [-]	0.260	0.360
permanent wilting point [-]	0.100	0.130
heat capacity [$10^6 J/(m^3 K)$]	1.350	1.450
heat conductivity [$W/(Km)$]	1.74	1.25
fraction of sand [%]	65	10
fraction of clay [%]	10	15

RCM, using a regular latitude/longitude grid with a rotated pole and a terrain following height coordinate. The CLM includes the multilayer soil model TERRA (Schrodin and Heise (2001)). The evapotranspiration of plants is parameterized based on the Biosphere-Atmosphere Transfer Scheme (BATS) (Dickinson et al. (1986)). The parameterization of bare soil evaporation follows Dickinson (1984). In the TERRA soil model ten active layers for energy transport (up to a depth 15 m) are used. The bottom layer (10th layer from 7.66 m to 15.34 m depth) is the so called *climate layer*, where the annual mean temperature is prescribed as a boundary value (Doms et al. (2002)). For the hydrological section the same layers as in the thermal section are set, but only to a depth of around 4 m (8 layers). At the bottom boundary of the 8th layer only the downward gravitational transport is considered and capillary transport is neglected (Doms et al. (2002)). According to the soil type distribution the soil moisture is initialised at the beginning of the simulation by the forcing data and evolves freely without any correction or nudging by the driving data in the course of the simulation. The model has been used previously for the simulation of present and/or future climate conditions in the EU funded projects: PRUDENCE (<http://prudence.dmi.dk/>), ENSEMBLES (<http://ensembles-eu.org/>) and also in the *klimazwei* project funded by the German government (<http://www.klimazwei.de/> and <http://sga.wdc-climate.de>). For this investigation the model version 3.21 is used which is a pre-version of the CCLM4 (a merged version of COSMO-LM and the climate version CLM). It was validated in detail by Jaeger et al. (2008).

Gridded geographical distribution of soil type fields

RCMs usually include soil types derived from the FAO global soil map. The FAO developed an international standardized classification to describe soil characteristics (for details see *Soil Map of the World* (FAO/UNESCO (1974))). For climate modelers a gridded version known as *Digital Soil Map of the World* (DSMW) (FAO (1996)), with a spatial resolution of 5' by 5' (approx. 9 km x 9 km) is available. It contains the DSMW map and derived soil

properties such as soil depth, soil moisture storage capacity and soil drainage class.

For the regional scale the *International soil map of Europe* published by Stremme (1937) with a scale of 1:2 500 000 have been selected. This map contains eleven soil texture classes and two mixed classes and has been digitized and classified for areas of silt loam. These areas have been added to the FAO soil distribution map and used it as the second soil type distribution within our experiment (see the following section).

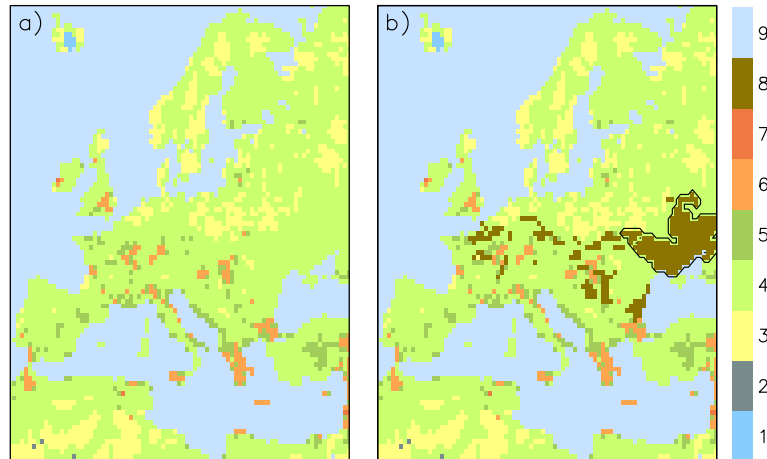


Figure 3.1: Soil type distribution derived from (a) FAO and (b) the same as a) but with silt loam areas added from the International Soil Map of Europe (1 - ice, 2 - rock, 3 - sand, 4 - sandy loam, 5 - loam, 6 - loamy clay, 7 - clay, 8 - silt loam, 9 - sea water). Black contour indicates the area of interest (cf. Figures 3.4, 3.5, 3.6, 3.8, and 3.7 and Chapter 3.3).

Experimental Design

The model domain covers Europe with a spatial resolution of 50 km and 32 vertical levels for the atmosphere. The pole of the rotated model grid is located at (50.75° N and 18° E) (cf. Figure 3.1 excludes the sponge zone). The simulations are driven by NCEP/NCAR re-analysis data (Kalnay et al. (1996)). In addition to the forcing at the lateral boundaries (Davies (1976)) a spectral nudging technique as described by Feser and von Storch (2005) has been applied. The soil type distribution used in RCMs is derived from FAO soil textures. The original three fractions (coarse, medium and fine) have been mapped to base porosities used in the model. After interpolation these mixed values have been assigned to the model used five standard soil types (sand, sandy loam, loam, loamy clay and clay) according to the individual porosity values in the models look-up table for the soil characteristics. Further surface properties include the definition of ice, rock and sea water.

Two 13-year CLM simulations have been performed covering the period 1993-2005. The simulations were initialized on January 1st, 1989, allowing a four year spin-up time to

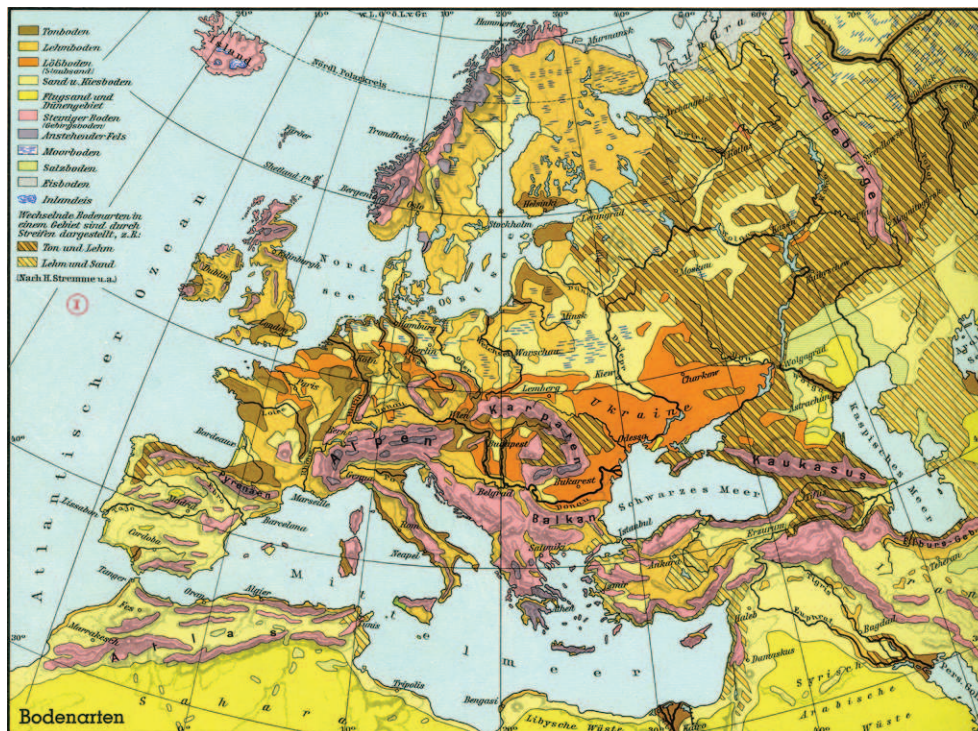


Figure 3.2: Part of the International Soil Map of Europe by Stremme (1937) from Diercke and Dehmel (1966).

reduce the influence of the initial soil moisture. One simulation has used the soil type distribution derived from the FAO dataset (hereafter referred to as the control simulation (CTL)). In the second simulation the same soil type distribution as for the control simulation has been used but with areas of silt loam from the *International soil map of Europe* (hereafter referred to as the modified simulation (MOD)). The areas of silt loam are not included in the FAO soil map, but other sources (e.g. Haase et al. (2007)) support the occurrence of silt loam. The associated soil parameters are listed in Table 3.1. For comparison of the modelling results the global high-resolution gridded temperature and precipitation data set CRU TS2.1 (Mitchell and Jones (2005)) has been used. This data set with a spatial resolution of $0.5^\circ \times 0.5^\circ$ covers the time period 1901-2002 and is based on in-situ measurements from a large number of stations.

3.3 RCM response on changing soil conditions

Based on the results of using different soil characteristic definitions (cf. Table 3.1), areas of silt loam in the modified simulation are initialized with a 9% higher soil moisture in all active soil layers compared to the control simulation that used sandy loam. After initialisation soil moisture develops freely without any correction or nudging during the

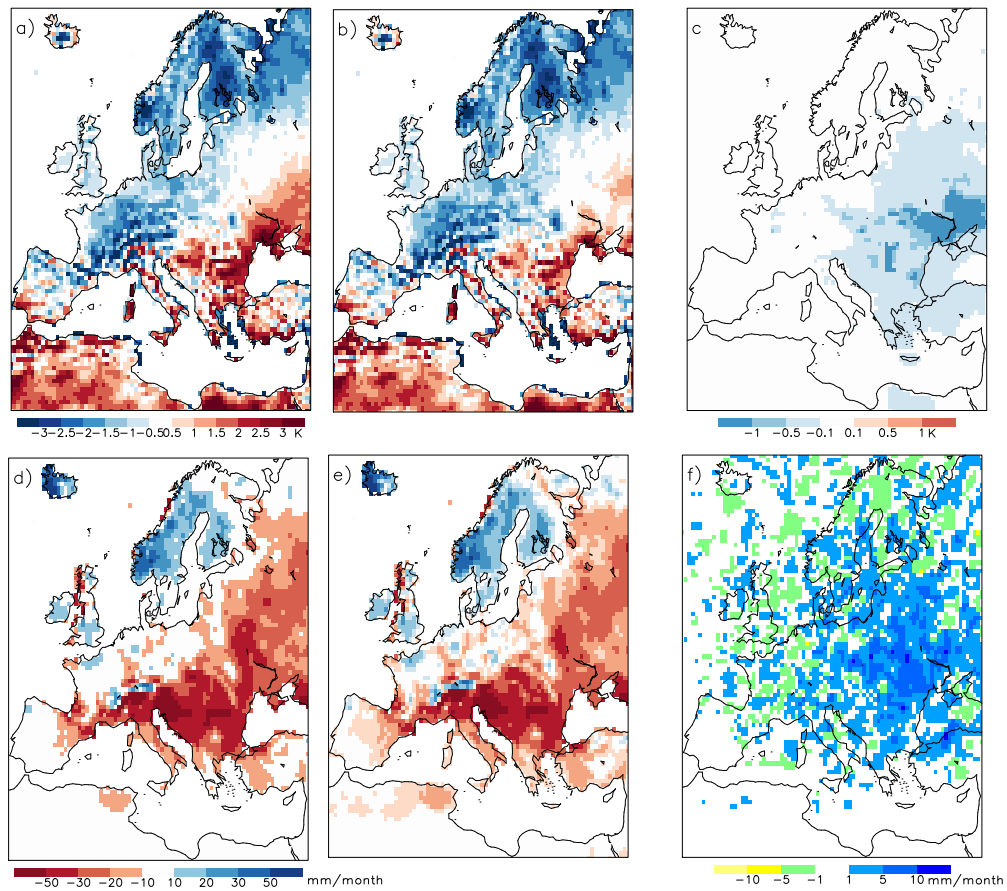


Figure 3.3: Top row: Bias of mean 2m-temperature over time period June-August compared to CRU data for the a) control simulation and b) modified simulation. c) difference between both simulations (MOD-CTL), Bottom row: Bias of the mean precipitation over the time period June-August compared to CRU data for the d) control simulation and e) modified simulation. f) difference between both simulations (MOD-CTL).

simulation. Figure 3.4-a) shows the mean annual cycles of soil moisture in all layers affected by the roots. Due to a mean root depth in this area of about 1.5 m, the upper seven soil layers are taken into account in these plots. The differences between both simulations can be seen in Figure 3.4-b) as the change MOD-CTL in relation to the amount which is available in the CTL simulation. The values are spatial averages over the connected silt loam area north of the Black Sea (3.1-b)) over the time period 1993-2005. During the whole simulation period using silt loam higher available soil moisture is observed in all active soil layers in the modified simulation. The upper four layers show a similar pattern with about 10-15 % more soil moisture during spring, autumn and winter and values up to 30 % during summer. The lower layers show values even of up to 75 % during spring time, which coincides with the annual maximum of moisture in all soil layers. In MOD a strong annual cycle of soil moisture is discernible in the lower soil layers (from the 5th layer downward). In the CTL simulation there is no annual cycle in the soil moisture for

the soil layers 7 to 10 (the most bottom). This can be traced back to the fact that due to small values for the saturation of the soil in this area there is not enough moisture available in the model to fill the lower soil layers. Figure 3.8 shows the temporal evolution of the available soil moisture in the root zone as percentage of the saturation. As the soil in both simulations is not at saturation it shows a constant increase of the values of about 10% over the whole year in MOD (cf. Table 3.2 for exact values). The Figures 3.9-g) and -h) show that this effect is limited to the silt loam area.

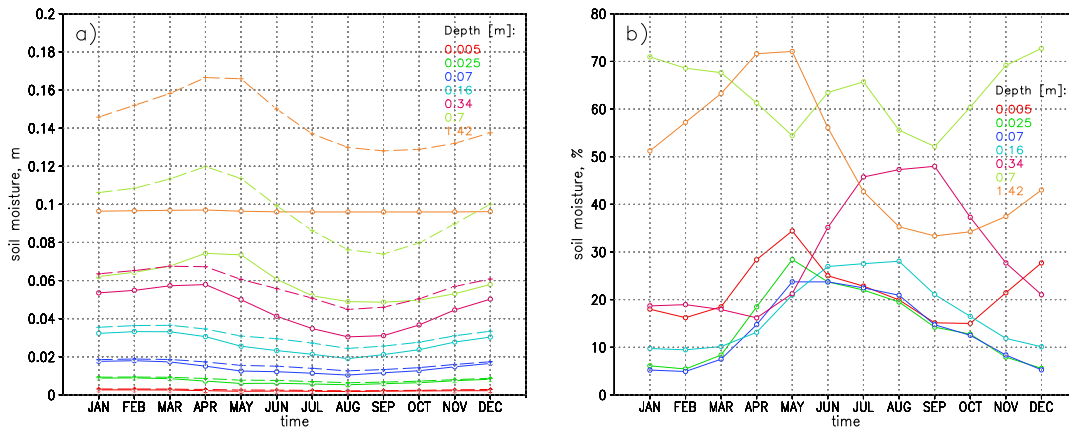


Figure 3.4: Mean annual cycle of soil moisture for all soil layers affected by the roots a) for CTL simulation (solid) and MOD simulation (dashed) and b) as the difference between MOD and CTL as the relation $(\text{MOD}-\text{CTL})/\text{CTL}$ and as the mean over the connected silt loam area north of the Black Sea (cf. Figure 3.1). The numbers indicate the mean depth of each soil layer, measured from the earth's surface.

Physical considerations explaining the differences in surface properties are related to increased soil moisture which leads to increased net solar radiation. The latter is due to a decrease in albedo (not shown) which increases the absorption of radiation at the surface. This effect is accompanied by a decrease of both surface temperature and therefore terrestrial outgoing radiation because more energy is used for evaporation. This decrease in the albedo is small with values about 1 to 3% in April and May and less than 1% during summer. This can be explained by the generally small values for soil moisture in these months, so that the increasing soil moisture has not a very big effect on the surface albedo. Further the decrease of surface albedo due to increasing soil moisture is masked by the large influence of the vegetation state. Teuling and Seneviratne (2008) investigated the dynamic of surface albedo and referred to the strong spectral response of vegetation to water stress. This agrees with results from Zaitchik et al. (2007).

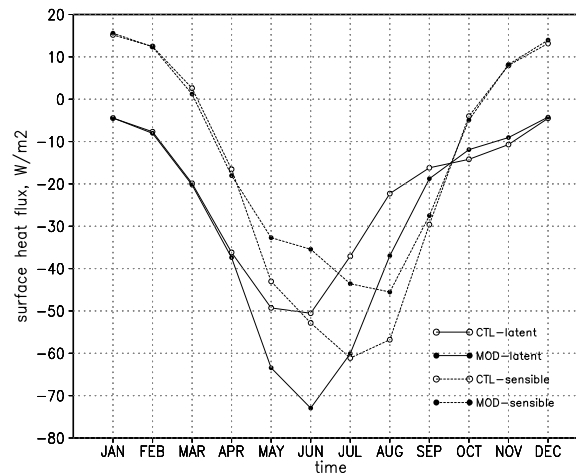


Figure 3.5: Temporal evolution of latent heat flux (circles) and sensible heat flux (squares) at surface, as mean annual cycle for connected silt loam area (cf. Figure 3.1). The values for CTL (solid) and MOD (dashed) integrations are spatially averaged over the connected silt loam area north of the Black Sea (cf. Figure 3.1).

Figure 3.5 shows the annual cycle of the surface latent heat flux. From May until August up to 60 % higher values for evaporation occur. Where e.g. in CTL in July an evaporation rate of -1.28 mm/day can be observed in MOD it is increased by -0.8 mm/day (see also Table 3.2). The changes in the heat fluxes are spatially limited on the grid points with the silt loam definition (cf. Figure 3.9-d) and -e).

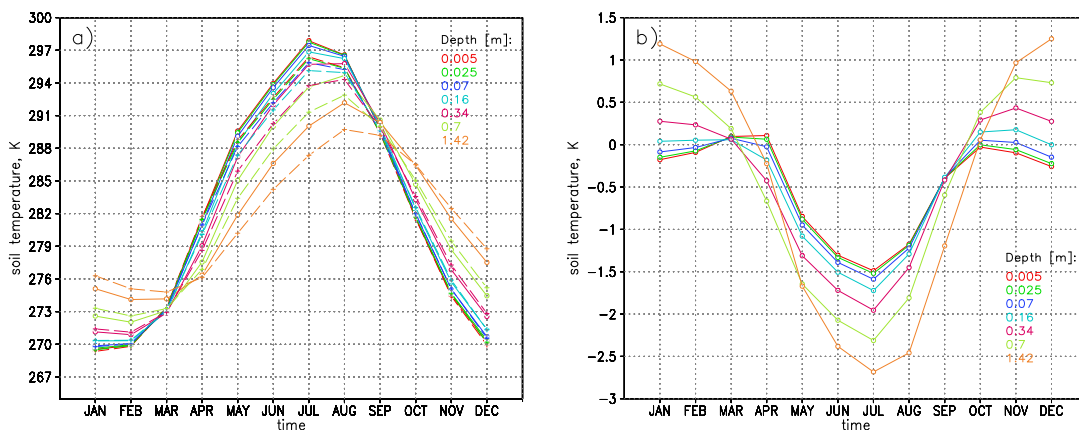


Figure 3.6: Mean annual cycle of soil temperature for all soil layers affected by the roots a) for CTL simulation (solid) and MOD simulation (dashed) and b) as the difference between MOD and CTL as the relation MOD-CTL and as the mean over the connected silt loam area north of the Black Sea (cf. Figure 3.1). The numbers indicate the mean depth of each soil layer, measured from the earth's surface.

The influence of higher soil moisture is also clearly reflected in the soil temperatures. Figure 3.6-a) shows the mean annual cycle of the soil layers temperatures in the root zone for

each simulation. Independent from model integrations the thicknesses of the upper layers is very small and is increased to the soil depth. Hence the amplitude of the temperature of the upper soil layers is very similar and the annual maximum occurs at about the same time in late July/beginning of August. The typical behaviour of the lagged heat transfer from the surface to the deep soil layers can be clearly identified. Due to the in general higher soil moisture conditions in MOD the amplitude of the soil layers temperature is reduced by up to 2.5 K compared to the CTL simulation. Hence, a weaker but more realistic annual cycle of soil temperature in the modified simulation results can be found. In MOD the described lag between the annual maximum temperature at surface and the lower soil layers is increased (cf. Figure 3.6-a)). This increased lag and as Figure 3.4-b) shows an increase of available soil moisture with depth an increase of differences in soil temperature is observed (cf. 3.6-b)). The difference in the 9th layer is smaller with values up to +/- 1 K and zero for the 10th layer (not shown) where the temperature is prescribed as a boundary value (cf. Section 3.2). In opposite to the upper soil layers within the lower levels differences between both simulations also occur during winter period. While the soil temperature decreases by up to 2.5 in summer (cf. Figure 3.9-f)) during the winter months the lower amplitude of the annual cycle of temperature leads to weaker cooling of the lower soil layers by 1.5 K in MOD compared to CTL.

As a result of increasing latent heat flux, the Bowen Ratio (the ratio between energy available for sensible heating and energy available for latent heating) decreases (e.g. from 1 to 0.5 in July) (see Figure 3.5). This leads to an increase of water vapour concentration in the boundary layer (Eltahir (1998)) and also to an increase of backscattered terrestrial radiation in the atmosphere. This, in combination with a decrease of ground and surface temperature results in an increase of net terrestrial radiation at the surface by up to 6 W/m^2 in July and August (see Table 3.2 for exact values).

Between May and August increases of relative air humidity (of about 6 %) and of specific humidity in July from $8.8 \cdot 10^{-3}$ in the control simulation to $9.6 \cdot 10^{-3}$ kg/kg in the modified simulation are evident. As the mean total cloud cover between May and August is 0.5, the increase of the cloud cover in the MOD simulation by 10 % is small (cf. Figure 3.9-c)). Hence in this time the changes in net solar radiation are also of low magnitude of about $-2.5 W/m^2$ (cf. Table 3.2 and Figures 3.9-a) and -b)).

Compared to the CRU data, summer precipitation in the modified simulation is still underestimated. However, an increase of simulated precipitation for both, large scale and convective precipitation can be seen. Figure 3.3 shows the mean differences in precipita-

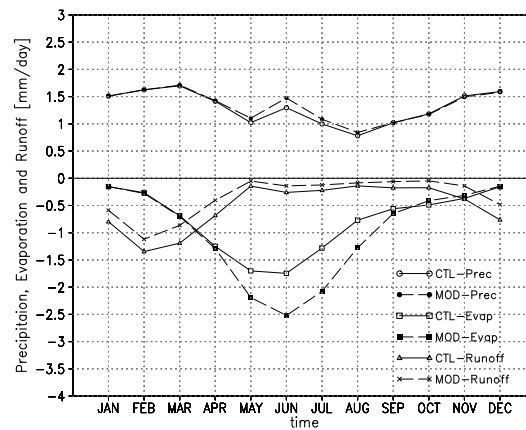


Figure 3.7: Temporal evolution of precipitation (dots), evaporation (squares), and runoff (triangle,cross) over the connected silt loam area north of the Black Sea (cf. Figure 3.1) in the CTL (solid) and MOD (dashed) integrations in mm/day.

tion summer (JJA) between the control and the modified simulations compared with CRU data for the period 1993-2002. In general, significant changes during May-September over Southeast Europe can be found. In the area of interest the total precipitation in summer is increased by up to 10 %, in July for example from 1 mm/day in CTL to 1.08 mm/day in MOD (see Table 3.2 for May and September).

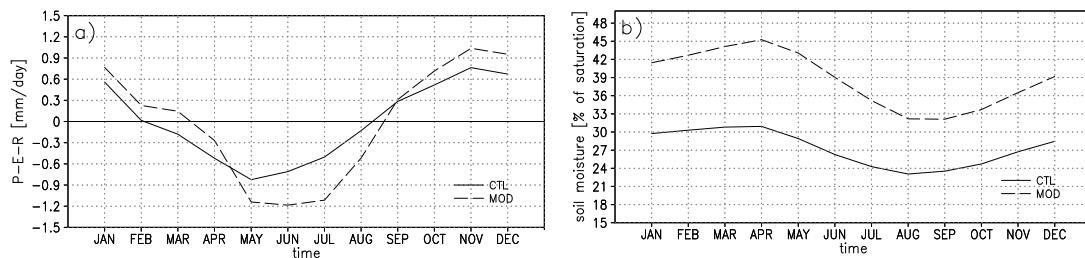


Figure 3.8: Temporal evolution of the a) net input of water in the soil (precipitation-evaporation-runoff) in mm/day and b) the relative soil moisture content in the root zone in % of saturation. The values for CTL (solid) and MOD (dashed) integrations are spatially averaged over the connected silt loam area north of the Black Sea (cf. Figure 3.1).

The mean temporal evolution of precipitation, evaporation and runoff as the spatial mean over the connected silt loam area north of the Black Sea (cf. Figure 3.1) is presented in Figure 3.7. From January to March and from September to December the precipitation rate is higher than the evaporation rate. As the soil layers are not at saturation the additional water can be stored in the soil. A part of this extra water is stored in snow.

Table 3.2: Summary of CTL and MOD experiments: mean of the 13 years simulated for the month May, July and September. The values are spatial averages over the connected silt loam area north of the Black Sea (cf. Figure 3.1). SW net denotes net shortwave radiation, LW net is the net longwave radiation, NR net radiation, LH latent heat flux, SH sensible heat flux.

Fields	Units	May			July			September		
		CTL	MOD	Δ	CTL	MOD	Δ	CTL	MOD	Δ
Hydrological cycle										
- Precipitation	mm/day	1.02	1.10	+0.08	1.00	1.08	+0.08	1.02	1.02	+0.00
- Evaporation	mm/day	-1.70	-2.19	-0.49	-1.28	-2.08	-0.8	-0.56	-0.65	-0.09
- Runoff	mm/day	-0.14	-0.05	+0.06	-0.22	-0.12	+0.10	-0.18	-0.06	+0.12
- Soil moisture										
→ (upper 10cm)	mm	2.05	2.58	+0.53	1.90	2.33	+0.43	1.95	2.23	+0.28
	% of sat	46.0	53.3	+7.3	42.8	48.0	+7.2	43.7	46.0	+2.3
→ (root zone)	mm	26.59	39.68	+13.09	22.32	32.44	+10.12	21.63	29.60	+7.97
	% of sat	31.5	43.1	+11.6	26.4	35.2	+8.8	25.6	32.1	+6.5
→ (total)	mm	45.87	72.86	+26.99	41.52	59.84	+18.32	40.83	55.21	+14.37
	% of sat	46.0	53.3	+7.3	42.8	48.0	+7.2	43.7	46.0	+2.3
Surface energy budget										
- SW net	W/m ²	179.58	177.32	-2.26	187.24	184.93	-2.31	115.98	117.14	+1.16
- LW net	W/m ²	-75.30	-71.05	+4.25	-78.19	-71.21	+6.98	-73.67	-72.21	+1.46
- Net Radiation	W/m ²	104.28	106.27	+1.99	109.05	113.72	+4.67	42.31	44.93	+2.26
- SH	W/m ²	-43.02	-32.70	+10.37	-61.11	-43.58	17.53	-29.60	-27.49	+2.11
- LH	W/m ²	-49.28	-63.41	-14.14	-37.09	-60.70	-23.61	-16.18	-18.75	-2.57

An increase of the soil moisture from September until April is observed (cf. Figure 3.8-a). From April onwards the increase of evaporation is substantial, while the rate is higher in the MOD simulation compared to CTL, due to the higher water storage especially in the spring time (cf. Figure 3.8-b). The evaporation increases in both simulations until June and decreases afterwards, due to the progress of the soil drying.

Figure 3.9-f) presents the changes between MOD simulation and the CTL in summer mean sea level pressure. In the greater area of interest an increase of surface pressure occurs of the order of 0-0.5 hPa.

3.4 Summary

In a number of different RCM simulations dry and warm biases over Southeast Europe have been observed. The hypothesis is tested that the biases are related to a false representation of soil properties in this region, based on divergences between the soil maps of Haase et al. (2007) and Stremme (1937) and that of FAO which is commonly used in (regional and global) climate models. Therefore two simulations with the RCM CLM have been carried out using default sandy loam and silt loam over an area north of the Black Sea. Key results of this study are:

Due to its higher porosity, silt loam assimilates more water during rainfalls than sandy loam. This leads to a 30 % to 75 % increase in soil moisture in the modified simulation compared to the control simulation. The wet ground leads to a decrease of surface albedo and thus an increase of net solar radiation. The air temperature decreases by up to 1.5 K

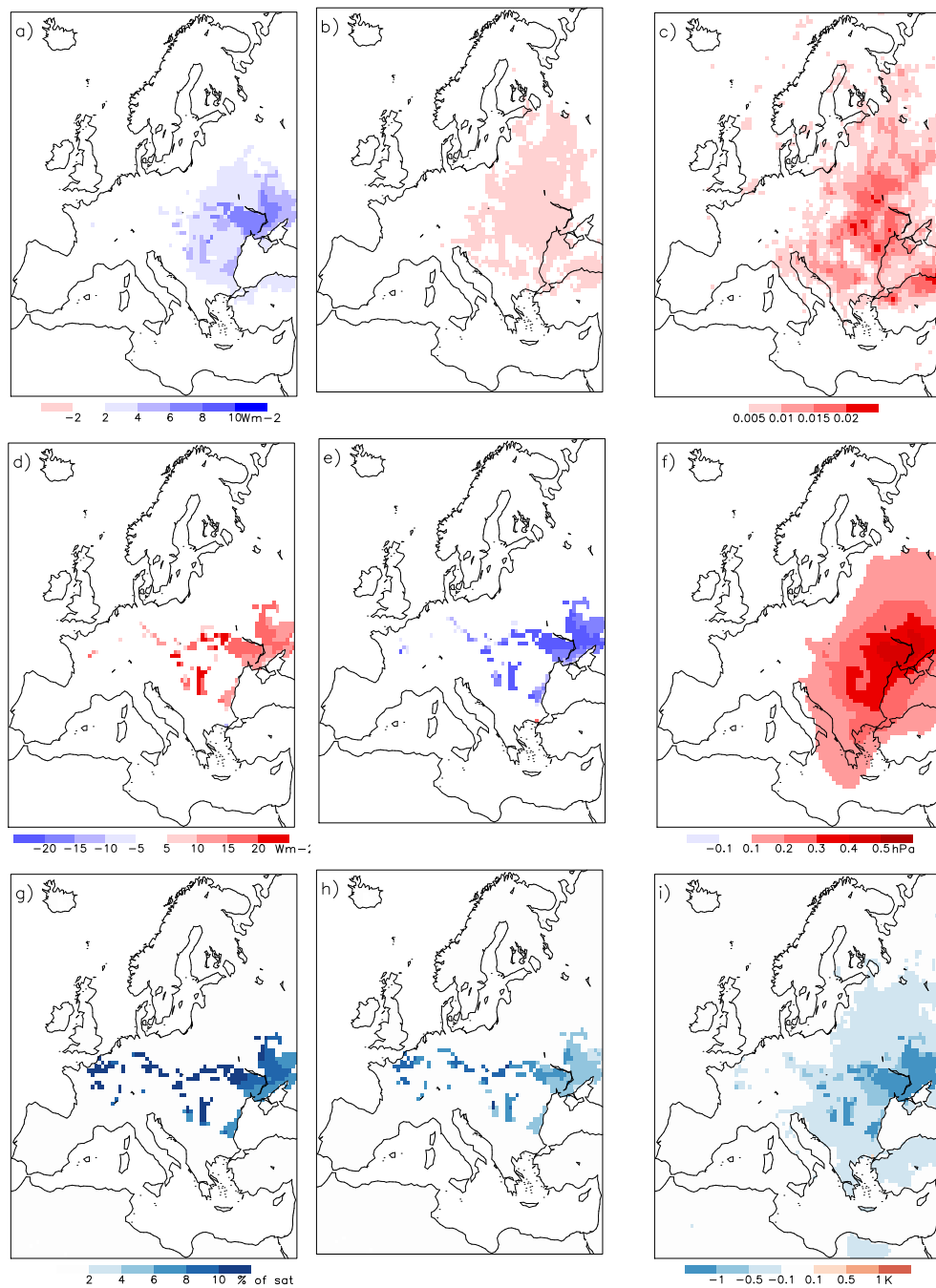


Figure 3.9: Difference between both simulations (MOD-CTL) over the time period June-August (1993-2005) for a) net longwave radiation, b) net shortwave radiation, c) total cloud cover, d) sensible heat flux, e) latent heat flux, f) mean sea level pressure, g) soil moisture in the root zone, h) soil moisture in the upper 10cm, and i) temperature in the upper soil layer.

because more energy is needed for evaporation. During summer a 60 % higher evaporation rate with increased humidity in air in the modified simulation compared to the control simulation have been found. In Southeast Europe the higher concentration of water within the boundary layer of the modified simulation causes more precipitation in the summer months. The study shows that heat fluxes and differences in soil moisture are limited

to the silt loam area, whereas radiation, total cloud cover and changes in mean sea level pressure also occur in a larger region.

It can be concluded that using a silt loam distribution from the *International soil map of Europe* combined with the FAO soil map improves models representation of the observed climate in the region with modified soil type. Nevertheless this modification fails to remove most of the model bias in Southeast Europe, because the area where the modification is performed is only a small part of the region affected by the "summer drying" bias. It can be nonetheless postulated based on our results that the specification of soil type is clearly important for such biases and may be relevant for other regions as well. It is a major contribution in reducing the phenomena of summer drying in the RCMs. The European Commission Joint Research Center (JRC) released the "European Soil Database" (European Commission (2004)). Based on this data Guillod et al. (2013) investigated the impact on European climate simulations and found similar results as have been presented in the present work.

The results confirm that improving the simulation of processes within the boundary layer strongly depends on the improvement of the simulation of soil moisture.

(Note: All results of this chapter have been published in Anders and Rockel (2009))

4 Main circulation pattern for Europe and the North Sea

4.1 Introduction

As stated in the overall introduction to this work results from regional climate models (RCMs) are getting more and more important in future wind climate assessment. An aim of this study is to carry out an evaluation of simulated coastal wind speeds from the regional climate model ensemble introduced in Section 2.3. From the regional climate models only the daily wind speed is available, but no information on prevailing wind direction of each day. However a dependence of the evaluation results from the direction of the wind is expected. To cover this important part of the analysis, weather regime classification is a helpful tool to investigate models ability of simulating surface wind speed in more detail. In the last decades weather regimes have been used to describe the synoptic situation per day and different weather regime classifications have been developed. The most famous ones from Baur et al. (1943) and Baur (1948) have been extended and revised by Hess and Brezowsky (1952) and Gerstengarbe et al. (1999). A similar classification by Lamb (1972) was made for the British Isles and another by Dittmann et al. (1995) for Germany. An overview on further weather regime classifications is given by Bissolli and Dittmann (2001).

In previous studies a correlation of large scale circulation and near surface variables, mostly temperature and/or precipitation has been shown (Buchanan et al. (2002), Fowler and Kilsby (2002), Post et al. (2002)). Buishand and Brandsma (1997) compared different circulation classification schemes for predicting temperature and precipitation in the Netherlands and identified advantages and disadvantages of the schemes. Trigo and DaCamara (2000) applied the classification by Jenkinson and Collison (1977) to investigate the influence on the precipitation in Portugal. They found a relation between the decrease in precipitation in March and a decrease on a wet weather regime in the same month.

Demuzere et al. (2009) used the automatic version the Lamb (Lamb (1972)) weather type classification method by Jenkinson and Collison (1977) to evaluate ECHAM5 pressure fields and to study trends in the frequency of occurrence of circulation patterns for the period 1860-2100.

In this section two objective regime classifications have been investigated to be a sufficient diagnostic tool to evaluate the present wind climate at the German and Dutch coastal area of the North Sea (cf. Figure 2.2). One classification was carried out for whole of Europe within the ENSEMBLES framework and was provided by Sanchez-Gomez et al. (2009), the other classification was carried out for all models and the forcing and is based on mean sea level pressure field in the area of the North Sea. For both classifications

mean occurrence and composites of mean MSLP pattern have been calculated for each regime and for the time period 1961 to 2000. Afterwards the composites of local wind observations have been derived depending on the weather regimes. Due to the applied methods in both classifications ERA40 and the RCMs do not necessarily show the same regime at each day. The agreement among the model simulations and ERA40 has been analysed in a last step.

4.2 Large Scale circulation pattern for Europe (provided by Sanchez-Gomez et al. (2009))

Sanchez-Gomez et al. (2009) used the simulation results from the regional climate model ensemble (cf. Section 2.3) to investigate the ability of the models to reproduce the large-scale atmospheric circulation of the driving ERA40 reanalysis data (cf. Section 2.2).

Description of the method

Sanchez-Gomez et al. (2009) carried out a cluster analysis applying the *k-mean* algorithm on the first 15 principle components of daily values of the ERA40 geopotential height at 500 hPa pressure level (Z500) for the time period 1961 to 2000. Via a Monte-Carlo-test the optimal number k of clusters was set to $k = 4$.

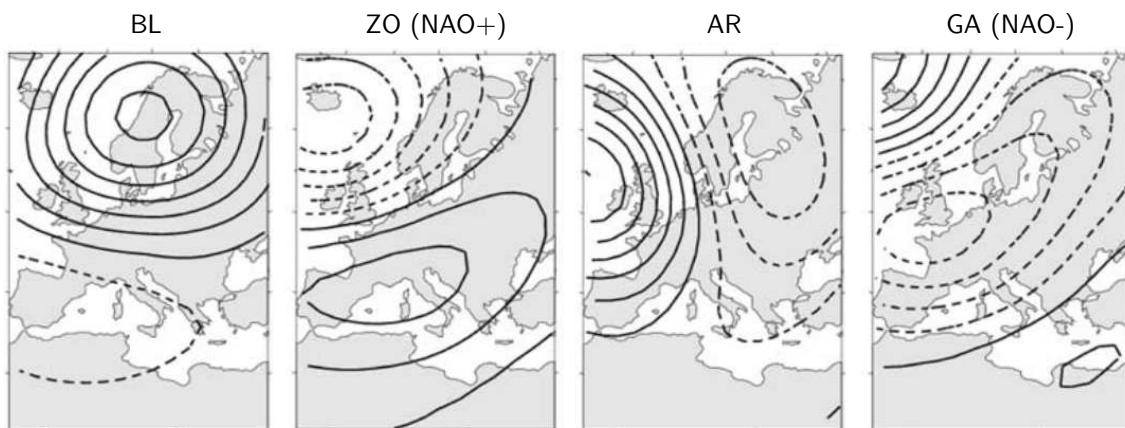


Figure 4.1: Composites of the weather regimes in winter (DJFM) for ERA40. From left to right: BL - Blocking, ZO - Zonal (NAO+), AR - Atlantic Ridge and GA - Greenland Anticyclone (NAO-). The isolines are the Z500 anomaly composites (solid lines: positive values, dashed lines: negative values). Contour interval is 30 gpm. (Source: Sanchez-Gomez et al. (2009))

The four weather regimes BL -Blocking, ZO - Zonal (NAO+), AR - Atlantic Ridge and GA - Greenland Anticyclone (NAO-) have been analysed for every day in the summer months (JJAS - from June to September) and the winter months (DJFM - from December to March) separately for the period 1961 to 2000. For every day within the given time

period one of the four weather regimes is set to describe the large-scale circulation. No “undefined day” exists.

During the Blocking regime a strong blocking cell can be found over Scandinavia. The higher pressure than normal over North Europe and lower values than normal over the Mediterranean lead to a strong pressure gradient in central Europe. In the Zonal regime, the NAO+ phase, the lower pressure than normal in Northern Europe and the higher pressure than normal over South and Southeast Europe lead to stronger mostly westerly wind over the northwest Atlantic. In the Atlantic Ridge regime, we can observe a positive anomaly over the Atlantic. The pressure gradient is in west-east direction. The Greenland Anticyclone (NAO-) regime presents a strong positive anomaly over west of Greenland and a negative anomaly over Europe. The pressure gradient is weak and this leads to low wind speeds over the whole area. (cf. Figure 4.1)

In order to analyse the large-scale circulation in the RCMs the *k – mean* algorithm has not been applied to the RCM output. Sanchez-Gomez et al. (2009) assumed instead that the structure of weather regimes will not vary between the models and reanalysis data. They projected the daily Z500 anomalies to the clusters centroids derived from ERA40 and checked the similarity by the use of the euclidean distance. This method has been applied to the 50km and the 25km spatial resolution RCM experiments. Depending on data availability simulation results of 13 RCMs have been used.

The complete description of the method can be found in Sanchez-Gomez et al. (2009).

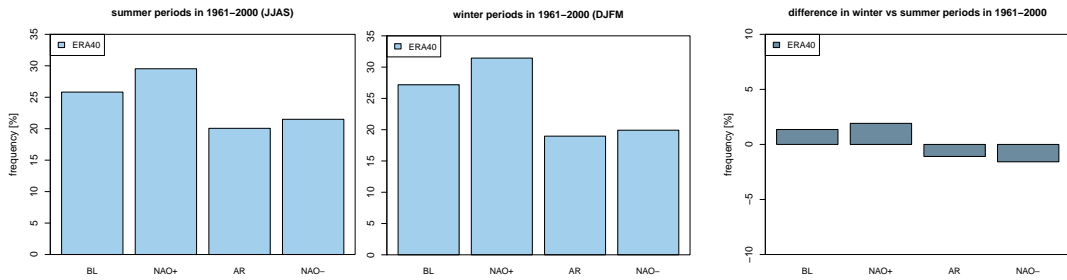


Figure 4.2: Relative occurrence frequency (%) of the four weather regimes Blocking (BL), Zonal (NAO+), Atlantic Ridge (AR) and Greenland Anticyclone (NAO-) derived from ERA40 reanalysis data within the time period 1961 to 2000 for summer (left) and winter (middle) and the difference of both (right).

Figure 4.2 shows the mean occurrence of the weather regimes in summer (left panel) and winter (middle panel) based on the regime data provided by Sanchez-Gomez et al. (2009) for the ERA40 reanalysis in 1961-2000. We can observe that the Zonal NAO+ occurs most in both seasons. The relation in the occurrence of the four regimes are about the same in the summer and winter months (cf. Figure 4.2, right panel). The Blocking frequency

matches the results of D'Andrea et al. (1998), who estimated an occurrence of about 23% for the northern hemisphere and longitudes between 0-30°E.

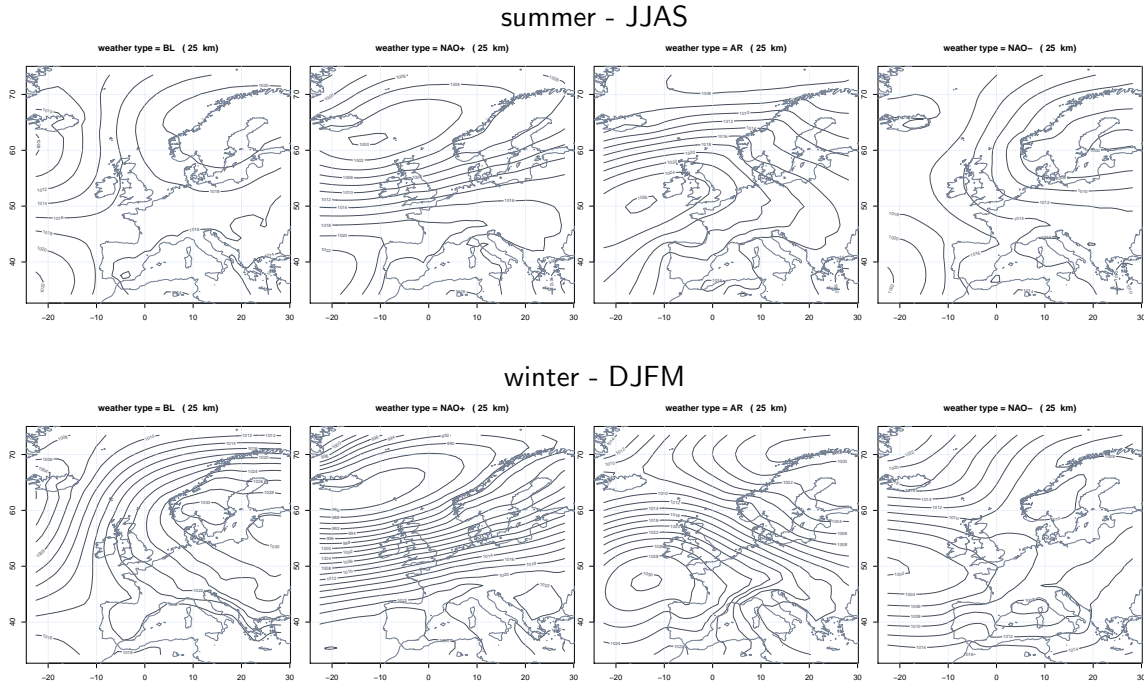


Figure 4.3: Composites of the mean sea level pressure in ERA40 during the four weather regimes in summer (JJAS) (upper row) and winter (DJFM) (lower row) within the time period 1961-2000.

While Figure 4.1 gives an overview on the mean pattern per regime of the geopotential height at 500 hPa Figure 4.3 shows the same but of the mean sea level pressure and additionally, the summer and the winter periods in 1961 to 2000 are separated. The gradients in winter are much stronger than in summer. Compared to the winter pattern the blocking in summer is weak. With focus on the North Sea the pattern for NAO- differs for the summer and winter months.

Agreement with station data

According to the analysis described in Section 5 it is important that the defined weather regimes represent the wind conditions in the area of interest, the German and Dutch coast. To decide whether the regime classification fits the requirements they have been compared to the local wind observational sites. Figure 4.4 gives examples for the wind characteristics at four different observations at the German and Dutch coast during the four weather regimes BL - Blocking, ZO - Zonal (NAO+), AR - Atlantic Ridge (AR) and GA - Greenland Anticyclone (NAO-) for the summer months (JJAS) and winter months

(DJFM) for 1971-2000. The wind roses show composites of the hourly observed wind speed and direction obtained by averaging over all the days for the same weather regime in the ERA40 data.

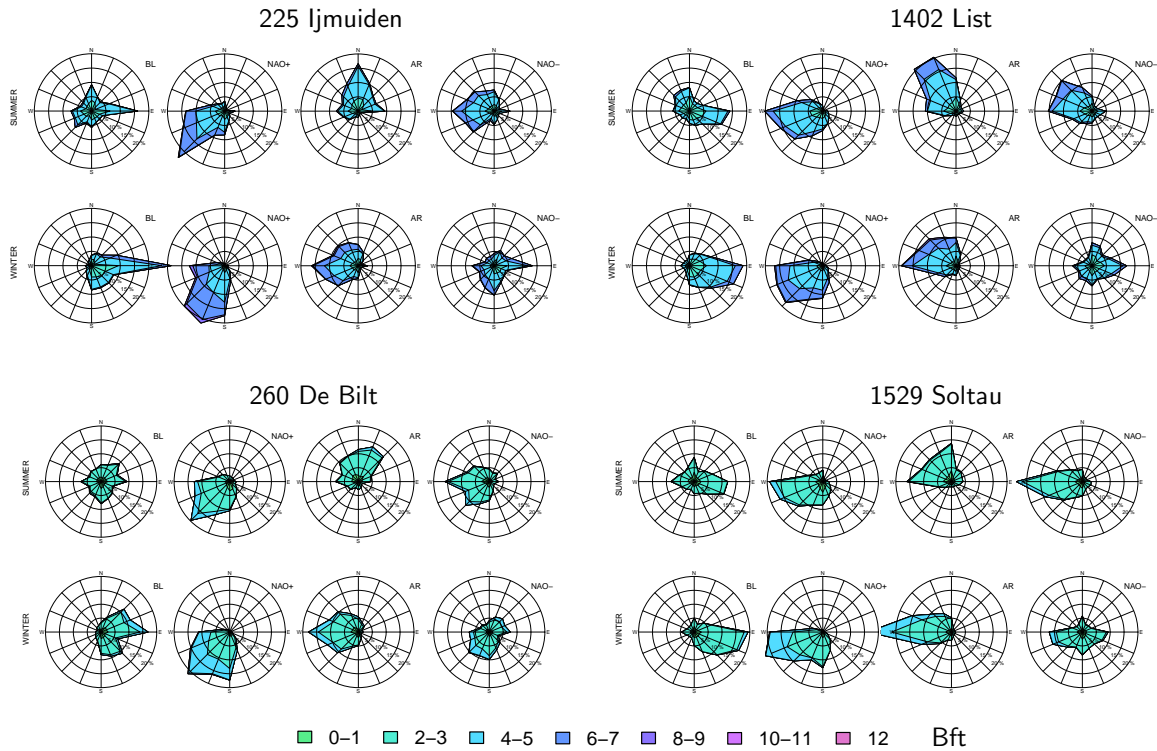


Figure 4.4: Wind characteristics at four stations (IJmuiden, List, DeBilt and Solttau) during the four weather regimes BL - Blocking, ZO - Zonal (NAO+), AR - Atlantic Ridge and GA - Greenland Anticyclone (NAO-) for the summer months (JJAS) and winter months (DJFM) within the time period 1971-2000.

In Figure 2.2 it can be seen, that the stations 225 - IJmuiden and 1402 - List are located near the coastline, whereas the stations 260 - DeBilt and 1529 - Solttau are inner land stations and located up to 100km far from the coast. This fact results in higher observed wind speeds at the coastal stations.

Only the wind roses for NAO+ agree at all stations and within the two seasons. They show clearly a western to southwestern wind direction of higher speeds for the German Bight. For AR and NAO- the wind conditions at the different stations are similar only within each season. In summer wind comes from the North and Northwest during AR regime, while in winter western directions are more dominant. The observations in summer show wind from the West during NAO- conditions, but there is no clear dominant wind direction during winter. During the Blocking conditions easterly winds seem to be slightly more common than from other directions, however this is more visible during the winter months.

Occurrence of the weather pattern over time and trends

In Figure 4.5 the occurrence of the four weather regimes from December to March in each year in the time period of 1961-2000 is shown. Additionally the trend has been calculated (blue line) and analysed for significance applying the parameter free Mann-Kendall-trend-test (Mann (1945), Kendall (1975)). This trend test does not presume a normal distribution of the data, but is very sensitive on autocorrelated data. With respect to a possible autocorrelation, the so called "Trend-Free-Prewhitening Procedure" after Yue et al. (2002) has been applied to the data in case of a high "lag - 1" -autocorrelation before testing for the Mann-Kendall-significance in the trend. The trend is significant if the level of significance, the p - value, is smaller than 0.05.

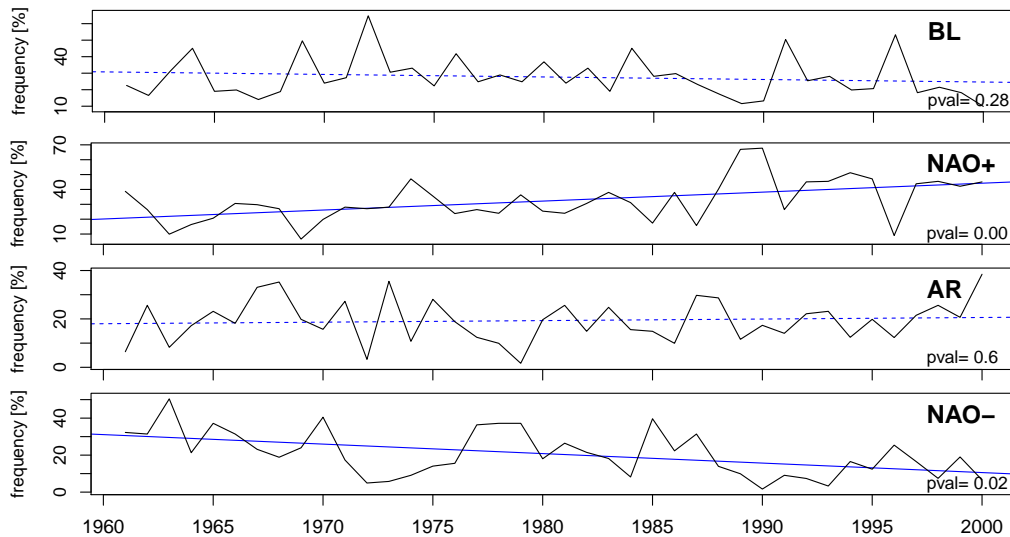


Figure 4.5: Annual occurrence of each regime in the winter months (December to March) in the time period of 1961- 2000 (black) and the linear trend (blue dashed line and in case of significance blue solid line).

While the regimes BL and AR do not show any change of the occurrence during the 40 years, a significant change can be observed in the trend of the NAO+ and NAO- regimes. These results are consistent with the Index of the North Atlantic Oscillation provided by the NOAA Climate Prediction Center (CPC (2000)) for the same time visualized in Appendix C.1. The NAO-index is widely used as a general indicator for the strength of the westerlies over the eastern North Atlantic and western Europe. In the positive phase of the NAO-index westerlies are dominant in this area, while in the negative phase the number of westerlies is reduced.

The correlations of the occurrence of the regimes NAO+ and NAO- and the NAO-index is 0.81 and 0.78. The significant positive and negative trend in the two regimes is caused by the strong positive phase of the NAO-index starting in the beginning of the 1980s. During

the summer months (June to September) the NAO-index is weak with high variation and with no long phases of positive or negative values (cf Appendix C.1). As expected, there is no significant change in the occurrence of one of the regimes during the summer season of the year (cf. Appendix E).

Agreement of the weather regimes between ERA40 forcing and RCM data

The agreement between the weather regimes detected in ERA40 and in each of the RCMs based on the 50km and the 25km spatial resolution simulations in percentages is shown in Figure 4.6. The agreement A_r in percentage is calculated by

$$A_r = \frac{N_r^{RCM} * 100 \%}{N_r^{ERA}} \quad , \quad (4.1)$$

where N is the number of days with the regime r in the ERA40 data, ERA , and the individual regional climate model, RCM . The upper graphs are for the summer period, the lower for the winter months. It can be clearly observed a higher agreement in winter for almost all RCMs than in summer. Highest agreement is with the CLM applied at the ETHZ and the GKSS Research Center, and the RCA3 applied at SMHI. Lowest agreement occur in the results from the models from CNRM and UCLM.

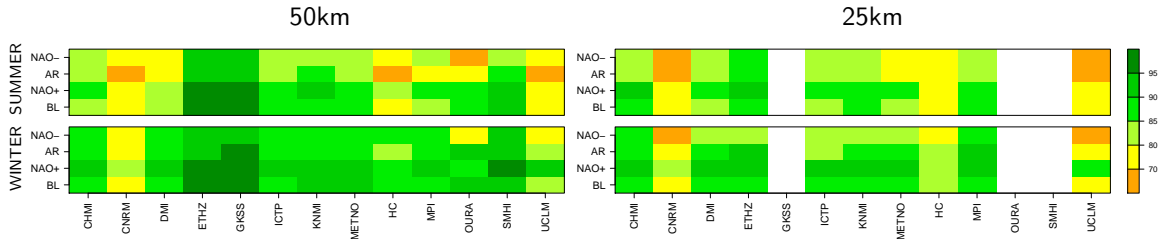


Figure 4.6: Agreement in detected weather regimes in the driving model ERA40 and the individual RCMs in percentages at a spatial resolution of 50km (left panels) and 25km (right panels) for summer (JJAS) (upper panels) and winter (DJFM) (lower panels) in 1961-2000

Compared to the agreement for the individual RCMs shown in Figure 4.6 in summer at only 47% of the possible days all models agree in the regime; in winter the agreement is higher with 63% (cf. Table 4.1).

Table 4.1: Total number of days per regime indicated in ERA40 (black) and number of days, where all RCMs and ERA40 show the same regime (green) for the time period 1961-2000

regime	ERA40	SUMMER		ERA40	WINTER	
		identical 50 km	identical 25 km		identical 50 km	identical 25 km
BL	444	204	203	499	327	320
NAO+	424	216	214	478	331	336
AR	367	135	161	282	168	196
NAO-	351	183	169	317	158	147

4.3 Weather regime classification for the North Sea (after Jenkinson and Collison (1977) and Loewe (2005))

The objective procedure to classify the atmospheric circulation near the surface for the North Sea applied at the Federal Maritime and Hydrographic Agency (Bundesamt für Seeschifffahrt und Hydrographie - BSH) goes back to investigations of Jenkinson and Collison (1977). This simple and efficient method is based on the areal pressure distribution at the mean sea level (MSLP) and the derivation of two representative indices for wind and vorticity. The definition of the circulation type, but also the identification of storm events are finally based on empirical relations between the two indices.

Until 2004 the BSH used daily distribution of mean sea level pressure of UK Met Office (UKMO) provided by the British Atmospheric Data Centre (badc.nerc.ac.uk/data/mslp) with a spatial resolution of 10° by 5° (longitude by latitude) at 16 grid points covering the North Sea and the surrounding (cf. Loewe (2005) and Loewe (2009)). As the MSLP data set ends in 2005 the BSH changed to NCAR/NCEP reanalysis data to derive the weather classification for the North Sea (Loewe (2013)).

Due to the fact that in this study the investigated regional climate models are forced by ERA40 reanalysis data the described method has been tested at the original UKMO MSLP data set and applied to the reanalysis data of ERA40, and also to the output of the RCMs. This allows the investigation of the models ability to reproduce the weather regimes and storm events within the time period 1961-2000. As the detailed description of the method can be found in Loewe (2005) and the Appendix D; in this chapter, just the criteria of the weather regime classification and the storm events are summarised.

Description of the method

As already mentioned above the classification basically uses empirical relations between the wind-index V^* and the vorticity-index ζ^* as listed in Table 4.2 (cf. Appendix D for calculation of these indices).

Table 4.2: Relations between wind-index V^* and the vorticity-index ζ^* to derive the weather classes.

condition	flow	type
$ \zeta^* < V^*$	directional	e.g. NW, wind direction
$ \zeta^* > 2V^*$	rotational	C (if $\zeta^* > 0$), cyclonic A (if $\zeta^* < 0$), anticyclonic
$V^* \leq \zeta^* \leq 2V^*$	hybrid	e.g. CW
$V^* \leq 6hPa \leq \zeta^* $	diffuse	UNC, unclassified

In this way 27 different weather types can be distinguished: beside the predefined 8 prevailed wind directions and the two possibilities on cyclonic or anticyclonic turbulences, 2x8 hybrid weather types can be defined. Additionally there is an unclassifiable type (UNC), which mainly occurs in combination with weak pressure gradients.

This method of weather type classification has been applied for different regions (Demuzere et al. (2009), Akkermans et al. (2012)), where the number and distance of the grid points used differs from 9 to 32 grid points and 2.5° by 5° (Akkermans et al. (2012)), 5° by 5° (Trigo and DaCamara (2000)) up to 10° by 5° (Linderson (2001), Buishand and Brandsma (1997)) respectively. Demuzere et al. (2009) tested different versions in grid point numbers and distance. By the number of unclassified stages they ended up with 16 grid points in an at least 5° by 5° grid. This assumption is dependent on the size and location of the region of interest.

As already mentioned, in Jenkinson and Collison (1977) and also at BSH, the grid was set up consisting of 16 grid points with a 10° resolution in zonal and a 5° resolution in meridional direction. As stated before in this study ERA40 mean sea level pressure data is used for the North Sea instead of the originally daily distribution of mean sea level pressure of UK Met Office applied at BSH. Sensitivity tests have been carried out to find the best configuration using ERA40 data compared to the results for weather type classification derived from UK MetOffice data. As some months in the reference data set are lost in the BADC database, the results of the sensitivity study for the time period 1961-1998, where no data is missing, are compared based on the MSLP from UKMO and from ERA40. Three configurations have been tested, where the number of grid points was fixed to 16, but the distance of these points was changed. Beside the originally used 10° by 5° grid, two other grids with a distance of 5° by 5° and 10° by 10° (cf. Figure 4.7) have been tested.

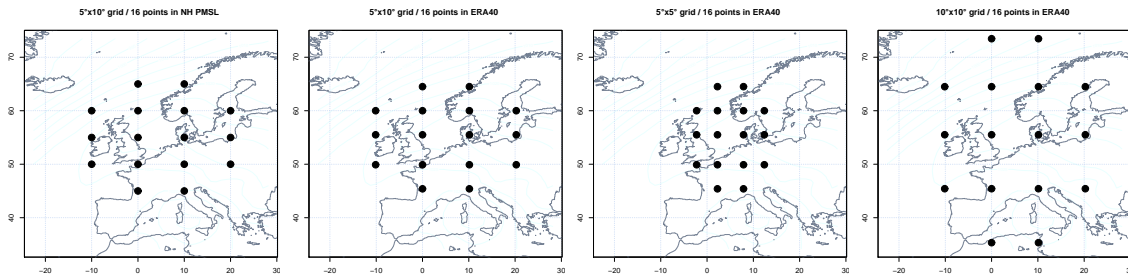


Figure 4.7: Visualization of the grid point locations used in the different sensitivity tests. *From the left to the right:* Location of the 16 points in the original data set of Northern Hemisphere PMSL from UKMO used at BSH in a grid space of 10° by 5° , in ERA40 at about the same locations, and with a distance of 5° by 5° and of 10° by 10° .

The resulting weather regimes for each day have been compared to the classification from BSH, which is used as the reference, using the available data from 1961-1998. Figure 4.8 shows the frequency of occurrence of each of the 27 classes within the given time period. While Demuzere et al. (2009) tried to find the best combination of grid point alignment to minimize the occurrence of the unclassified days, the overall aim of the sensitivity test in this study was to identify the grid point alignment where the results of the classification are closest to the classification derived at BSH. As expected the classification using ERA40 in the 10° by 5° grid has the highest similarity (cf. Figure 4.8).

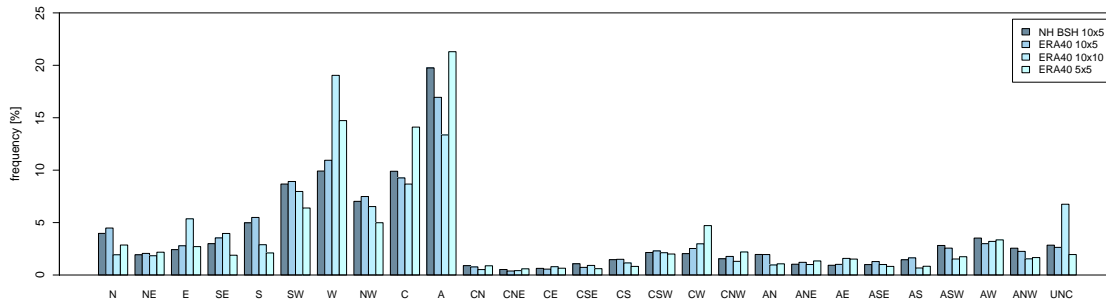


Figure 4.8: Relative occurrence frequency (%) of the 27 weather regimes based on UK Metoffice and ERA40 daily mean sea level pressure fields at the different 16 grid points (cf. Figure 4.7) within the time period 1961 to 1998.

With respect to a robust investigation of wind speed depending on their directional component all hybrid types have been grouped to one of the pure directional or the centred types. The hybrid types are separated from the pure centred or directional type by two straight lines with a slope of ± 1 and ± 2 respectively (cf. Loewe (2009)). Therefore the allocation of the hybrid types to the main classes has been defined via a straight line with a slope of $\sqrt{2}$. In this way the 27 weather types have been reduced to 11 classes (8 directional, 2 dominated by the vorticity and one class for unclassifiable cases) (cf. Figure 4.9.). Their distribution in the summer and the winter half year for the time period 1961 to 1998 is shown in Figure 4.10.

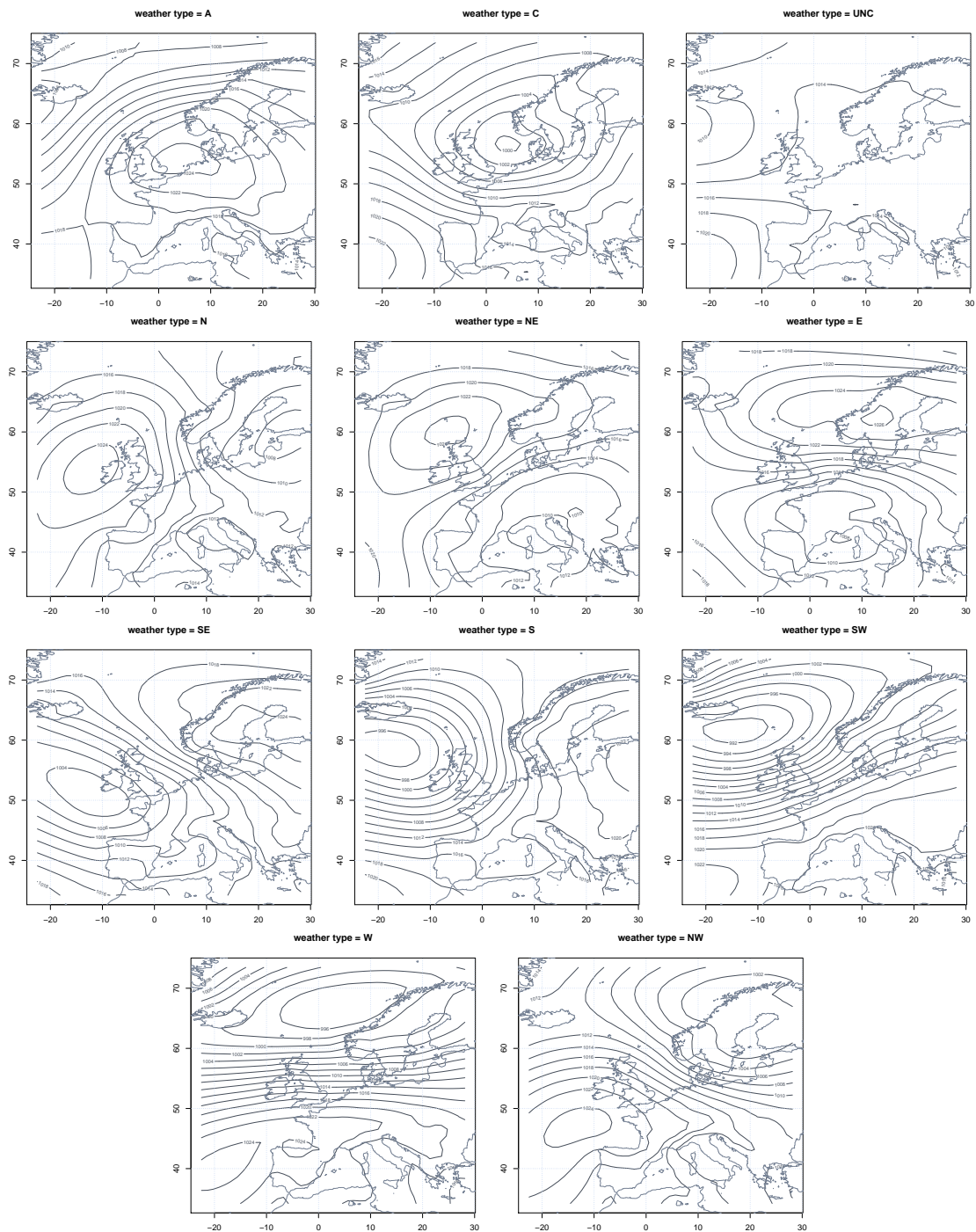


Figure 4.9: Composites for the 11 weather types (8 directional, 2 dominated by the vorticity and 1 unclassifiable cases) derived from ERA40 daily MSLP fields, averaged over the time period 1961-1998.

Figure 4.11 (left and middle plot) shows the same distribution as Figure 4.10 but only based on the 10° by 5° grid ERA40 data and for the whole period of the analysis 1961-2000. The very right plot in Figure 4.11 indicates the differences between the summer and winter distribution of the regimes. In winter western and southwestern wind directions

are more dominant compared to the occurrence in the summer months while wind from northern directions is reduced. The number of unclassified cases is smaller for the winter months than for the summer months.

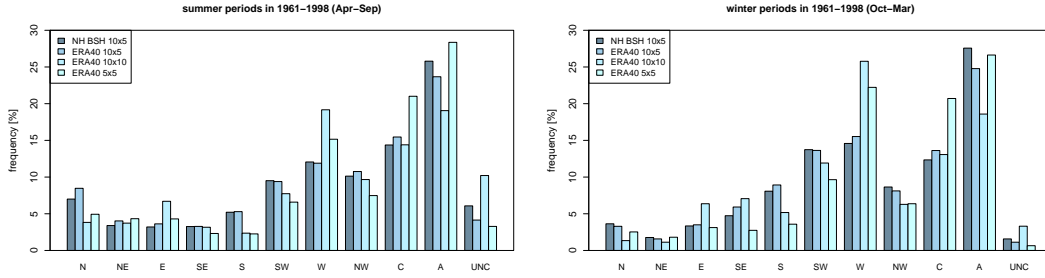


Figure 4.10: Relative occurrence frequency (%) of the 11 weather regimes based on UK Metoffice and ERA40 daily mean sea level pressure fields using the different configurations of the 16 grid points (cf. Figure 4.7) for the time period 1961 to 1998.

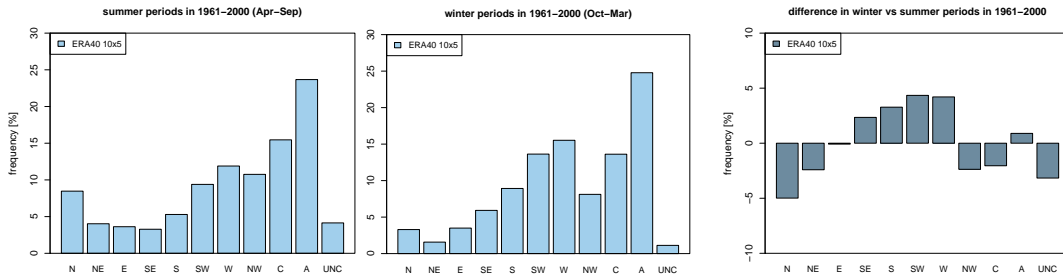


Figure 4.11: Relative occurrence frequency (%) of the 11 weather regimes based on ERA40 daily mean sea level pressure fields with the 16 grid points on the 10° by 5° grid (cf. Figure 4.7) for the time period 1961 to 2000 for summer (left) and winter (middle) and the difference of both (right).

Beside the weather types also storm events can be identified and quantified. The storm index G^* is calculated from the wind- and vorticity-indices

$$G^{*2} = \sqrt{V^{*2} + \zeta^{*2}/4} \quad (4.2)$$

The original thresholds to distinguish between the different storm intensities were defined by Jenkinson and Collison (1977) and applied to UKMO MSLP. Days with a storm index > 30 are categorized as gale, > 40 as severe gale, and > 50 as very severe gale. Due to a comparison to the NCEP/NCAR reanalysis Loewe (2013) identified an inhomogeneity in the UKMO MSLP fields. Before 2002 the daily MSLP data is based on one instantaneous value of time each day. Thereafter the data was calculated as a mean of 4 time steps a day.

Table 4.3: Reanalysis data set dependent thresholds for storm-index G^* to define storm categories

	G^* (hPa) <			severity	type
	UKMO	NCEP I	ERA40		
30	28.3	29.0		gale	G
40	36.6	37.9		severe gale	SG
50	44.6	45.2		very severe gale	VSG

With respect to the storm index the smoothing of the fields due to this averaging leads to an underestimation of the detected storms using the common thresholds described above. As the NCEP/NCAR reanalysis daily MSLP fields are calculated in the same way via fitting a Pareto-II-distribution on the storm index, Loewe (2013) derived new thresholds valid for NCEP/NCAR daily MSLP data. The common thresholds from Jenkinson and Collison (1977) used for UKMO MSLP and the new calculated thresholds adapted for NCEP/NCAR MSLP are listed in Table D.2 in the first and second column. In this study daily mean MSLP fields from ERA40 reanalysis data but also from regional climate models are used and require a recalculation of valid thresholds as well. Therefore, the same kind of distribution has been fitted to the gale index derived from ERA40 reanalysis data. The recalculated thresholds valid for the reanalysis data set from ECMWF are listed in Table D.2 in the third column and are very close to the values for NCEP/NCAR, as expected.

Agreement with station data

The mean observed wind conditions at the locations described in Section 2.1 have been analysed depending on the prevailing weather regime. Wind roses for the winter period in 1971-2000 at 4 locations for the 11 regimes are shown in Figure 4.12. Similar to Figure 4.4 the locations are 225 - IJmuiden and 1402 - List located near the coastline, and the stations 260 - DeBilt and 1529 - Soltau located inland.

It can be clearly seen that the defined regimes reflect the local wind characteristics (cf. Figure 4.9). During the regimes A - Anticyclonic and C - Cyclonic wind comes from all directions and the wind roses from the directional types (N, NE, E, SE, S, SW, W, NW) show the prevailed wind direction clearly. During the regimes with southern wind directions the wind is slightly shifted to the right. It can be observed that wind from northern directions and from the West is deflecting to the right over land after hitting the coast which is caused by the sudden increased roughness at the surface and the Coriolis force (cf. Figure 4.12, wind roses for N, NW, W). The results for the summer period look very similar and can be found in the Appendix E.5.

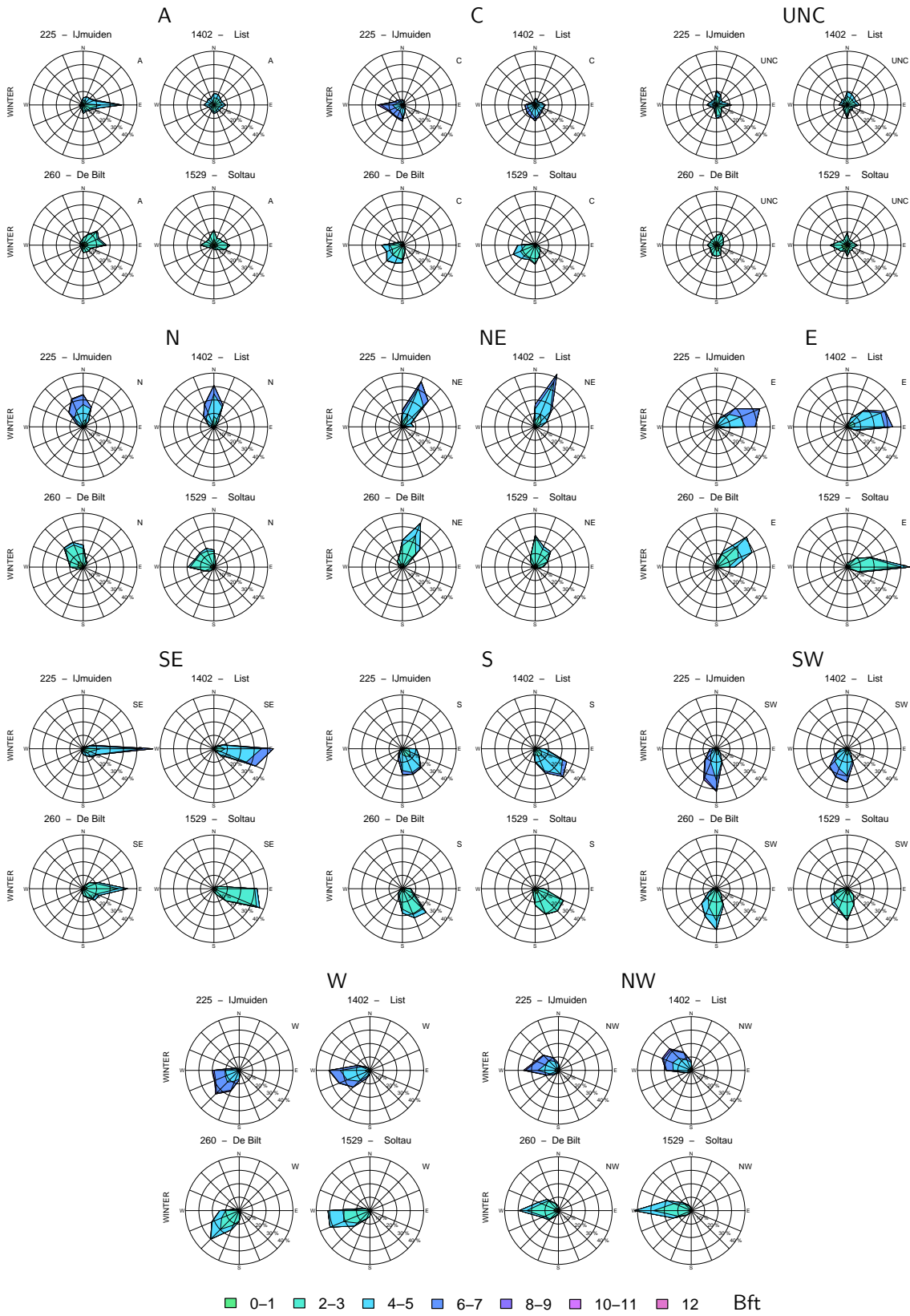


Figure 4.12: Mean wind characteristics at four stations (as Figure 4.4) for the 11 weather regimes for the winter half year (Oct-Mar) in 1971 to 2000.

Occurrence of the weather pattern over time and trends

Figure 4.13 shows the annual occurrence of the eleven weather regimes from October to March in the period of 1961 to 2000. The trend (blue line) is tested for significance applying the Mann-Kendall-trend-test described in the section before (see also Figure 4.5).

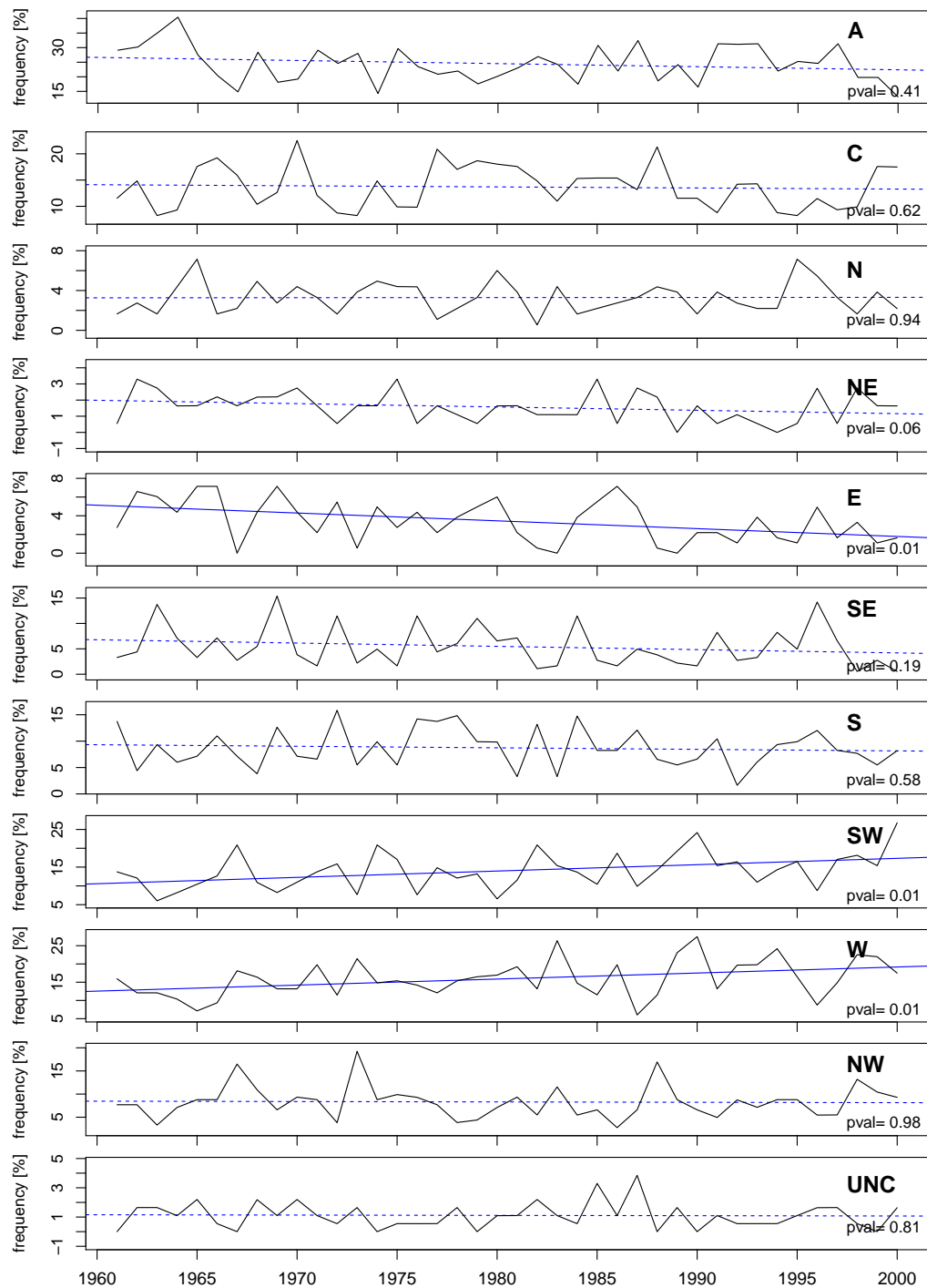


Figure 4.13: Annual occurrence of each regime from October to March in the time period of 1961- 2000 (black) and linear trend (blue dashed line and in case of significance blue solid line).

While in summer no significant change in the occurrence of one of the regimes can be detected (cf. Appendix E) in the six months from late autumn to early spring, the number of days with a main circulation pattern with western wind directions over the North Sea area increased while the number of days with eastern and southeastern directions decreased. These trends are dominated by the strong positive phase of the NAO index especially in the months January to March starting in the beginning of the 1980s (cf. Appendix C.1), as already stated before in the same section.

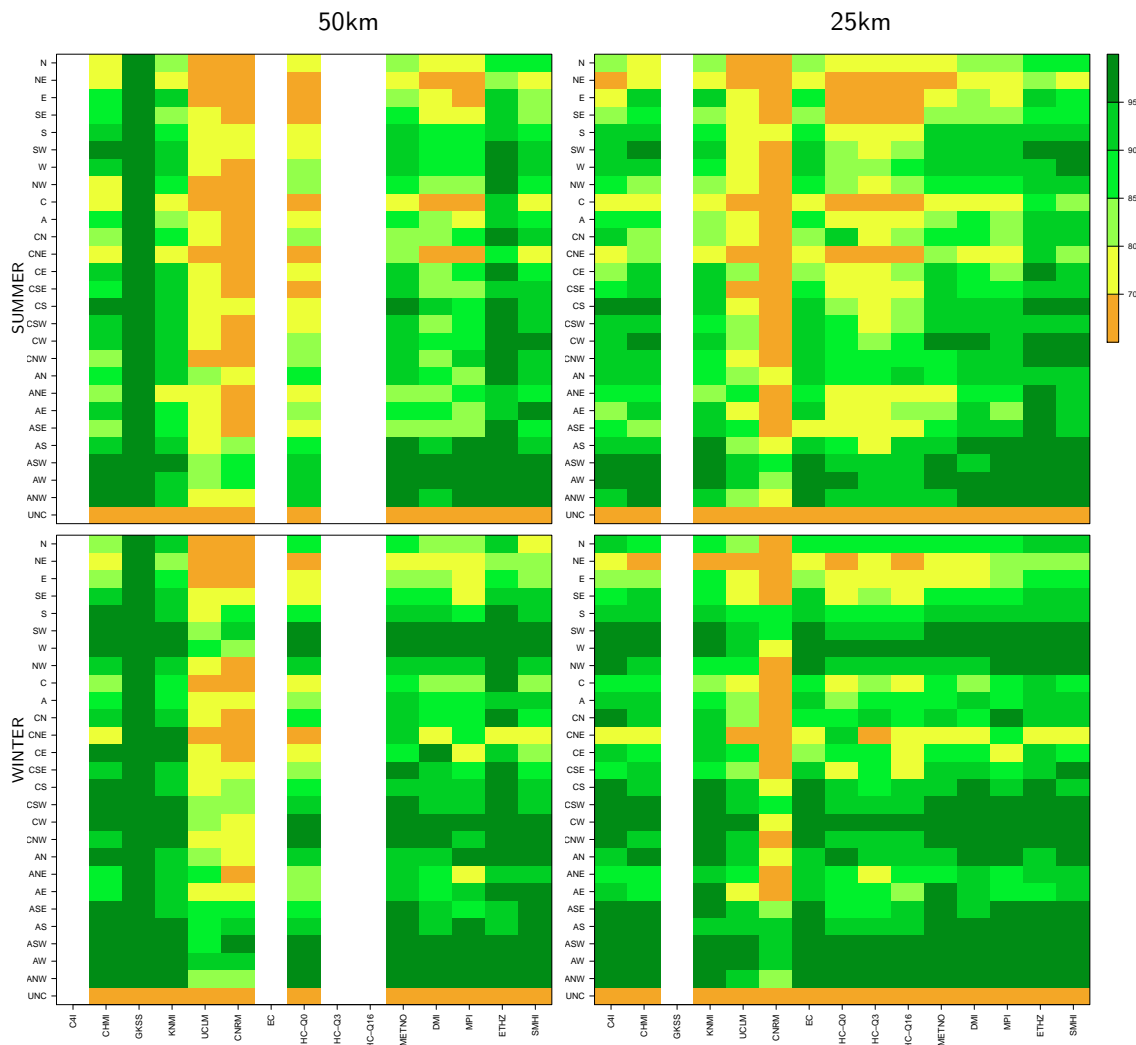


Figure 4.14: Agreement in detected weather regimes in the driving model ERA40 and the individual RCMs in percentages at a spatial resolution of 50km (left panels) and 25km (right panels) for summer half year (Apr-Sep) (upper panels) and winter half year (Oct-Mar) (lower panels) for the period of 1961 - 2000.

Agreement of the weather regimes between ERA40 forcing and RCM data

In the next step the classification method described before and in Appendix D has been applied to the mean sea level pressure fields from all regional climate model simulations

described in Chapter 2.3. Figure 4.14 summarizes the agreement of the weather pattern derived from original ERA40 mean sea level pressure field and the weather types calculated from ERA40 driven regional climate model simulations. The agreement has been derived by applying the Equation 4.1 where in this case the number of the regimes is 27.

In the 50 km simulations the regional climate model CLM used at GKSS and ETHZ performs best with agreement of often higher than 95 %, while in the simulations with the higher spatial resolution of 25 km several models show a high agreement e.g. the HIRLAM regional climate model applied at C4I, METNO and DMI, the RCA3 developed at SMHI, the CLM applied at ETHZ or the RCM REMO from the MPI. Very low agreement in the derived weather regimes compared to those ones derived from the forcing ERA40 with values down to <70 % can be observed in both resolutions with the ALADIN model applied at CNRM and especially in the coarser resolution with PROMES from UCLM. In general the models perform better in winter than in summer.

Table 4.4: Total number of days per regime (27 classes) indicated in ERA40 (black) and number of days, where all RCMs and ERA40 show the same regime (coloured) in the period of 1971-2000. Red indicates values, where the number of cases is too small for statistics; Green, where the number of cases is sufficient.

regime	ERA40	SUMMER		ERA40	WINTER	
		identical 50 km	identical 25 km		identical 50 km	identical 25 km
N	369	103	91	131	35	30
NE	169	41	29	57	5	8
E	141	43	33	124	38	33
SE	151	38	25	221	116	99
S	232	94	79	386	233	227
SW	375	173	153	635	470	491
W	495	218	187	744	533	537
NW	475	147	120	344	161	152
C	542	92	74	453	146	120
A	1919	307	275	885	421	432
CN	43	15	8	38	19	13
CNE	26	3	4	10	4	3
CE	39	19	12	21	8	7
CSE	37	15	13	43	23	17
CS	76	32	25	86	50	53
CSW	122	58	50	145	107	111
CW	129	61	46	142	94	99
CNW	103	45	40	82	53	50
AN	175	76	78	61	33	36
ANE	102	33	34	31	17	16
AE	50	17	14	51	24	28
ASE	48	16	17	83	52	48
AS	55	31	26	121	91	96
ASW	105	57	67	185	154	161
AW	144	99	99	209	178	180
ANW	136	78	74	122	90	94
UNC	232	0	0	58	0	0

Beside the total number of days per regime and season indicated in ERA40 (in black) for the time period of 1971-2000 Table 4.4 shows the number of days per regime, where all RCMs and ERA40 show the same regime (coloured). Red indicates values, where the number of cases is too small for statistics. An agreement is given if the RCMs show the same or, in case of the directional types, a neighbouring regime. In summer we observe slightly better results with the models at 50km spatial resolution than at 25km, where in winter the differences in the two resolutions are very small. High agreement up to 88 % can be seen for the regimes with wind from western directions, while the agreement is low with values of 8 % for northeastern wind directions and the cyclonic type. As the hybrid eastern types occur in low frequency, the number of days where all models show the same regime is, from the statistical point of view, too small for further investigations (cf. Table 4.4, red coloured values).

Table 4.5: Total number of days per regime (11 classes) indicated in ERA40 (black) and number of days, where all RCMs and ERA40 show the same regime (coloured) in the period of 1971-2000. Red indicates values, where the number of cases is too small for statistics; Green, where the number of cases is sufficient.

regime	ERA40	SUMMER		ERA40	WINTER	
		identical 50 km	identical 25 km		identical 50 km	identical 25 km
N	479	51	46	179	24	26
NE	226	16	12	76	3	6
E	180	27	13	158	29	20
SE	180	18	12	277	82	72
S	306	70	64	486	182	191
SW	501	116	118	815	405	432
W	626	164	134	929	424	430
NW	587	84	71	447	113	112
C	842	62	46	739	101	83
A	1331	226	201	1304	355	374
UNC	232	0	0	58	0	0

Table 4.5 shows the same as Table 4.4 but here the 27 regimes are reduced to the number of 11 as described in this Section before. Compared to the analysis of the 27 regimes using the 11 regimes the number of days where forcing and RCMs show the same regime is lower with values up to 53 %. The advantage of using only 11 regimes is that the total number of cases is increased and further statistical evaluation of wind speed is more robust. To increase the number of days with the same regime the two models with the lowest performance in reproducing the daily regimes, the PROMES from UCLM and the model ALADIN developed at the CNRM, have been left out. This results in values of up to 70 % of the possible days where the ERA40 and all of the RCMs show the same regime. Again, the same as in the large spread of the 27 regimes, in the 11 regimes also

the NE regime shows the lowest agreement among the models, whereas the agreement in the western directions is highest.

Table 4.6: Same as Table 4.5, but without RCMs from UCLM and CNRM: total number of days per regime (11 classes) indicated in ERA40 (black) and number of days, where all RCMs and ERA40 show the same regime (coloured). Red indicates values, where the number of cases is too small for statistics, in Green where the number of cases is sufficient.

regime	ERA40	SUMMER		ERA40	WINTER	
		identical 50 km	identical 25 km		identical 50 km	identical 25 km
N	479	104	111	179	60	71
NE	226	33	31	76	9	13
E	180	49	26	158	50	42
SE	180	39	26	277	109	102
S	306	111	98	486	243	241
SW	501	212	193	815	568	544
W	626	292	269	929	647	636
NW	587	206	184	447	233	244
C	842	145	134	739	248	259
A	1331	446	411	1304	595	597
UNC	232	2	1	58	0	0

4.4 Summary

One main aim of this thesis is to evaluate surface wind speed at the German and Dutch coast simulated by the regional climate model ensemble introduced in Section 2. Due to the fact that from the models only daily wind speed but no prevailing daily direction of the wind was available, weather regimes could be a helpful tool to close this gap. In previous studies it has been shown that there is a correlation between large scale pattern and near surface variables (e.g. Buishand and Brandsma (1997), Demuzere et al. (2009), Akkermans et al. (2012)).

Two objective weather regime classifications have been analysed to describe the synoptic situation per day. The first classification for Europe was provided via the ENSEMBLES framework by Sanchez-Gomez et al. (2009). The other method is a classification by Lamb (Jenkinson and Collison (1977)), which is approved at the Federal Maritime and Hydrographic Agency (Bundesamt für Seeschifffahrt und Hydrographie - BSH) and centered over the North Sea. This method has been adapted to the ERA40 forcing and RCM output. The classification by Sanchez-Gomez et al. (2009) distinguishes between 4 regimes, the Blocking regime, the Zonal regime, the Greenland Anticyclone regime and the Atlantic Ridge regime. The relative occurrence of the regimes in winter and summer is about the same. Composites of the mean sea level pressure in ERA40 during the regime show in the

Blocking and the Greenland Anticyclone regime a diverse picture for summer and winter. With focus on the area of interest, the German and Dutch coast, compositing wind roses for observations show no clear prevailing wind direction for the regimes. While e.g. during the AR regime in winter wind comes from the West, in summer the main wind direction is North to Northeast for the same regime.

The objective classification by Jenkinson and Collison (1977) uses values for mean sea level pressure at 16 locations centred over the North Sea. Beside the predefined 8 prevailed wind directions and the two possibilities on cyclonic or anticyclonic turbulences, 2x8 hybrid weather types can be defined. In this way 27 different regimes can be distinguished including a class of unclassifiable cases. The 27 regimes could be reduced to a number of 11 by allotting the hybrid types to the directional or the centred types. As the classification is carried out for the North Sea the different regimes clearly reflect the mean wind characteristics at the stations.

Comparing the wind roses for the individual observations leads to the assumption that the regime classification for Europe carried out by Sanchez-Gomez et al. (2009) does not fit the requirements to carry out the regime dependent evaluation of the models with a focus to the German and Dutch coast. Instead, the evaluation of the surface wind speed will be based on the second classification carried out for the North Sea using the method from Jenkinson and Collison (1977).

5 Representation of Surface Wind Speed in the Multi Model Ensemble

5.1 Introduction

The knowledge of the wind climate at specific locations is of vital importance for risk assessment, engineering, and wind power assessment. In the last decade the energy market is in transition from conventional energy (e.g., coal and oil) towards renewable energy resources (e.g., solar power and wind energy). One goal of the European Commission is to cover 15.7% of EU's electricity needs by wind energy resources by 2020 (Moccia et al. (2011)). As an installation of an effective network of wind power plant, the estimation of future changes in wind climate is important. Several studies investigate the wind conditions under a changing climate (Pryor et al. (2005a), Pryor et al. (2005b), Najac et al. (2009), Leckebusch and Ulbrich (2004), Pryor and Schoof (2010), Pryor et al. (2012)). The focus shifts to offshore regions, as the potential for wind energy over sea is larger than over land. Only few observations over sea are available, for example, light ships, oil platforms or existing wind farms and, obviously, there is a lack of a dense and consistent measuring network. With the help of meso-scale and micro-scale models this lack can be overcome. They provide homogenous wind field data, available for further studies and analysis.

Another important application of an appropriate wind climate assessment is storms and storm related losses. Storm climatology can be derived from observed mean sea level pressure, from reanalysis data and climate models. Donat et al. (2011) investigated long term regional trends of wind storm occurrence in Europe using the 20th Century Reanalysis (20CR). They found decadal-scale variability in the occurrence of wind storms since 1871, including a period of enhanced storm activity during the early 20th century. Matulla et al. (2008) used annual and seasonal statistics of local air pressure characteristics as proxies for storminess across Northern Europe. They state significant changes throughout the past 130 years in European storm climate with significant variations on a quasi-decadal timescale. Krueger and Storch (2011) derived daily geostrophic wind speeds from geographical triangle of surface air pressure from regional climate model data and investigated the correlation to area-maximum surface wind speeds. Storm activities in relation to weather pattern and North Atlantic Oscillation (NAO) have been analysed by Suselj et al. (2010), Donat et al. (2010) and Matulla et al. (2008) and identified a strong decadal correlation. Cavicchia et al. (2014) investigated storm trends in the Mediterranean; Krueger et al. (2013) in the North-Atlantic.

In the studies mentioned before results from global and regional climate models have been analysed, hence they are getting more and more important to enlarge the investigation

for wind climate from local to regional scale. In several studies regarding wind climate assessment based on model results, the question has been raised: Can regional models add value to the global models? Main findings in a study by Feser et al. (2011) are, that regional models can add value, but only for certain variables and locations with characteristics valid for a larger region. With help of GCM- and RCM-simulations, Leckebusch and Ulbrich (2004) investigated the relationship between cyclones and extreme windstorm events over Europe. It is clearly visible that with the higher temporal and spatial resolution, especially in near coastal areas the RCM lead to an improvement in simulating the extreme wind speeds compared to the GCM. For open ocean areas Winterfeldt and Weisse (2009) show no adding value for RCM modelling compared to reanalysis forcing in the wind speed frequency distributions, whereas in near coastal regions RCM results - especially for higher wind speed percentiles - are closer to the observations than the forcing data. Focussing on near-surface wind speed over Europe Rockel and Woth (2007) identified that most of the RCMs have not been able to simulate wind velocities higher than 8 Bft.

The overall aim of the present study is to investigate the ability of regional climate models to simulate surface wind speed. Hereby, coastal regions are in special focus, as this is for models a challenging small transition zone between water and land. From one grid point defined as land to the neighbouring water grid point elevation is changing as the surface roughness length. This coastline causes to a strong disturbance in the general flow. The RCM ensemble investigated in this section was provided by the partners from the EU-funded ENSEMBLES-project. The model ensemble was introduced in Section 2.3. In the following section the mean wind conditions at the German and Dutch coast are investigated based on observation data at 10 m above ground provided by the DWD and the KNMI (cf. Section 2.1). Mean annual values and the variability for daily wind speed, the seasonal cycle, but also main wind directions in each month of the year are analysed. Statistics on maximum wind speed, percentiles and the number of storm days will give an overview on the storm activity in this area. The influence of the NAO is demonstrated by examples. Afterwards, the calculation of the different skill for quality and added value assessment are listed, followed by the results from the comparison of RCMs and ERA40 to the observations. As the model output for wind speed is only available without any information on the daily prevailing wind direction, the results of the comparison are investigated according to the daily leading weather regime derived from the MSLP field described in Section 4.3.

5.2 The mean wind conditions in the Southern North Sea and the German Bight

The coastal areas are strongly influenced by the maritime effect, the slow reacting ocean. In opposite to a moderate climate or continental climate the marine climate is mainly indicated by a smaller annual but also daily cycle for temperature and much higher values for mean wind speeds. During high pressure weather regimes, especially in the warm season, the areas are controlled by local land-sea-circulation or land-sea-breezes. Anyway there are big differences between the eastern and the western coasts of the continents.

The Belgisch coast, the Netherlands coast and the German west coast are windward coasts, the main wind direction is West to Southwest. These winds blow onshore or parallel to the coast. To analyse the mean wind condition in more detail the station data described in Section 2.1 is used. The data with no breaks are available for the two time periods: 1971 - 1983 and 1971 - 2000.

Mean annual wind speed and variability

The mean annual wind speeds \bar{x}_0 at almost all stations vary between 3.8 and 4.8 m/s with a standard deviation σ_0 between 1.7 and 2.3 m/s (cf. Table 5.1). The values at List and IJmuiden are higher having a mean annual wind speed of 7.0 and 7.3 m/s and a standard deviation of 2.8 and 3.1 m/s, respectively. These stations are located directly at the coastline in a very flat terrain. Other exceptions are Soltau and DeBilt. Soltau is located inland, far from the coast. The value for mean annual wind speed is 2.9 m/s with a standard deviation of 1.3 m/s. The distance to the coast, when considering the main wind direction, from the station DeBilt is smaller than for the station Volkel. However the values for mean annual wind speed and standard deviation are higher in Volkel. The time series for the surface wind speed at DeBilt is quite homogeneous, but the instrument is located on the top of a building of the KNMI. So the environment of the measurement is quite rough. Due to this fact the mean annual wind speed is 3.2 m/s with a standard deviation of 1.5 m/s (cf. for Volkel it is 3.9 and 1.9 m/s, respectively).

Beside the described values Table 5.1 summarizes also the values for mean annual wind speed and standard deviation over the months from October to March (*Oct-Mar*) and from April to September (*Apr-Sep*). The division of the year into two seasons, which is relevant for the wind analysis, is based on the analysis of the mean annual cycle and the storm activity in each month (see below). For the period between October and March the values are slightly higher for both wind speed and standard deviation.

Table 5.1: Statistical values for the German and Dutch observations for daily mean wind speed [m/s] covering the time period 1971 to 2000

ID	Name	\bar{x}_0	σ_0	$\bar{x}_0^{Oct-Mar}$	$\sigma_0^{Oct-Mar}$	$\bar{x}_0^{Apr-Sep}$	$\sigma_0^{Apr-Sep}$
1529	Soltau	2.9	1.3	3.1	1.4	2.7	1.2
1402	List	7.0	2.8	7.2	2.8	6.9	2.7
1474	Bremen	4.3	1.9	4.7	2.1	4.0	1.7
1438	Schleswig	3.8	1.6	4.1	1.8	3.5	1.4
1444	Hohn	4.1	2.1	4.5	2.2	3.7	1.7
1497	Oldenburg	3.7	1.7	4.1	1.8	3.4	1.5
9007	Wittmundhafen	4.7	2.3	5.2	2.5	4.3	1.9
1730	Jagel	4.8	2.3	5.2	2.6	4.4	2.0
260	De Bilt	3.2	1.5	3.6	1.6	2.9	1.2
270	Leeuwarden	4.9	2.2	5.4	2.4	4.5	1.9
375	Volkel	3.9	1.9	4.2	2.0	3.5	1.7
350	Gilze-Rijen	4.0	1.8	4.3	1.9	3.7	1.5
225	IJmuiden	7.3	3.1	7.5	3.2	7.0	3.0

Mean annual cycle

Looking at the mean annual cycle calculated from the mean wind speed in each month over the measurement period, it is possible to identify a small variability for most of the observations (cf. Figure 5.1). For the shorter time period from 1971 to 1983, the mean annual cycles vary in the range of 1.1 m/s up to 2.0 m/s. For the longer period from 1971 to 2000 the range is slightly smaller with values between 1.0 and 1.8 m/s.

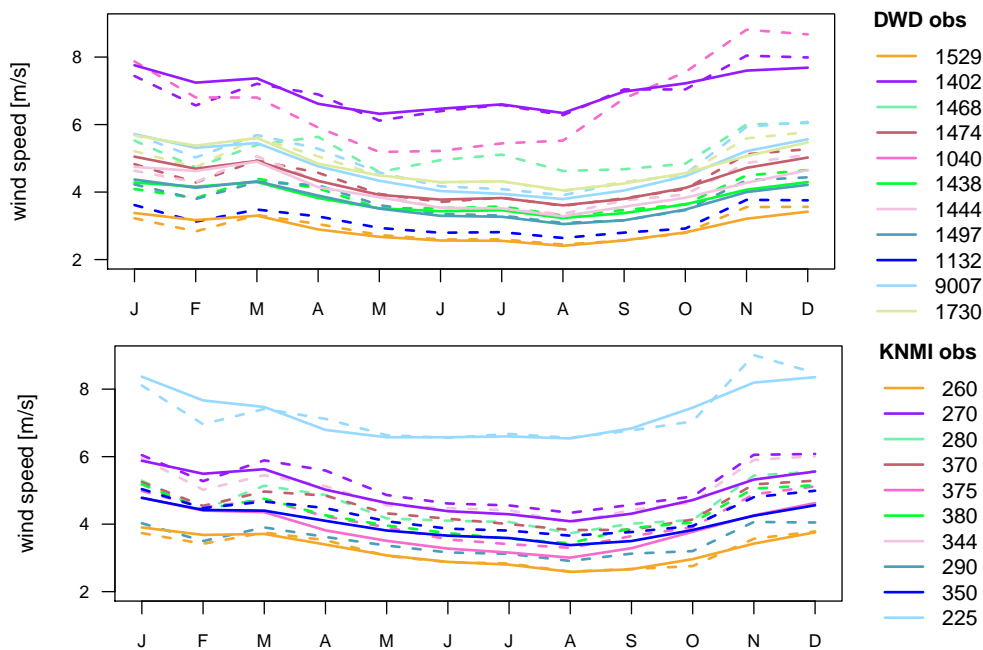


Figure 5.1: Mean annual cycle of wind speed observations from the DWD (upper panel) and from the KNMI measuring network (lower panel) for the time periods 1971 to 1983 (dashed line) and 1971 to 2000 (solid line).

One exception for the short time slice is the station at the island Helgoland (ID 1040), which is located far from the coast and where high wind speeds are observed. Another exception is the station IJmuiden (ID 225) located directly at the coast line. The range of the mean annual cycle of the mean wind speed for Helgoland for the shorter period is 3.2 m/s, for IJmuiden it is 2.5 m/s. For the 30-year time period, the value for the variability of the annual cycle for the station IJmuiden is 1.8 m/s, which is in the range of the others.

Wind direction

For the German and Dutch coast the winds blow most of the year mainly from western directions. Figure 5.2 shows an example for the distribution of the mean wind directions in each month of the year for the time period 1971-2000 for the measurements in IJmuiden (ID225), List (ID1402), DeBilt (ID260) and Soltau (ID1529). Winds from the South play an important role during winter, where an occurrence of up to 40 % of wind events can be recognized. In summer their part is only 20 %. The influence of northern winds in winter is very low, but higher during the spring and summer months. Exceptions are the inner land stations Hohn (ID1444), Jagel (ID1730) and Schleswig (ID1438), which are located close together. Here northern and southern winds occur very seldom.

In summer the main wind direction for all stations is from the West. Winds from eastern directions can be detected over the whole year between 15 % and 30 % in each month. In springtime northern wind directions are dominant at some stations. In autumn and winter wind blows mainly from southern and western directions. The analysis of the wind directions per months supports the separation of the year into the two parts, summer and winter half year, as the wind climate within each of the seasons is very similar.

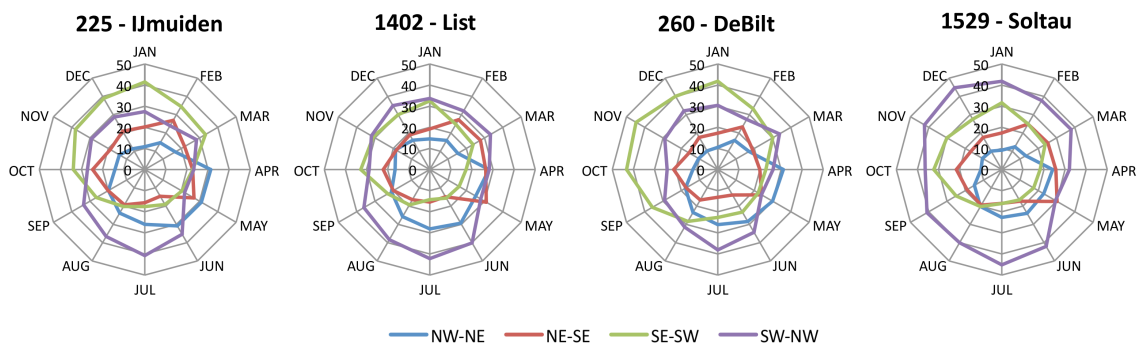


Figure 5.2: Frequency of the wind directions in each month of the year as mean over the time period 1971 to 2000 for IJmuiden, List, DeBilt and Soltau (from the left to the right).

Spatial correlations

Figure 5.3 shows the correlations between the observations within the same measuring network covering the time from 1971 to 2000 in dependence of the distances. The two different colors indicate the seasons. As expected the correlations to measurements in small distances are higher and smaller with increasing distance. Up to a distance of about 100km the correlation is larger than 0.8. This investigation reflects the size of synoptic phenomena at the mesoscales. The correlations are higher for the months October to March where wind speed is more often dominated by large scale processes than for the months April to September where the mean wind speed is smaller and local effects are more important.

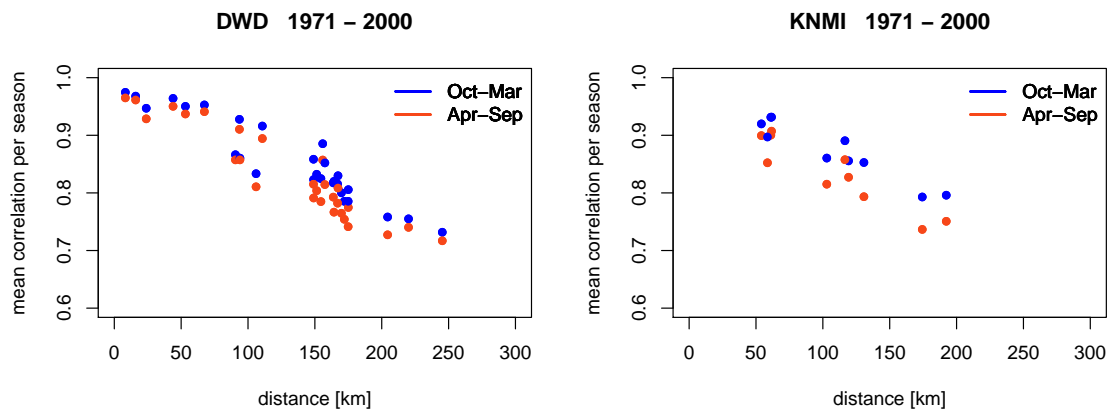


Figure 5.3: Correlation between all observations in dependence of the distances to each other in the two measuring networks from the DWD (left) and the KNMI (right) in 1971-2000.

Maximum wind speed and percentiles

The values for daily maximum wind speed and 50th, 90th, 95th and 99th percentiles of daily mean and daily maximum wind speed for all observations are summarized in Table 5.2 and 5.3. For the period of 1971 to 2000 the values for the 95th percentile of the daily mean wind speed of most of the observations are between 5.5 and 9.3 m/s. As expected, due to the exposition directly at the coast line for List and IJmuiden 5 % of the daily mean wind speeds are higher than 12.1 m/s and 13.1 m/s, respectively. In general the values for the 95th and the 99th percentile of the hourly observations are 0.5 m/s to 1 m/s and 1 m/s to 2 m/s higher as for the derived daily mean wind speeds (not shown).

Table 5.2: Statistical values for the German and Dutch observations for daily maximum wind speed covering the period of 1971 to 2000.

ID	Name	\bar{x}_{0max}	σ_{0max}	$\bar{x}_{0max}^{Oct-Mar}$	$\sigma_{0max}^{Oct-Mar}$	$\bar{x}_{0max}^{Apr-Sep}$	$\sigma_{0max}^{Apr-Sep}$
1529	Soltau	9.4	3.9	9.9	4.1	9.0	3.5
1402	List	15.0	5.3	15.4	5.6	14.6	5.2
1474	Bremen	11.1	4.5	11.6	4.7	10.6	4.0
1438	Schleswig	11.1	4.4	11.6	4.7	10.6	3.9
1444	Hohn	10.9	4.4	11.4	4.6	10.4	3.8
1497	Oldenburg	10.7	4.5	11.2	4.7	10.2	4.0
9007	Wittmundhafen	12.0	4.9	12.6	5.1	11.4	4.3
1730	Jagel	11.9	5.0	12.4	5.4	11.4	4.4
260	De Bilt	10.1	4.0	10.7	4.2	9.5	3.4
270	Leeuwarden	11.9	4.5	12.4	4.8	11.3	4.0
375	Volkel	10.2	4.0	10.6	4.2	9.6	3.6
350	Gilze-Rijen	10.8	4.2	11.2	4.4	10.3	3.6
225	IJmuiden	13.7	5.1	14.1	5.3	13.0	4.8

Table 5.3: The 50th, 90th, 95th and 99th percentile values for the German and Dutch observations for daily mean and daily maximum wind speed covering the period of 1971 to 2000.

ID	Name	\bar{x}_0^{p50}	\bar{x}_0^{p90}	\bar{x}_0^{p95}	\bar{x}_0^{p99}	\bar{x}_{0max}^{p50}	\bar{x}_{0max}^{p90}	\bar{x}_{0max}^{p95}	\bar{x}_{0max}^{p99}
1529	Soltau	2.7	4.7	5.5	6.9	8.8	14.7	16.7	21.5
1402	List	6.7	10.8	12.1	14.6	14.3	22.5	25.5	31.4
1474	Bremen	4.0	6.9	8.0	10.1	10.4	17.0	19.5	25.0
1438	Schleswig	3.5	6.0	6.9	8.7	10.4	17.0	19.4	24.9
1444	Hohn	3.7	6.9	8.1	10.4	10.3	16.7	19.0	23.8
1497	Oldenburg	3.5	6.1	7.0	8.9	9.9	16.6	19.1	24.4
9007	Wittmundhafen	4.3	8.0	9.2	11.8	11.3	18.5	21.1	26.7
1730	Jagel	4.4	8.0	9.3	12.1	11.3	18.5	21.6	26.8
260	De Bilt	3.0	5.3	6.1	7.7	9.3	15.4	17.5	21.6
270	Leeuwarden	4.6	7.9	9.2	11.5	11.3	18.0	20.6	25.0
375	Volkel	3.5	6.6	7.6	9.6	9.3	15.4	17.5	22.1
350	Gilze-Rijen	3.7	6.5	7.4	9.3	10.3	16.0	18.5	23.1
225	IJmuiden	6.8	11.7	13.1	15.6	12.7	20.9	23.0	28.3

Number of storm days and storm activity

The German Weather Service, DWD, defines a storm day as a day where the daily maximum 10-minutes-mean wind speed is equal or bigger than 8 Beaufort. The daily maximum wind speed at the DWD stations has been provided by the DWD. For the KNMI stations the daily maximum has been derived from the observed maximum hourly wind speed values.

According to this definition, the mean number of storm days per month at the KNMI stations and DWD stations in the time period 1971 to 2000 is calculated and shown in Figure 5.4. Due to its location, the highest number of storm days is counted in List (ID1402). At this station in the summer months June to August between 5.5 and 6 storm days occur per month in average within the 30 years; in the winter months the values are higher and

12 to 13 storm days can be observed in months November to January (cf. Figure 5.4 upper panel). The other German stations count a lower number of storm days during the year. Schleswig (ID1438) and Hohn (ID1444) as two neighboring stations show similar results. In the summer months (June, July and August) 0.7 to 1.2 storm days are counted; in the late autumn and winter months November, December and January 3.5 to 5.8 storm days occur in average. Although Jagel (ID1730) is located in between these two stations the number of counted storm days is higher than these from Schleswig and Hohn. Here 1.6 to 1.8 storm days are counted in each of the summer months, in autumn and winter months 5.7 to 7 storm days occur. A reason for the different numbers of storm days per month in Jagel compared to Schleswig and Hohn can be differences in the stations near-by surrounding.

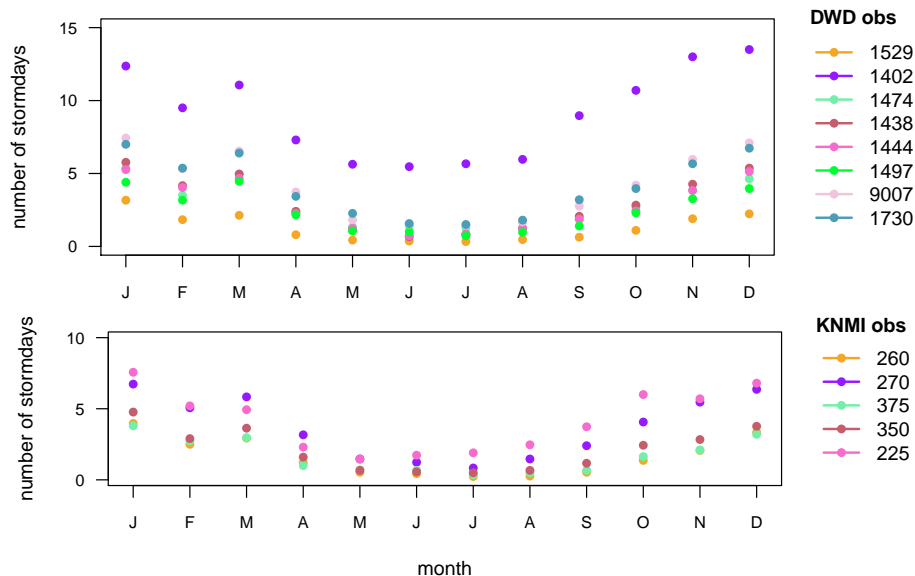


Figure 5.4: Number of stormdays in observations from DWD (upper panel) and observations from KNMI measuring network (lower panel) for the time period 1971 to 2000.

The results are similar for the observations at the Dutch coast. As expected highest values occur at the coastal station IJmuiden (ID225). During the summer months 1.7 to 2.5 storm days per month are counted, during November to January 5.7 to 7.6 storm days occur. Anyway, the number of counted storm days in each month is smaller in IJmuiden compared to List. In late autumn and winter months the values at IJmuiden (5.7 to 7.6) are quite similar to those from Volkel (5.5 to 6.7). The observations at DeBilt (ID260), with the values 0.2 to 0.4, show the smallest number of storm days during the summer months. Based on this analysis, the highest storm activity can be defined as the period October to March. Figure 5.5 shows the number of stormdays in each of the core storm

months in individual years from 1971 to 2000 for the KNMI observation at Leeuwarden (ID 270). The right panel is a lowpass filtered result from the original values from the left panel using a filter of 3-years length. Loewe (2009) defines that the real core storm season in each year lasts over three months. While until the beginning of 1980s the core period was present mainly in November/December, its occurrence moved towards January and February by 1983 until at least the year 2000, the end of this analysis. The years between 1983 and 1995 are the time period with an especially high storm activity compared to the periods before and afterwards. Similar like the NAO index the storm activity underlies large quasi-cycled variances at an intra decadal base. The month wise 3-years filtered storm activity (cf. Figure 5.5, right panel) filters out cycles smaller than 3 years and enhances variability in the range of 6 to 9 year periods.

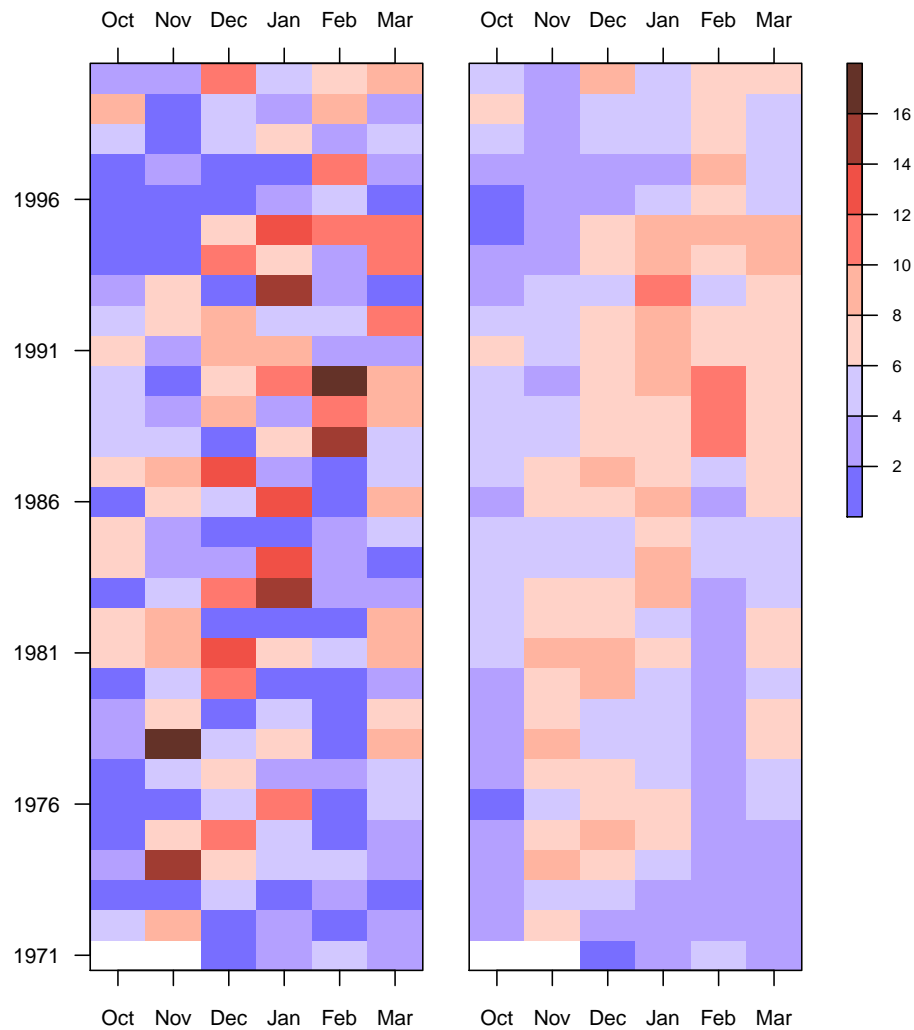


Figure 5.5: Total storm frequency at Leeuwarden (ID 270) for the period of 1971 to 2000 from October to March calculated in number of days. Months Oct, Nov and Dec refer to the previous year. Total number of storm days per month (left panel) and number of storm days after applying a 3-year time-progressive low-pass filter (right panel).

The influence of the North Atlantic Oscillation (NAO) on the wind climate in the North Sea

As already stated in Section 4 the prevailing western circulation at midlatitudes is important for the European climate. It directs oceanic air masses inland over the continent. A strong western circulation leads to mild and wet weather and strong winds over most of Europe, especially in winter. In contrast, a weak or blocked western circulation causes generally cold and dry winters and hot and dry summers. In this context the NAO index determines the intensity of the western circulation in Europe. NAO is the large-scale fluctuation in atmospheric pressure in the Atlantic ocean between the high-pressure system near the Azores and the low pressure system near Iceland. The fluctuation in this pattern leads to variations in the European climate, as already stated in Section 4.

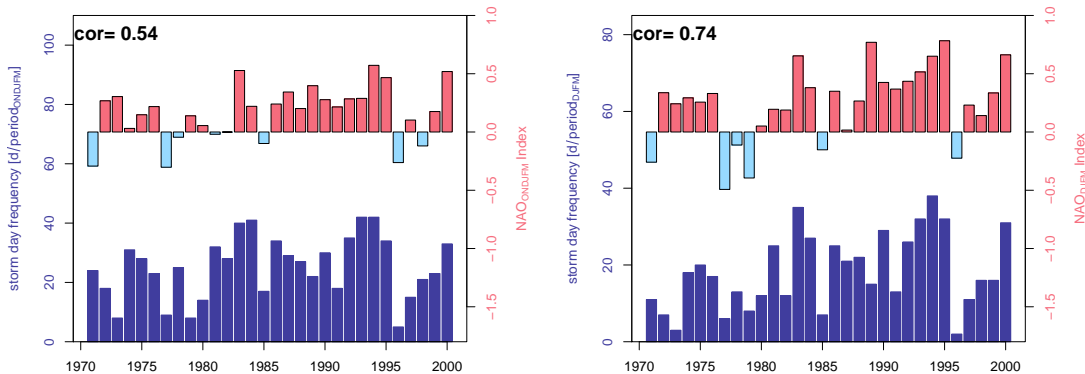


Figure 5.6: Total number of storm days per seasons at Bremen (ID1474) (dark blue bars) and the mean NAO index (red and light blue bars for positive and negative values) from 1971 to 2000 for October to March (ONDJFM) (left panel) and for December to March (DJFM) (right panel). Correlation coefficient is calculated based on Pearson (1895).

The storm activity over the North Sea can be quantified by the state of the NAO. Figure 5.6 shows the total number of storm days per season at Bremen (ID 1474) and the mean NAO index from 1971 to 2000 for October to March (ONDJFM) and for December to March (DJFM). The calculated temporal correlation after Pearson (1895) is 0.54 for the 6-months-season and 0.74 for the shorter season. The higher correlation coefficient results from the much stronger NAO-signal in this period of the year (cf. Appendix C). Based on a weather classification derived from vorticity and a wind index for the North Sea, Loewe (2009) distinguished between storm, heavy storm and very heavy storm. He got similar results as in this study, but found a slightly higher correlation of about 0.7 for all storms. In the present study the highest values for temporal correlation can be found for Oldenburg (ID1497) and Leuwarden (ID270) with a value of 0.7.

As expected, the storm activity and the NAO-index show a clear tendency to a high storm frequency in combination with a positive phase of the NAO-index. This agreement can especially be seen in long positive phases of the NAO 1989 - 1995. On the other hand winter periods with low storm activity (and very low temperatures) go together with a negative NAO - phase (1979, 1985-1987, 1996). The linear correlation is not stationary. The calculation of a rolling correlation shows low correlation coefficients before 1973, a very high correlation 1974 - 1989 (up to 0.89), and a weaker correlation after 1989 with values of about 0.7 (Loewe (2009)).

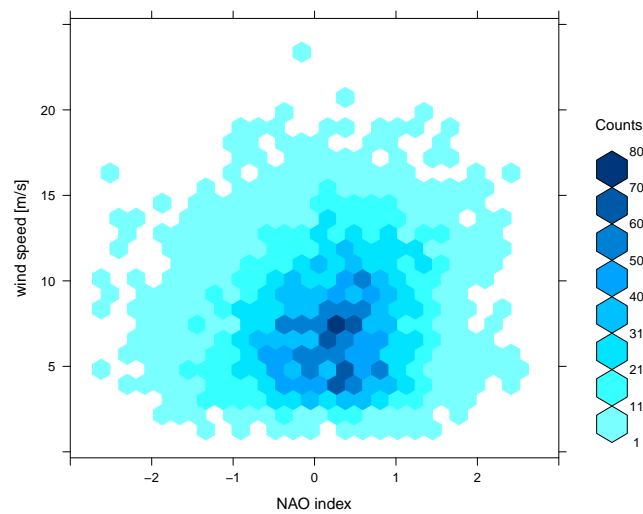


Figure 5.7: Hexagonal density of daily maximum wind speed depending on the daily NAO index in winter season (Oct-Mar) at IJmuiden (ID225) in the time period of 1971 to 2000.

The Figures 5.7 and 5.8 combine the daily maximum wind speed and the daily NAO-index in a so called *hexbin*-plot for the observation in IJmuiden (ID225). The plotting area is divided into hexagonal bins. In each covering hexagon the number of events is counted. While Figure 5.7 shows the results for the whole storm period October to March, Figure 5.8 shows the same but separated for the late autumn season (Oct to Dec) and late winter/early spring season (Jan to Mar). The Figures support the hypothesis stated before that high wind speeds occur more often on days with a positive NAO-phase.

Additionally the Figures 5.8 identify a stronger tendency to the positive NAO-phase in the second half of the winter season (Jan-Mar), while in the first half of this season (Oct-Dec) high wind speeds occur about the same in positive and negative NAO-phases. From January to March the NAO-index has a clear positive phase since about 1982, while the NAO-index for October to December does not show any longer or shorter positive (or negative) phase (cf. Appendix C).

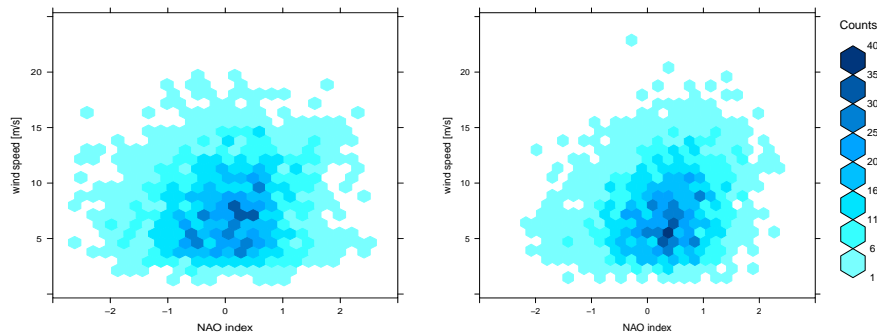


Figure 5.8: Hexagonal density of daily maximum wind speed depending on the daily NAO index at IJmuiden (ID225) in the time period of 1971 to 2000 for October to December (left panel) and January to March (right panel).

5.3 Methods and Measures

For comparison between the RCM output and observation data, Winterfeldt and Weisse (2009) interpolated simulated wind speeds from the RCM from the four grid points surrounding the measurements location in a bilinear way. This procedure is common for grid points over the ocean. In the present study wind speed at the coastline and over land is analysed. In this case it is not useful to interpolate different grid point values since the grid points contain a different fraction of land and sea and, according to this, may have very different values for roughness length which strongly influence the calculated surface wind speed.

In a first step, the grid cell from the regional climate model, as well as the ERA40 reanalysis, covering individual station was used for bias, standard deviation, root mean squared error (RMSE), and quantiles assessment. To estimate a possible added value of using a RCM for wind speed simulation than the reanalysis directly two skill scores are introduced. Additionally these skill scores have been modified in a way to analyse the added value of the RCM in relation to the ERA40 compared to observation data and the other way round (see Equations 5.5 and 5.7).

In the second step, not only the covering grid cells, but also 8 surrounding grid cells in the RCMs are taken into account for analysis and comparison. Due to the coarse resolution of the ERA40 reanalysis data only the covering grid cells are used. The comparison of the surrounding grid cells from the RCMs always refer to the data from the covering grid cell in the reanalysis data.

The **ensemble mean** has been calculated on the daily basis referring to the available RCMs for both spatial resolutions. This results in 10 integrated RCMs for the two spatial resolutions, 25km and 50km. The results from the ensemble mean are indicated by the abbreviation ENSmean. The **bias** and the **standard deviation** are standard statistical methods and are not described in further detail.

The other measures used are:

Pearson Correlation Coefficient

The correlation coefficient after Pearson Pearson (1895) is given by

$$Corr = \frac{1}{n-1} \sum_{i=1}^n (x_i - y_i)^2 \quad , \quad (5.1)$$

where x is the simulated wind speed by a RCM and y the observation timeseries, both of the same length n .

Root Mean Squared Error

The Root Mean Squared Error is a quite common measure for model skill and expresses relation between the bias and the standard deviation of the differences between two datasets.

The RMSE is given by

$$RMSE = \sqrt{\frac{1}{n} \sum_{i=1}^n (x_i - y_i)^2} \quad , \quad (5.2)$$

where x is the simulated wind speed time series from a RCM and y the observation data, both of the same length n .

Brier - Skill Score

The Brier Skill Score (BSS) is defined, e.g. von Storch and Zwiers (1999), by

$$BSS = 1 - \frac{\sigma_F^2}{\sigma_R^2} \quad , \quad (5.3)$$

where σ_F^2 and σ_R^2 represent the error variances of the "forecast" F (the time series of regionally modelled wind speeds) and the reference "forecast" R (the time series of ERA40 wind speeds). Since the error variances are computed relative to the same predictand, in this case the respective time series of observed wind speeds within a certain time period, the BSS is equivalent to

$$BSS = 1 - \frac{RMSE_F^2}{RMSE_R^2} , \quad (5.4)$$

where the $RMSE_F^2$ and $RMSE_R^2$ are the mean squared errors of the "forecast" F and the reference "forecast" R, respectively. By definition the Brier Skill Score can vary between $-\infty$ and $+1$. For the value 1 the forecast exactly matches the observations. Negative values indicate a better performance of the reference, positive values indicate an added value of the reference forecast in comparison to the reference.

Additionally in the present study, a modified BSS is introduced with a range of -1 to 1. Values from -1 to 0 indicate an added value for wind speed taken directly from ERA40 compared to wind speed from RCM, values between 0 and 1 indicate an added value for wind speed from RCM compared to the one from the reanalysis. "0" means both models, the RCM and ERA40 are of about the same quality. None of the models is closer to the observation than the other.

$$BSS_{mod} = \begin{cases} 1 - \frac{RMSE_{RCM}^2}{RMSE_{ERA40}^2} & \text{for } RMSE_{RCM} \leq RMSE_{ERA40} \\ \frac{RMSE_{ERA40}^2}{RMSE_{RCM}^2} - 1 & \text{for } RMSE_{ERA40} < RMSE_{RCM} \end{cases} , \quad (5.5)$$

Perkins - Skill Score

This score adapted by Perkins et al. (2007) is a very simple measure to estimate the relative similarity between simulated and observed Probability Density Functions (PDF). In detail it allows a comparison of the coverage of two histograms (cf. Equation 5.6). In each predefined bin of the probability distribution of the simulation Z_{mod} and the observation Z_{obs} the smaller value is taken and accumulated over all bins n . As a result, a value between 0 and 1 is calculated, where 1 indicates a perfect simulation compared to the observations, a value close to 0 means that the PDFs from the simulation and the observation almost do not overlap at all.

$$S = \sum_1^n \min(Z_{mod}, Z_{obs}) \quad (5.6)$$

The Perkins Score has been modified similar to the BSS_{mod} by calculating the difference between the Skill Scores from the RCM S_{RCM} and the ERA40 S_{ERA40} to indicate a possible added value of the RCMs according to Equation 5.7.

$$PSS_{mod} = S_{RCM} - S_{ERA40} \quad (5.7)$$

The value -1 means a full agreement between the PDFs from ERA40 and the observations and no similarity between the PDFs from the RCM and that ones from the observations. The value 1 is the opposite and indicates the gained value when considering the RCM.

5.4 Near surface wind performance of the multi model ensemble

The daily mean wind speed and daily maximum wind speed provided by the regional climate models and ERA40 (cf. Section 2.3) was compared to observations applying the different skill scores described in the section before. As already stated the wind speed from the observation covering grid cell in each RCM in the two spatial resolutions is used for evaluation, but also the 8 surrounding grid cells in the models have been taken into account. From ERA40 the provided wind speed only from the covering grid cell is used and is the same in the plots independently from the two different spatial resolutions available from the RCMs.

Bias

The mean annual bias in the daily wind speed derived from the model grid boxes and the observations shows a range of -2.8 m/s to +3 m/s with the tendency to more cases of overestimation can be observed (cf. Figure 5.9). For the observation data at Soltau (ID1529), Hohn (ID1444), Schleswig (ID1438) and Oldenburg (ID1497) almost every model overestimates the surface wind speed (-0.5 to 2.5 m/s). At Hohn (cf. Table 5.1, mean: 4.1 m/s, std: 2.1 m/s) the mean annual bias with values of -0.5 to 2 m/s, is within the observed standard deviation. In comparison for the stations Jagel (ID1730) and Bremen (ID1474) (mean: 4.8 m/s and 4.3 m/s, std: 2.3 m/s and 1.9 m/s, respectively) the bias of the RCMs is smaller (between -1.2 and 1 m/s) and within the standard deviation of the station data. The wind speeds are in general overestimated by the regional climate models PROMES (UCLM) and HadCM (HC). The bias of the ERA40 data is in the range of -1.5 to 1.5 m/s. The mean annual bias of the RCM ensemble mean is quite small and for the most of the cases smaller than the bias in the ERA40 data.

The results for the two spatial resolutions are mostly very similar. The RCMs in the higher resolution often show reduced values for the mean annual bias compared to the coarser

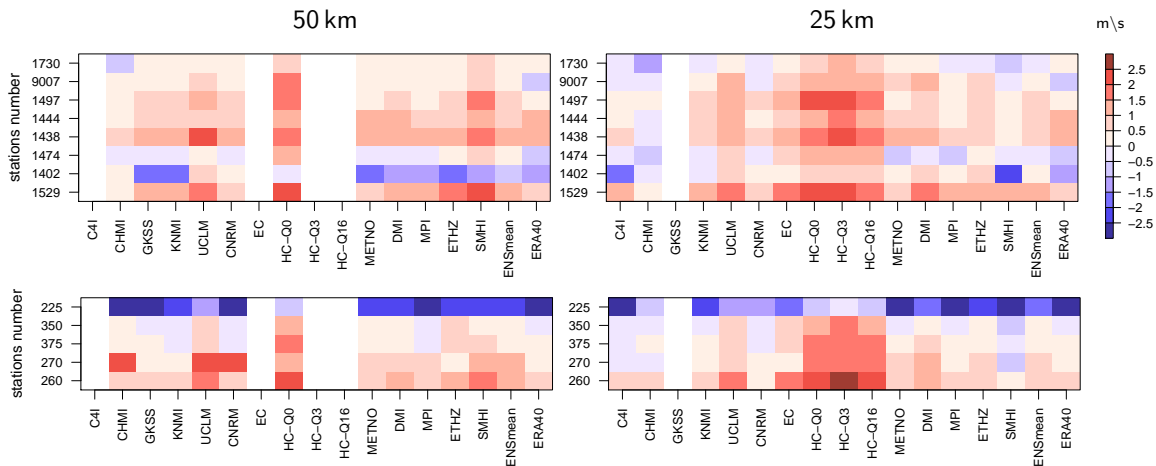


Figure 5.9: Mean annual bias of simulated wind speed by regional climate models at certain locations in the DWD network (upper row) and KNMI network (lower row) for the two different spatial resolutions 50km (left column) and 25km (right column) within the time period 1971–2000.

resolution. For example, for List (ID1402) the negative mean annual bias can be reduced with increased model resolution. While in the coarser resolution the models underestimate the observed wind speed over the whole year, in the results from the 25 km simulations the underestimation can be seen only in summer. In contrast in winter the models mainly overestimate the wind speed at this location.

In both resolutions, 50 km and 25 km, for most of the cases the mean annual bias (0.5 – 2.5 m/s) is within the standard deviation of the observations. Exceptions are from the RCM perspective the simulations with the Headley Center model (HC-Q0, HC-Q3 and HC-Q16), and from the observational perspective Soltau (ID1529), where for some RCMs, the mean annual bias is out of the range of the observed standard deviation.

All results have been tested for statistical significance, which mainly the smaller biases failed. Plotted are all results with respect to identify certain behavior of individual models at all locations or an individual observation where most of the RCMs show the same tendency.

Generally, there is a seasonal cycle in both, in the mean annual cycle the same as in the counted cases where the bias is within the range of the observed standard deviation. The bias is lowest in March with an relative error of -30 % to +50 % compared to the observed monthly wind speed. While in March and April the models slightly underestimate the observed wind speed, from Mai onwards a slight overestimation can be detected. This overestimation increases within the following months and is highest from the end of August until the beginning of November with values of up to +100 %. From November onwards the bias is getting smaller again.

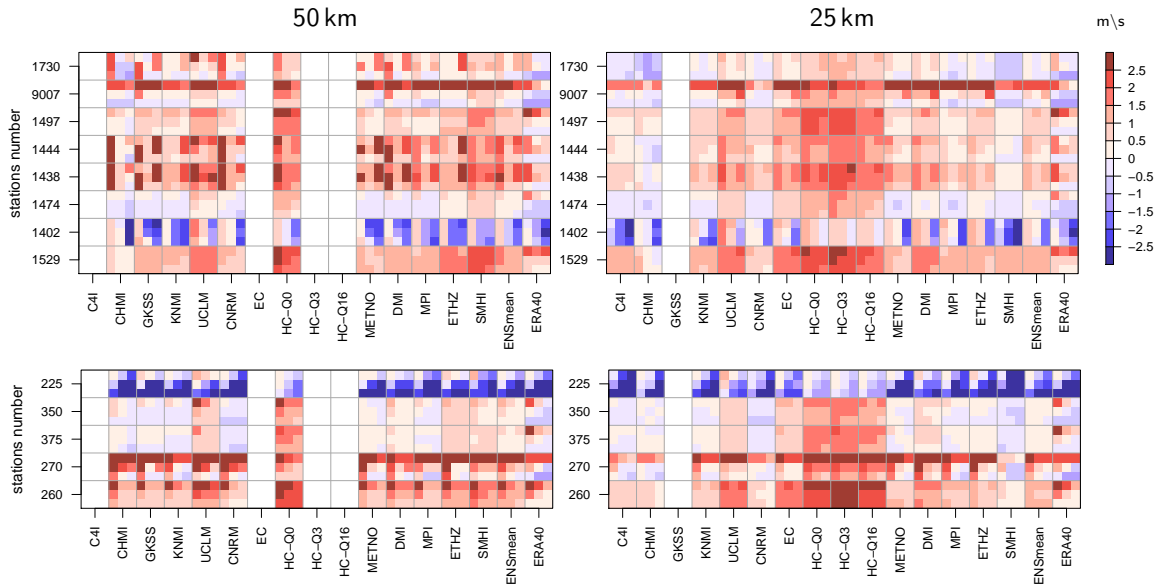


Figure 5.10: Mean annual bias of simulated wind speed by regional climate models at certain locations in the DWD network (upper row) and KNMI network (lower row) for the covering grid box and the 8 surrounding grid boxes for the two different spatial resolutions 50km (left column) and 25km (right column) within the time period 1971-2000.

The results for the bias calculation of the 8 surrounding grid boxes are shown in Figure 5.10 and support the choice of using the station covering grid cell from the models for wind speed evaluation. The simulated wind speed in the neighboring grid cells show a higher bias than this one from the covering grid cell. Additionally, for the coastal stations and near coastal stations like, for example, List (ID1402) and IJmuiden (ID225) but also Wittmundhafen (ID9007) and Leeuwarden (ID270) the bias in the neighboring grid cells clearly reflects the land-sea-distribution in each RCM (cf. Figures 5.10 and 5.27). Due to the higher spatial resolution and the smaller represented area the results for the bias among the nine grid boxes is more homogeneous in the 25 km than in the 50 km simulations. Although the model CLM applied at the HZG (former GKSS) is using the spectral nudging approach, the results for the bias are in the same range as for the other regional climate models.

Annual cycle

The calculated annual cycle of observed and simulated monthly mean wind speeds (cf. Figure 5.11) reflect the results for the bias analysed in the section before. The models are able to reproduce the observed annual cycle. Some models even show the slight increase of mean wind speed in March compare to February. Only at List (ID1402) especially the RCMs in the higher resolution overestimate the magnitude of the annual cycle.

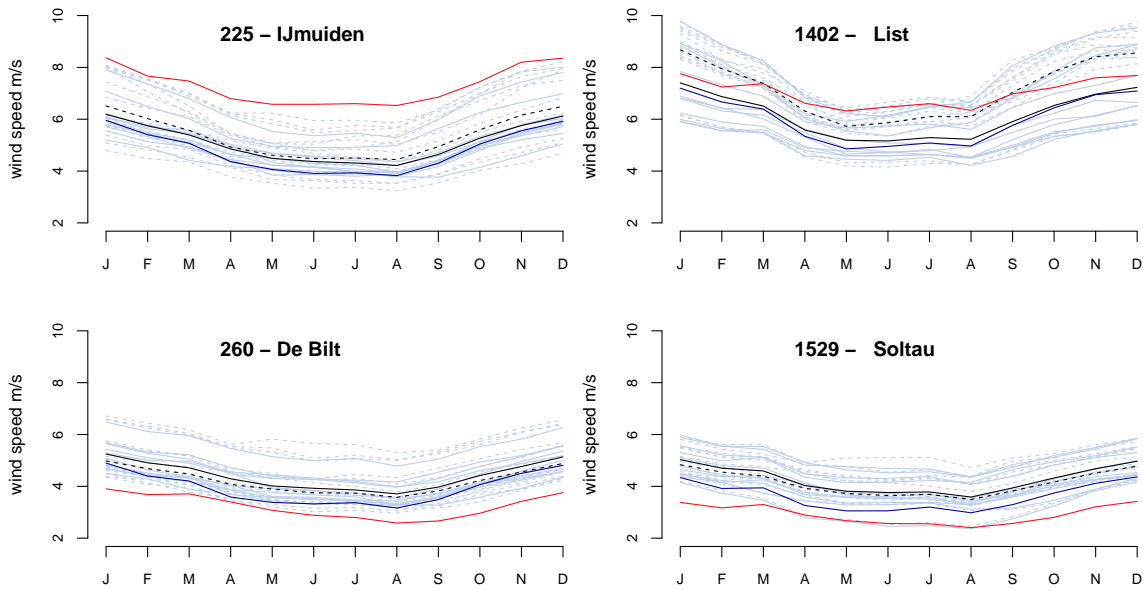


Figure 5.11: Mean annual cycle of the observed (red line) and simulated wind speeds by ERA40 (blue line), the individual regional climate models in 50km (solid grey lines) and 25km (dashed grey lines) spatial resolution and the corresponding ensemble means (black solid and dashed lines) at IJmuiden (ID225), List (ID1402), De Bilt (ID260) and Soltau (ID1529) within the time period 1971-2000.

Standard deviation

Figure 5.12 shows the values for the normalized standard deviation of the simulated wind speed at certain locations. The model data is normalized to the observed standard deviation (STD). The differences in the STD are small and in most of the cases the STD of the observations is represented by the models. At some locations like e.g. Soltau (ID1529) and DeBilt (ID260) the STDs is overestimated by about 50%, at IJmuiden (ID225) an underestimation of the variability by the models of about 50% can be observed. There is a small annual cycle in the normalised STD (not shown). In the winter months there is almost no difference between the observed and the simulated STD, in the summer months the differences are slightly bigger. This fact can be addressed to the generally small variability in surface wind speed and, compared to the winter months, the more important local effects during the summer months. In summer months the STD is underestimated by the ensemble mean by 50%.

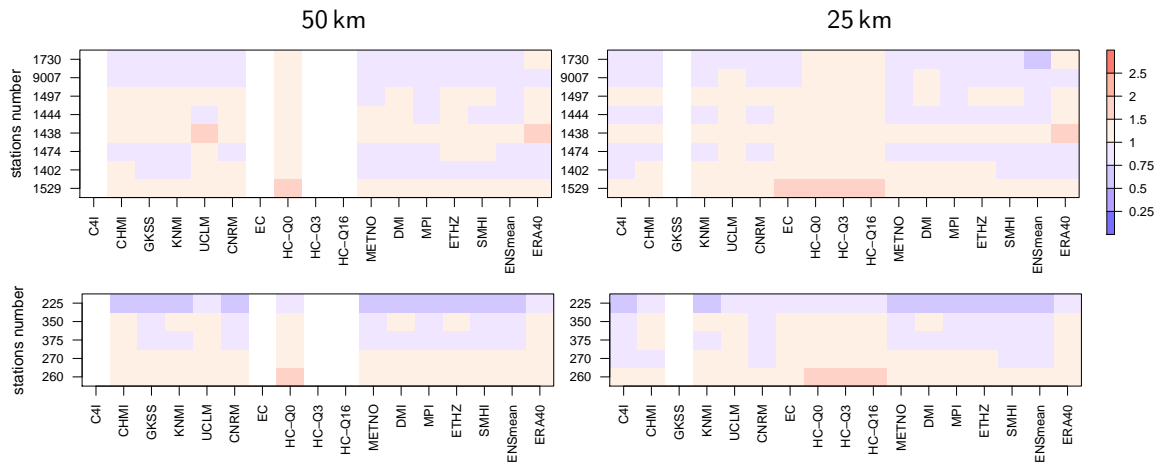


Figure 5.12: Normalized standard deviation of the simulated wind speed by the regional climate models at certain locations in the DWD network (upper row) and KNMI network (lower row) for the two different spatial resolutions 50km (left column) and 25km (right column) within the time period 1971-2000.

Temporal correlation

The calculated correlation for the time period 1971-2000 between the simulated and observed wind speeds is in general low with values between 0 and < 0.9 (cf. Figure 5.13). The model results for the months December and January are with values of 0.7 - 0.95 higher correlated with the observations than for June until August, where in most cases the correlation is smaller than 0.5.

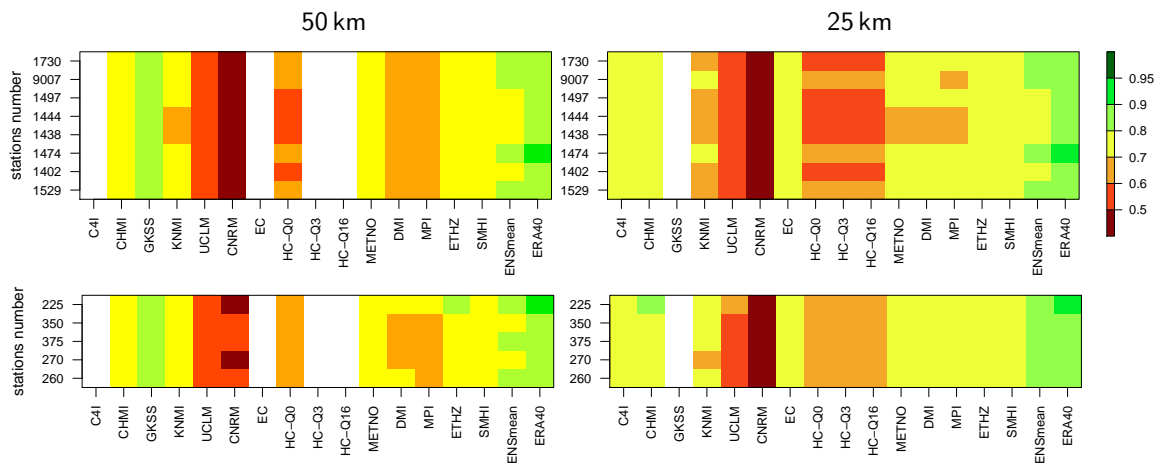


Figure 5.13: Correlation between simulated wind speed by the different regional climate models and observed wind speed at a certain location in the DWD network (upper row) and KNMI network (lower row) for the two different spatial resolutions 50km (left column) and 25km (right column) within the time period 1971-2000.

One exception is the regional climate model CLM applied by the HZG (former GKSS). As already stated, the model uses the spectral nudging approach described by von Storch

et al. (2000). Although the nudging is relatively weak and only applied to the large waves in the middle and higher atmosphere it positively effects the simulation of surface wind speed. The values for correlation are most of the time higher than 0.8 and reach 0.95. Compared to the other RCMs, for this model simulation the annual cycle in the correlation is very small (not shown).

In contrast, the values for the correlation for the regional climate models UCLM, CNRM and the HC runs are very low for the whole year. The RCM ensemble mean is higher correlated with the observations than each individual model (except the HZG (GKSS) model). Especially during the winter months the values are quite high and in the range of 0.8 to 0.9. The wind speed provided by ERA40 is highly correlated with the observations over the whole year with values between 0.75 and 0.95. It should be taken into account that data of several observations have been assimilated into the reanalysis simulation, but not very regularly, with large deviations in the assimilation frequency. However, the correlation in ERA40 is also high, e.g., for Schleswig (ID1438) and IJmuiden (ID225), although these observations have not been used for assimilation.

Root Mean Squared Error

The root mean squared error combines the results from bias and correlation (cf. Equation 5.2) and should therefore reflect the results shown before.

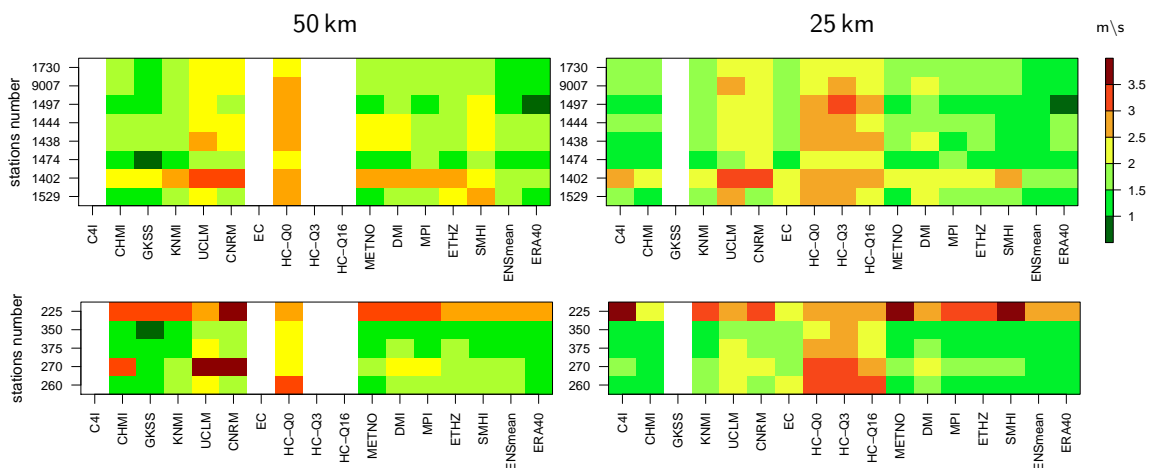


Figure 5.14: RMSE of simulated wind speed by the regional climate models at a certain location in the DWD network (upper row) and KNMI network (lower row) for the two different spatial resolutions 50km (left column) and 25km (right column) within the time period 1971-2000.

As shown in Figure 5.14 the range of values for the RMSE is between 0 m/s and > 3.5 m/s, thereby for most of the RCMs it is between 1.5 m/s and 2.5 m/s. The largest RMSE is reached by CNRM model ALADIN, where low values for the correlation have been

observed. According to the higher values for biases at List (ID1402) and IJmuiden (ID225) also the RMSE is high for all RCMs (cf. Figure 5.14). As it has been seen in the results for the correlation again the GKSS model CLM, the ensemble mean and the ERA40 have lower values for the RMSE (<2 m/s and in some cases even <1 m/s, excepting IJmuiden). In the annual cycle of the RMSE, smaller values for the summer compared to the winter months can be identified (not shown).

Brier Skill Score (modified)

Figure 5.15 shows the modified Brier Skill Score with specifications of the BSS (cf. Equations 5.4 and 5.5) within the time period 1971-2000. Analysis of BSS_{mod} as the combination of each RCM's RMSE and this one from ERA40 show no clear added value for the regional climate models. For the locations Hohn (ID1444), Schleswig (ID1438) and IJmuiden (ID225) an added value for the regional climate models applied by the C4I, CHMI, KNMI, METNO, DMI, MPI, ETHZ, SMHI but also the ensemble mean can be observed.

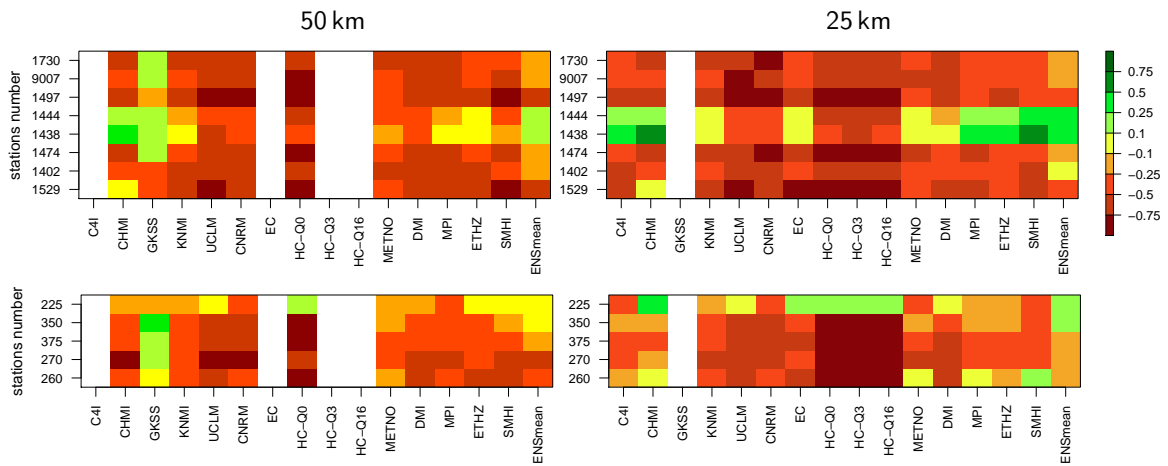


Figure 5.15: Modified Brier Skill Score at certain locations in the DWD network (upper row) and KNMI network (lower row) for the two different spatial resolutions 50km (left column) and 25km (right column) within the time period 1971-2000. (cf. Equation 5.5)

Although Hohn and Schleswig are located very close to Jagel (ID1730) (cf. Figure 2.2) the results are very different. The observed wind speed at Jagel is well represented in ERA40 as well as in the RCMs. No added value for any of the RCMs can be observed. Unlike in the case of Jagel, the observed wind data from Schleswig is not assimilated and the bias in ERA40 is higher than for the RCMs. At this station most of the RCMs show a very robust sign for an added value. Additionally, for the coastal station IJmuiden (ID225) an added value can be seen for some models, but not for List (ID1402). Whether an observation

is close to the coastline or not gives not a clear answer about the behavior according to the BSS. The fact of using spectral nudging approach or not is remarkable and is again dominant in the results. The CLM applied by GKSS including a spectral nudging is able to give an added value compared to ERA40 for most of the locations. This added value is dominated by the good model performance from late summer months until the end of spring (not shown).

Percentiles

Figure 5.16 shows the differences in percentiles calculated as the bias between the percentiles derived from the simulated and the observed wind speed at four selected locations. Positive values indicate an overestimation of wind speed percentiles by the models, negative values indicate an underestimation. Note that the very low and very high percentiles (1%, 2%, 5% and 95%, 98%, 99%) are of special interest, due to their relation to extremes, and have been therefore added to the plots. The larger the distance between the inland stations and the coastline, the larger is the overestimation of the modeled wind speed percentiles compared to the observations (cf. Soltau in Figure 5.16).

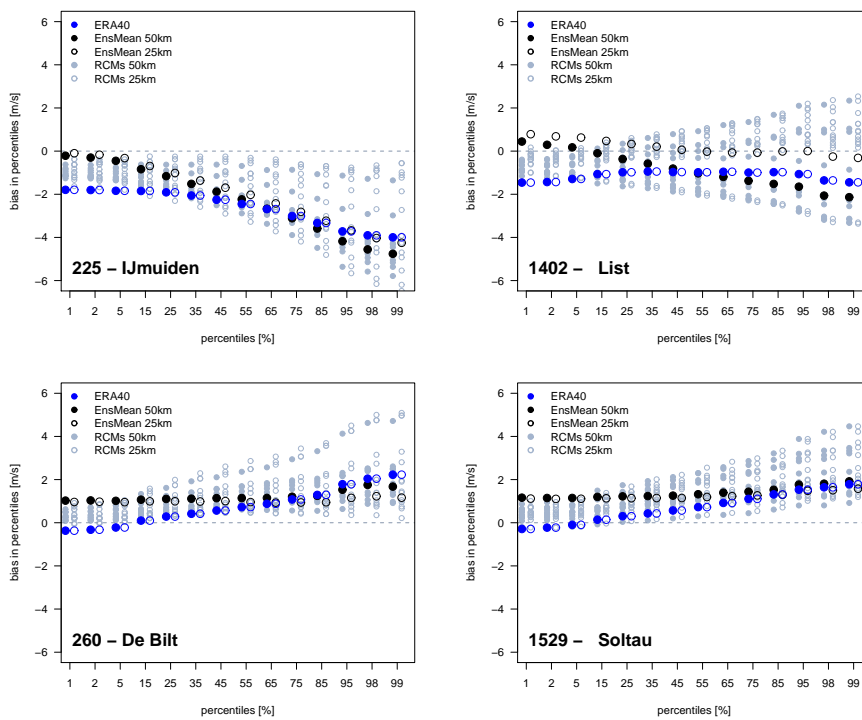


Figure 5.16: Bias in percentiles as the difference of percentiles derived from simulated wind speeds by ERA40 (blue), the individual RCMs (grey) and the RCM ensemble mean (black) for the two spatial resolutions 50km (filled circle) and 25km (open circle) at IJmuiden (ID225), List (ID1402), De Bilt (ID260) and Soltau (ID1529) within the time period 1971-2000.

At IJmuiden all models for both spatial resolutions underestimate all percentile values by 0 to 7 m/s. The observed percentiles at List (ID1402), the second station located very close to the coastline are partly underestimated by the models. While the lower percentiles are underestimated by the models in both spatial resolutions, the medium and higher percentiles are overestimated by the models in the 25km resolution and underestimated in the coarser resolution of 50km. Only the RCMs from C4I and SMHI are underestimating all percentile values at List in the 25km resolution. While ERA40 is underestimating all percentile values at this station, the RCM ensemble mean at 25 km spatial resolution almost perfectly fits the observed wind speed percentiles for List. It can be stated that at 6 out of the 13 locations the RCM ensemble mean at 25 km resolution is often closer to the observed percentiles than ERA40. Two of these stations are List and IJmuiden. Hence in the case of percentiles there is a clear added value for the higher resolved ensemble mean compared to ERA40. But also among the model resolutions, the higher resolution leads at most of the locations to better results in percentiles performance. At 10 locations out of the 13 the RCM ensemble mean at 25 km is performing better than the coarser resolved ensemble mean. At the other three locations the results for both resolutions are very similar.

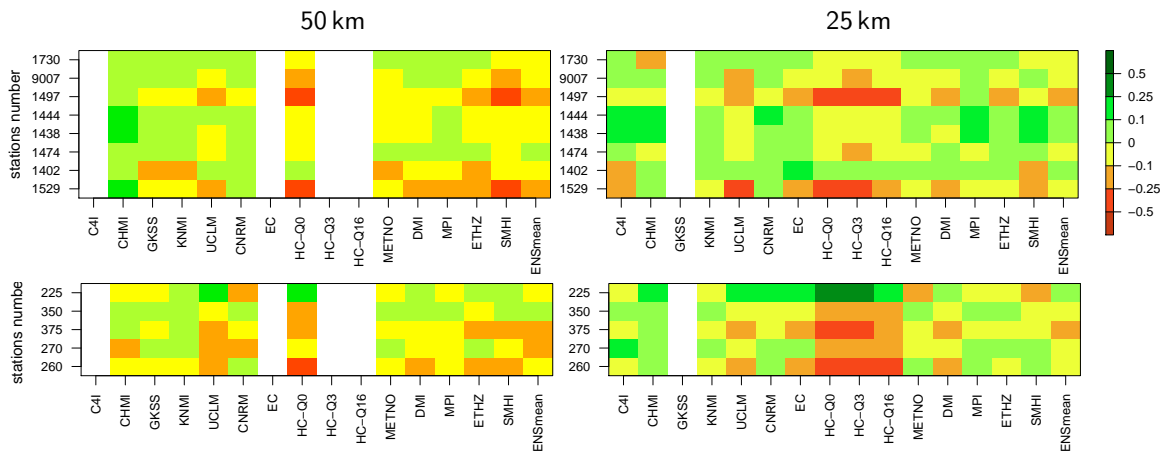


Figure 5.17: Modified Perkins Skill Score at certain locations in the DWD network (upper row) and KNMI network (lower row) for the two different spatial resolutions 50 km (left column) and 25 km (right column) within the time period 1971-2000. (cf. Equation 5.7)

Perkins Skill Score and Probability Distribution

By comparison of the similarity of the observed and the simulated wind speed distributions the Perkins Skill Score is another measure to investigate a possible added value of the

use of regional climate models compared to the forcing reanalysis data from ERA40 (cf. Equations 5.6 and 5.7). The results of the 50km simulation do not show a clear pattern for a certain station or a certain RCM (cf. Figure 5.17). Compared to the analysis of the Brier Skill Score the results for the Perkins Skill Score show more cases for an added value of the regional climate models. In general the Perkins Skill Score of the RCMs is compared to the one from ERA40 smaller for the inland observations far from the coast like e.g. Soltau (ID1529). For the distribution, the use of spectral nudging does not seem to be important. The results for the CLM simulation performed by the GKSS are not different from other RCM simulations. In the 25 km simulations the distributions in almost all RCMs are much closer to the observation at Hohn (ID1444), Schleswig (ID1438) and Jagel (ID1730) than the ERA40 data, especially in winter (not shown). In summer the simulated wind speeds from the RCMs are closer to the observations at List (ID1402) and IJmuiden (ID225).

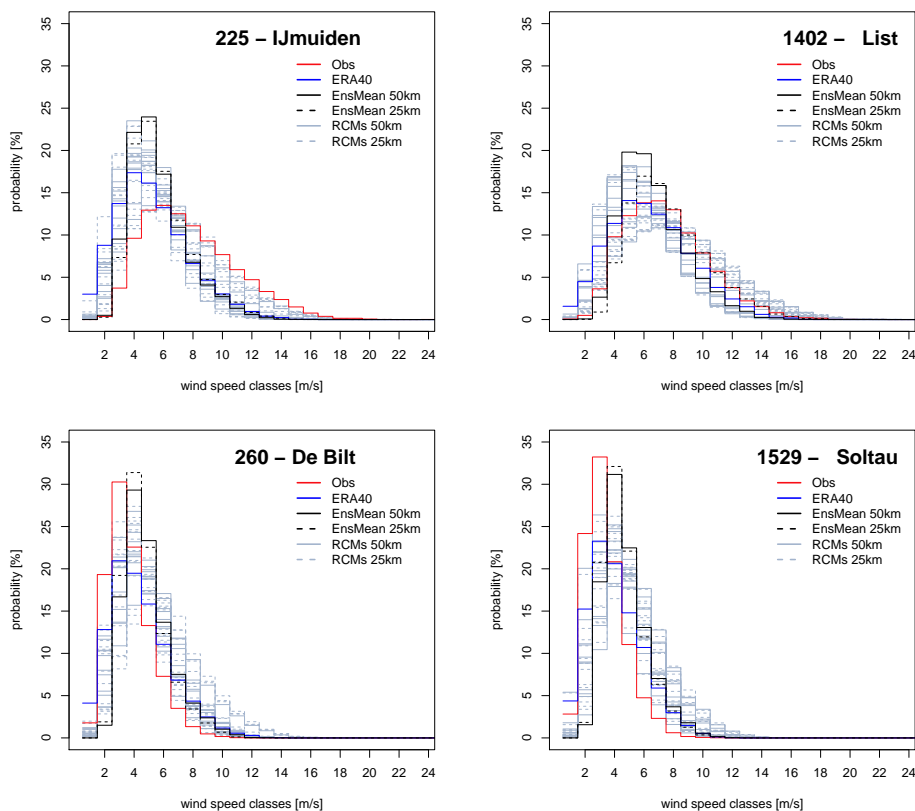


Figure 5.18: Histograms indicating the distribution of daily observed and simulated wind speed at IJmuiden (ID225), List (ID1402), De Bilt (ID260) and Soltau (ID1529) within the time period 1971-2000.

Figure 5.18 gives four examples for the observed and simulated distributions of surface wind speed at IJmuiden (ID225), List (ID1402), DeBilt (ID260) and Soltau (ID1529) for the time period 1971-2000. Among the RCMs, the variability of the daily wind speed

distribution is high. DeBilt and Soltau, both inland stations, show very similar results. At these stations, all models, ERA40 the same as the RCMs, underestimate the occurrence of wind events of low wind speeds and overestimate the number of high wind speed events. ERA40 underestimates the wind speed in the medium range of 3 to 4 m/s, while some of the RCMs and especially the ensemble means can reach this peak in the wind speed distribution, although, with a small shift to higher wind speed values.

The distributions of measured wind speeds at IJmuiden and List are very similar and cover a wide range of wind speed values. While the results for the inland stations for the simulated wind speed are quite similar, at this two coastal stations the results from the RCMs and ERA40 differ. At IJmuiden, none of the models, ERA40 the same as the regional climate models, is able to reproduce the observed distribution. In contrast to the results for the inland stations the models overestimate the occurrence of low wind speed events and underestimate the high wind speed events. Anyway the RCMs are closer to the measured distribution than ERA40. At List the results are slightly different. Most of the RCMs at 50km underestimate the high wind speed events, but most of the results at the 25km resolution overestimate the measured number of events. A clear difference is visible among the results from the 50 km and 25 km simulations. This finding covers the results in the subsection before, where percentile values at different locations are analysed.

Taylor diagramms

While the Figures 5.12, 5.13 and 5.14 show the results for normalized standard deviation, correlation and root mean squared error as an overview of all observations compared to model results, the Taylor diagrams (Taylor (2001)) in Figure 5.19 combine the three parameters for selected locations. In this way it is possible to identify an added value either using regional climate models instead of direct use of model results from reanalysis data or simulating wind speed in coarse or higher spatial resolution (50 km vs. 25 km) depending on certain location.

Figure 5.19 gives four examples for analysed wind speed time series in Taylor diagrams. Due to the highest values for correlation the regional climate model CLM applied at GKSS and ERA40 data perform best at all stations. The ensemble mean can also reach correlations around 0.8 at all sites, where the results for the individual RCMs show lower values for correlation. An added value of the higher spatially resolved data of 25 km compared to 50 km can be identified for the MPI regional climate model REMO at all measuring sites. An increased correlation in the 25 km simulations can also be seen, but with smaller extend in the results from regional climate models from the DMI, CHMI and UCLM. For the models from KNMI and CNRM the values for correlation are constantly smaller for

the 25km simulation compared to 50km. In these cases no added value can be identified. The results from the HC are very similar, independent from the spatial resolution but also in the sensitivity factor (Q0, Q3 and Q16).

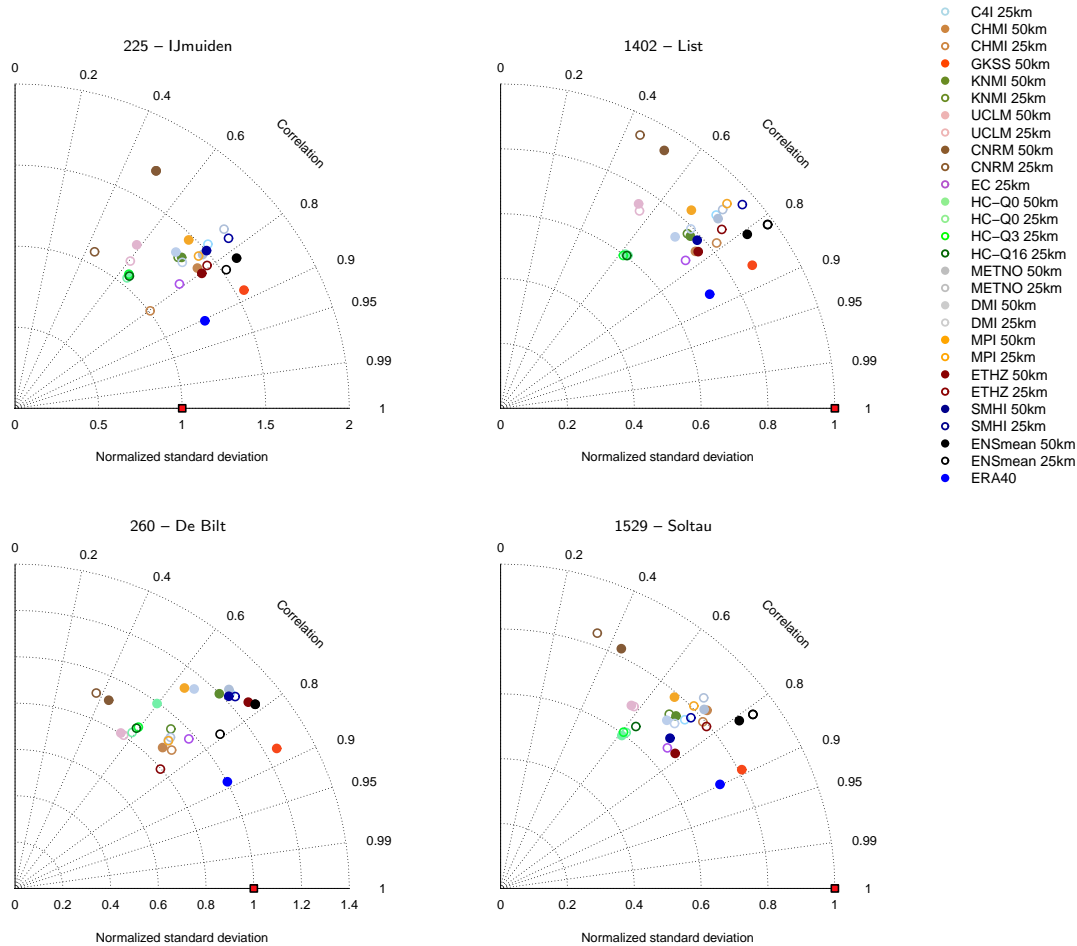


Figure 5.19: Taylor diagram for daily mean wind speeds at IJmuiden (ID225), List (ID1402), De Bilt (ID260) and Soltau (ID1529) within the time period 1971-2000 for the two different spatial resolutions 50km (filled circle) and 25km (open circle).

Daily maximum wind speed

Regional climate models are able to calculate the maximum wind speed for a predefined time period. Differences in the results can be seen if the models apply a wind gust parameterisation. For all models daily maximum wind speed is available, but for 5 out of the 15 models also daily maximum wind speed including gust is offered. A comparison to ERA40 is not possible, as this parameter is not available from the reanalysis.

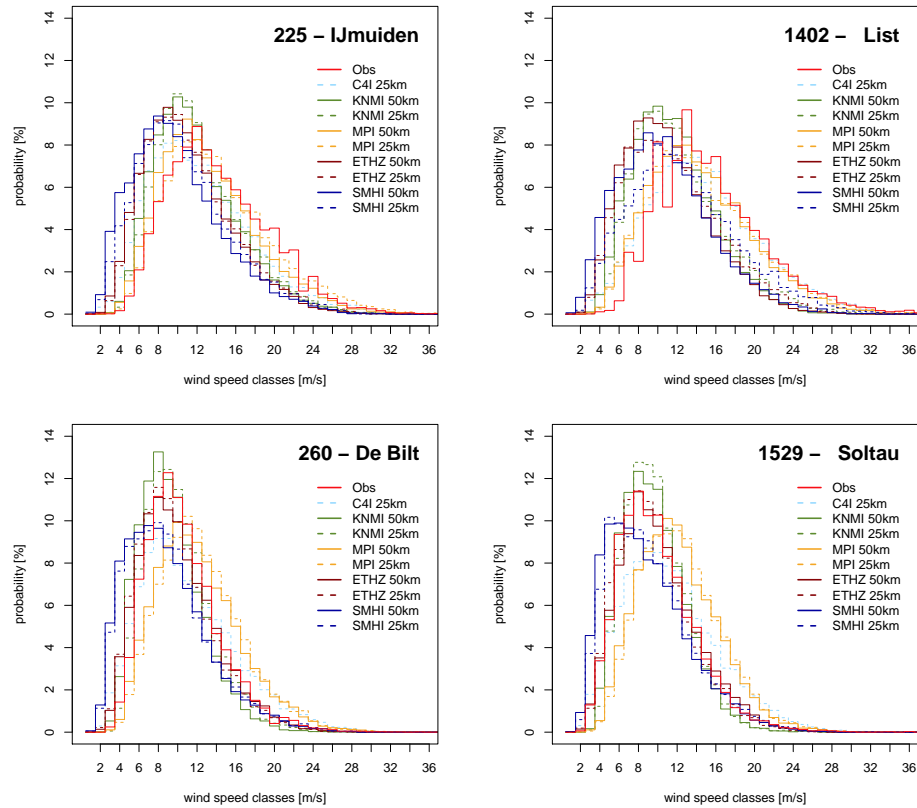


Figure 5.20: Histograms indicating the distribution of daily observed and simulated maximum wind speed (incl. gusts) at IJmuiden (ID225), List (ID1402), De Bilt (ID260) and Soltau (ID1529) within the time period 1971-2000.

The observed mean annual maximum wind speed distributions at all stations cover a wide range of values. The models are able to reproduce the observed maximum wind speed distribution, in dependence of the stations location and whether the gust parameterisation was included or not. The results from simulated maximum wind speed without gusts have been compared to the observations according to mean values, probability distribution and percentiles. The models are not able to capture the range nor distribution of the observations and are not further investigated, only the model results including wind gust parameterisation fit the observations well and are investigated in the following.

Figure 5.20 shows the results of the daily maximum wind speeds observed and simulated by the models including gusts. At IJmuiden and List all models overestimate the mean annual maximum wind speed probability in lower wind speed conditions ($< 12\text{m/s}$) and underestimate the higher values. The simulation results being closest to the distribution of the observations are the ones from REMO (MPI) and RCA3 (C4I). In general, both models simulate slightly higher values for maximum wind speeds as the other models. In consequence both models overestimate the mean annual maximum wind speed at the land

stations like DeBilt and Soltau (cf. Figure 5.20, lower panels). This fact can also be seen in the results for the bias in percentile values shown in Figure 5.21. The models underestimate the percentile values up to -5 and -8 m/s compared to the observed values for the coastal stations. The bias is smaller at inland locations due to the generally lower values for maximum wind speed. At these locations the models capture the observed values very well. REMO and RCA3 perform best for the coastal stations, while CLM (ETHZ) performs best for inland stations showing constant small biases over all percentiles.

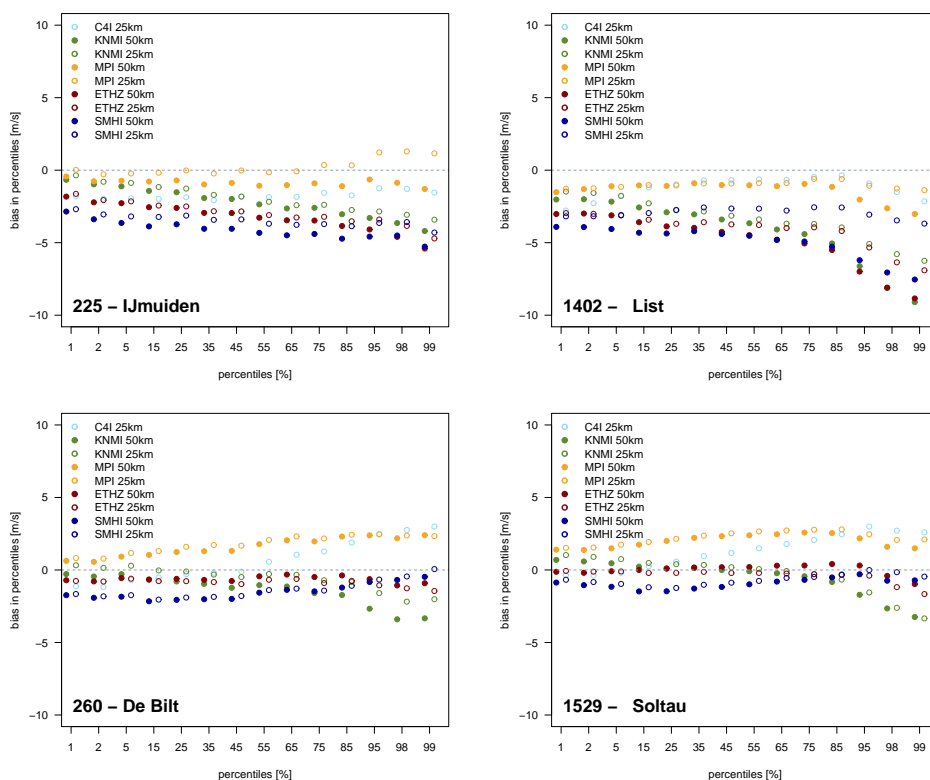


Figure 5.21: Bias in percentiles as the difference of percentiles derived from simulated daily maximum wind speed (incl. gusts) by the RCMs for the two different spatial resolutions 50km (filled circle) and 25km (open circle) at IJmuiden (ID225), List (ID1402), De Bilt (ID260) and Soltau (ID1529) within the time period 1971-2000.

The correlation between observations and the simulated daily maximum wind speeds is represented in the range of 0.6 and 0.8. The standard deviation indicating the temporal variability of daily maximum wind speeds is well captured by the regional climate models. REMO and RCA3 (from C4I) have a smaller variability than observed, whereas KNMI'S model RACMO overestimates the variability constantly. For the REMO simulations at 25km spatial resolution for all stations the values for correlation are constantly higher compared to the results from the 50km simulation (not shown).

5.5 Regime-dependent validation of simulated surface wind speeds

From the regional climate models introduced in Section 2.3 only wind speed data is available but no information on the prevailing direction of the wind per day. With respect to this deficit, weather regime classifications carried out for Europe and the North Sea have been tested in Chapter 4 to close this gap and provide a directional component to the given daily wind speed information. The classification after Jenkinson and Collison (1977) carried out in the present work with special focus on the North Sea fits the requirements in describing best the synoptic situation per day (cf. Section 4.3).

The investigations from the previous Section 5.4 are repeated, but depending on the direction of the wind. It should be tested, whether the models are able to reproduce the wind climate dependent on the daily leading weather regime. The analysis in this section is based on those days, where for all RCMs and ERA40 the same regime is set (cf. Table 4.5). The whole analysis has been made for all simulations on both spatial resolutions, 50 km and 25 km. Shown are only the results for the 25 km simulations.

In a last step, the simulations from the model CLM are selected, as these runs performed best in both spatial resolutions and to increase the robustness of the results by using a higher number of agreed days per regime.

Bias

While Figure 5.9 shows the mean bias per RCM and for ERA40 compared to different observation data for the 30-year time period 1971 – 2000, Figure 5.22 shows the same but for the 25 km simulations only and depending on the leading weather regime for summer and winter at four locations. With respect to the robustness and to avoid misinterpretation, the results for the regimes SE, E, NE and UNC in summer and N, NE, E and UNC in winter are blanked out, as the number of days within the individual season, where all models show the same regime, is below the statistically critical number of 30 (cf. Table 4.5).

Basically, the results for bias reflect the findings in the previous section. The aim of the regime dependent validation is to identify regimes, where most of the RCMs show a different result compared to other regimes. Looking at all panels in Figure 5.22, none of the regimes stands out from the crowd at all locations the same. Only for the German locations the RCMs and partly ERA40 show a slightly more positive bias for wind speeds from south-western (SW) wind direction. For the observations in the Netherlands none regime occurs to be special in the bias results. Additionally, at the individual locations, there are regimes at which most of the RCMs behave the same but differently from other regime conditions. At e.g. List (ID1402) in the 25 km simulations, the regime W and SW

in both seasons, summer and winter, show higher overestimation as other regimes. The wind speed is more overestimated for the regimes C and SW at the stations Schleswig (ID1438), Hohn (ID1444) and Oldenburg (ID1497). At Volkel (ID375) and at De Bilt (ID260) the RCMs and ERA40 show an overestimation of up to 60% for the regime NW in both seasons.

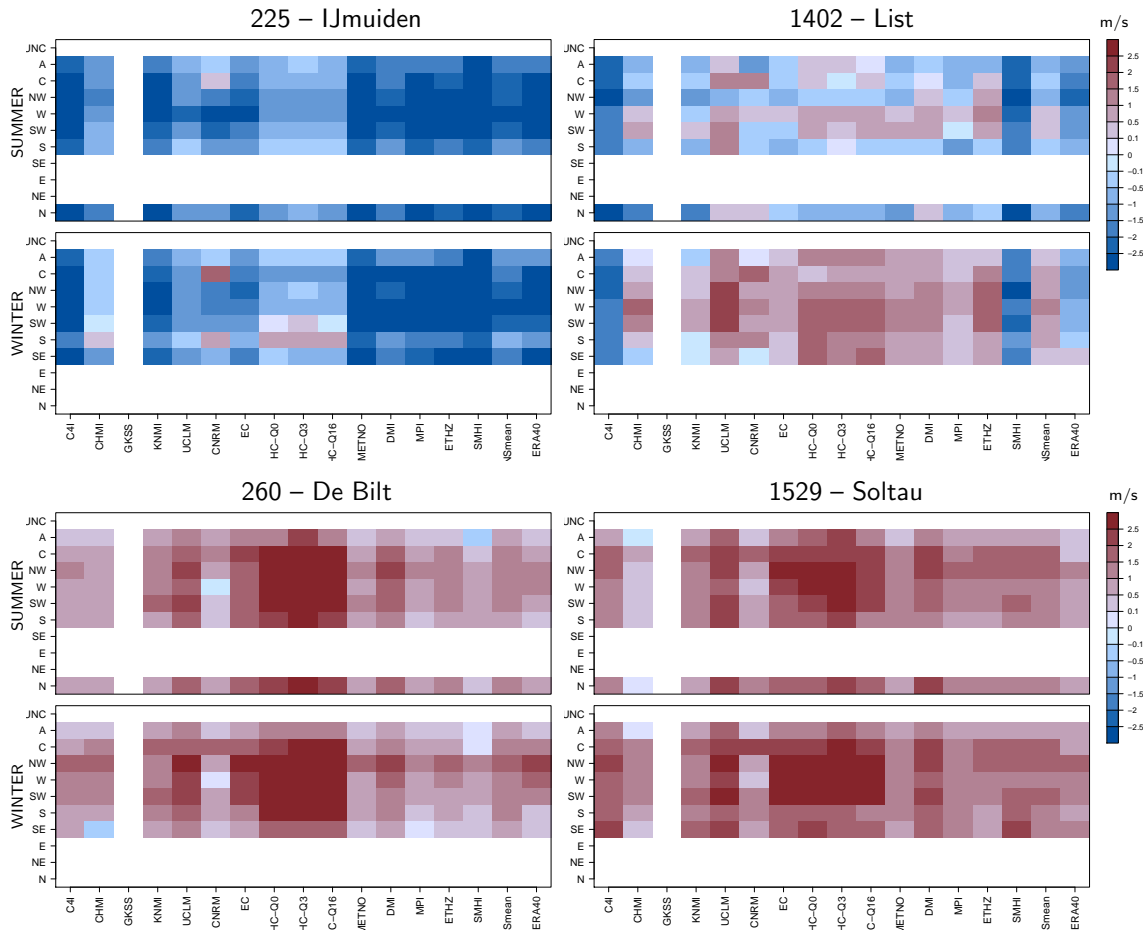


Figure 5.22: Mean seasonal bias per weather regime between simulated wind speed by the regional climate models at 25 km spatial resolution and the observations at the locations IJmuiden (ID225), List (ID1402), De Bilt (ID260) and Soltau (ID1529) within the time period 1971–2000.

Standard deviation

Figure 5.23 shows the differences in the standard deviations (normalized to the observations) between the regional climate model results and the observations at the four locations IJmuiden (ID225), List (ID1402), De Bilt (ID260) and Soltau (ID1529). The RCMs, the same as ERA40, over- and underestimate the observed values by approximately +/- 80%. Similar to the results for the bias, one regime shows the highest overestimation for all locations the same. While in the bias the wind speed from south-western direction (SW) and during cyclonale (C) conditions was highest, in the standard deviation only the regime

C points out. For the Dutch locations, the regime C does not play a special role. Instead, at De Bilt and Volkel all models overestimate the standard deviation by 25 % to 80 % for the regime NW, while the standard deviation during all other leading regimes is smaller and between $\pm 30\%$. At IJmuiden during summer and SW the standard deviation is slightly higher underestimated compared to other regimes.

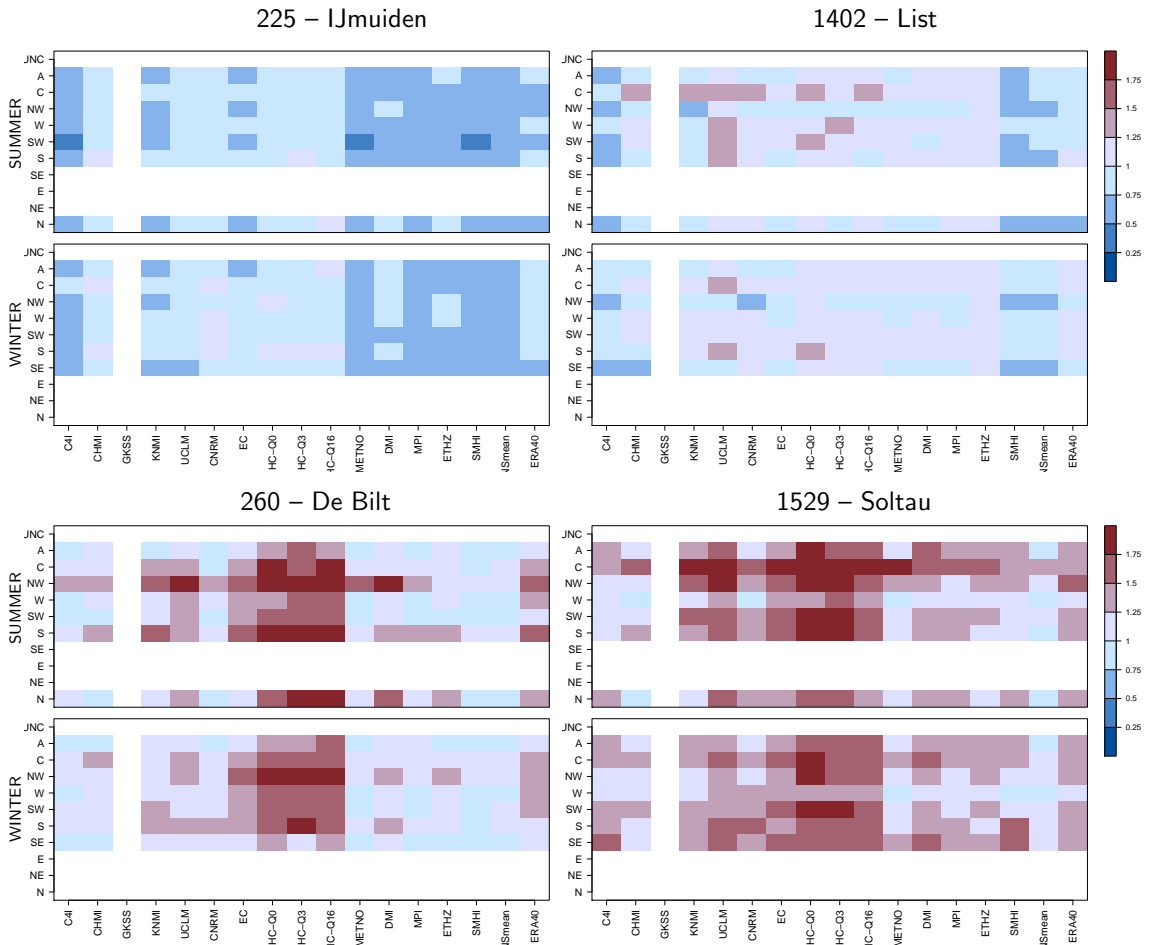


Figure 5.23: Differences in the normalized standard deviation per weather regime between simulated wind speed by the regional climate models at 25 km spatial resolution and the observations at the locations IJmuiden (ID225), List (ID1402), De Bilt (ID260) and Soltau (ID1529) within the time period 1971–2000.

Perkins skill score

The added value concerning the RCMs ability to reproduce the observed wind speed distribution in comparison to ERA40 is shown for different locations in Figure 5.24. The Perkins skill score defined by the Equations 5.6 is modified (cf. Equation 5.7) in the way, that positive values indicate the RCMs added value, negative numbers demonstrate the better agreement of ERA40 with the observed distribution per regime. In Figure 5.17

the Perkins Skill score was already presented for all RCMs at the different locations, but independent from prevailing wind direction. There, the location Ijmuiden (ID225) stands out from the other locations in the way, that most of the RCMs covered the observed wind speed distributions better than ERA40. In Figure 5.24, the RCMs show an added value for the regimes A, C, NW and S in summer and for S and SE in winter, at this location.

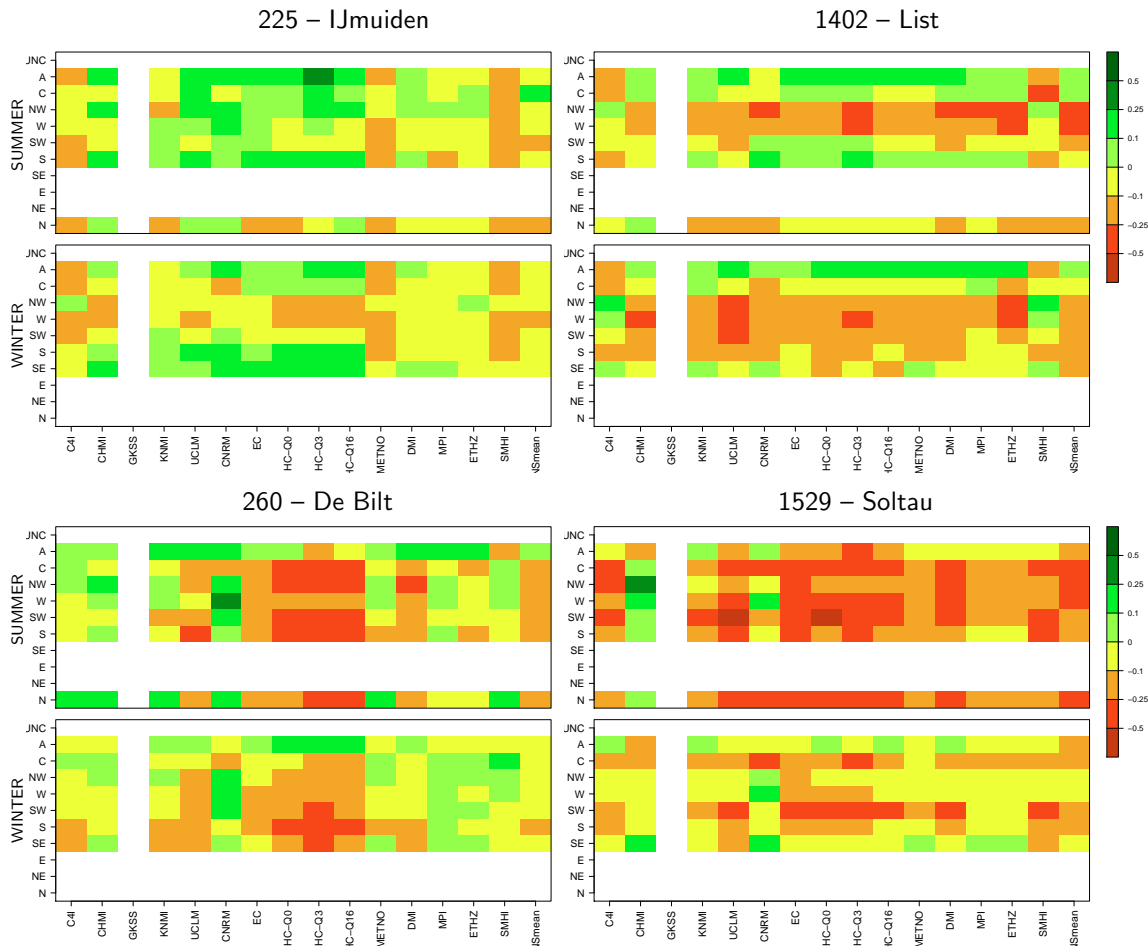


Figure 5.24: Perkins skill score per weather regime between simulated wind speed by the regional climate models at 25 km spatial resolution and the observations at the locations IJmuiden (ID225), List (ID1402), De Bilt (ID260) and Soltau (ID1529) within the time period 1971–2000.

At most of the locations, the RCMs show an added value for the regime A, where the wind direction is diverse. In contrast, for the regimes NW, W and SW for most of the locations ERA40 covers the observed distribution better than the RCMs and the Perkins Skill score is negative. At the locations Schleswig (ID1438), Hohn (ID1444) and Jagel (ID1730) the RCMs show for most of the regimes a positive Perkins score in both seasons (not shown). The RCMs can not add value for most of the leading wind directions at the locations Soltau (ID1529), De Bilt (ID260), Wittmundhafen (ID9007) and Oldenburg (ID1497) (not shown).

Increase of robustness of the previous results

In the previous investigation some of the regimes have been identified, in which the RCMs behave in the same way but differently compared to other regimes and independent from the location. Anyway, there is no information for the blanked out regimes due to too few cases per season. To increase the number of analysable days per regime and include in this way the missing regimes, from the results from Section 5.4 the most promising simulations have been chosen. With respect to institutional interest it has been reduced to the CLM simulations. For these three simulations, two for the 50 km spatial resolution and one for 25 km, the total number of days, where these simulations and ERA40 show the same regime in the period 1971 – 2000, have been identified and are listed for different seasons in Table 5.4. The number of agreeing days is very different among the regimes and within a season. In this way, a number below the accepted 30 cases was found only for the very short 3-month-seasons October to December (OND) and January to March (JFM) and both for NE. The seasons have been defined according to the mean wind conditions in the North Sea (cf. Section 5.2) and the analysis of the NAO and NAO index in Section 5.2 and Appendix C. The following investigations have been carried out for all different seasons and periods.

Table 5.4: Total number of days per regime (11 classes) indicated in ERA40 (black) and number of days, where GKSS-CLM and ETHZ-CLM in both resolutions and ERA40 show the same regime (coloured) in the period of 1971-2000. Red indicates values, where the number of cases is too small for statistics; Green, where the number of cases is sufficient.

regime	ERA40 ident		ERA40 ident		ERA40 ident		ERA40 ident		ERA40 ident	
	ONDJFM	ONDJFM	AMJJAS	AMJJAS	OND	OND	JFM	JFM	DJFM	DJFM
N	479	283	179	126	122	63	95	63	166	82
NE	226	107	76	42	46	16	34	26	82	31
E	180	128	158	112	93	30	53	82	186	94
SE	180	122	277	204	178	100	136	104	274	131
S	306	222	486	365	322	183	242	182	410	237
SW	501	385	815	688	555	367	430	321	640	446
W	626	468	929	789	602	401	481	388	770	542
NW	587	401	447	328	303	170	237	158	421	229
C	842	515	739	496	550	277	393	219	632	312
A	1331	987	1304	1006	870	500	630	506	1214	686
UNC	232	33	58	5	39	3	29	2	55	2

In a first step the bias and the standard deviation have been calculated according to the method in the previous section, but reduced to the three RCM simulations and using of more days per regime, as described before. Five locations have been selected, indicating very interesting results with diverse values per regime. Figure 5.25 shows the mean

bias between the simulated wind speed from the RCMs and ERA40 and the observation data at Heligoland (ID1040), Bremerhaven (ID1468), Jagel (ID1730), Leeuwarden (ID270) and De Bilt (ID260) for the season December to March within the time period 1971 – 1983.

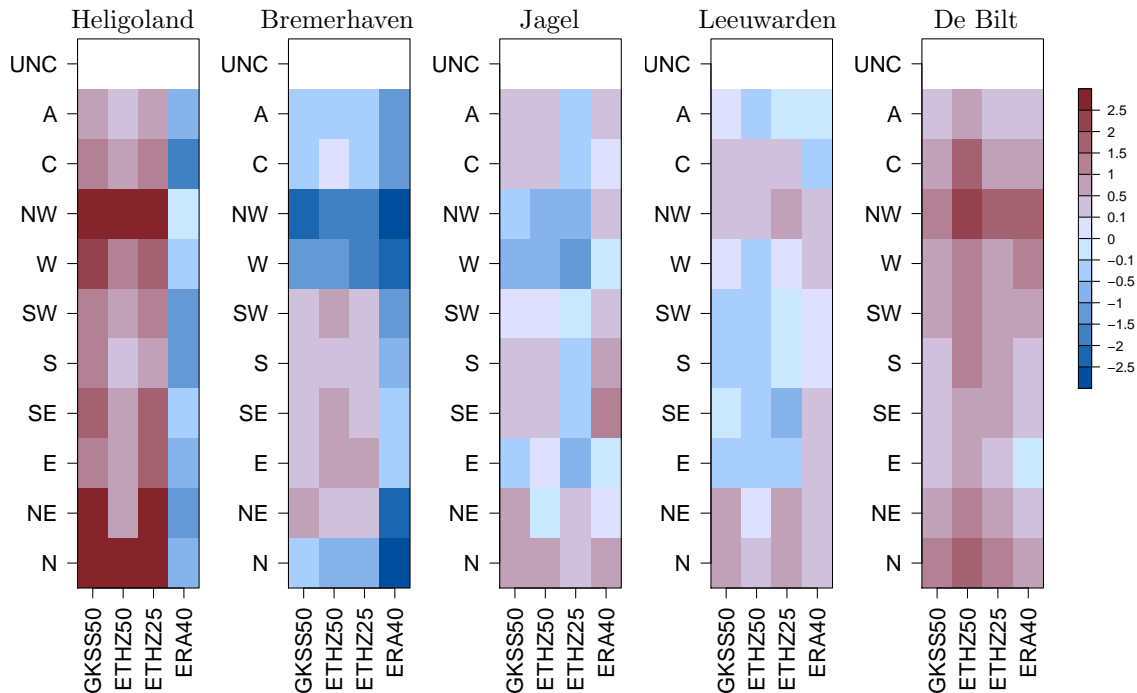


Figure 5.25: Mean seasonal bias [m/s] per weather regime of simulated wind speed by the regional climate models at the locations Heligoland (ID1040), Bremerhaven (ID1468), Jagel (ID1730), Leeuwarden (ID270) and De Bilt (ID260) during December to March within the time period 1971–1983.

Heligoland (ID1040)

Heligoland consists of two islands about 46 km off the German coast, with sizes of 1 km² and 0.7 km². The main island consists of the "Upper Land" and the "Lower Land". Most of the houses and the harbour are located in the Lower Land. The Upper Land is a plateau with a height of 61 m above the sea level at its highest point. The wind speed observation is located in the Lower Land. Lindenberg et al. (2012) focused in their study on Heligoland and investigated the influence of the changes in the measuring location, as the site was moved at the end of 1989 from the Lower Land to a mole further away from the influencing island. The change of the location is the reason, why this observation data is only used for the short time period 1971 – 1983.

The covering grid cell in the RCMs define this location as water, with an elevation of 0 m, and a surface roughness defined for open ocean. The results for the regime dependent wind speed evaluation in Figure 5.25 show differences depending on the wind direction. The RCMs show a general overestimation of the wind speed, which results from the low

roughness length and the fact, that the island does not exist in the models. ERA40 underestimates the observed wind speed, which should not be analysed here. Additionally, the RCMs show a larger overestimation for the wind speed from the Northwestern, Northern and Northeastern direction. This can easily be associated with the location of the Upper Land and the second smaller island in relation to the observation site. The Upper Land has a shadowing effect on the observation site for wind speed from the NW directions, the Lower Land from the North and the smaller island from the Northeast directions.

Bremerhaven (ID1468)

The results for the mean bias in Bremerhaven (cf. Figure 5.25) can also be traced back to the station's surrounding. The measuring site is located in the harbour at the eastern side of the river Weser, west of the city in an urban area. Hence, the wind speed measurement is disturbed by urban areas from almost all sides, except from the Northwestern and Western wind direction, where the wind only comes from the water. The higher observed wind speed from the Northwestern direction can not be captured by the models, as there is no differentiation of these structures around the station in the models.

Jagel (ID1730)

The location of the station in Jagel is a very flat area on the site of a big military airport. There are two in an acute angle crossing runways. The main runway is in the direction SW-NE, the second runway in about WSW-NNE direction. The RCMs fit the observed wind speed values very well with a bias between -1.2 m/s and 1.3 m/s. Similar to the results for Bremerhaven some regimes stand out by collective overestimation or underestimation of the observed wind speed. The analysis for the wind roses at this station in relation to the leading weather regime showed the documented slight turn to the south. In this way the main wind direction at the measuring site is West-South-West for the regime "W" and for the regime "NW" the wind comes from West-North-West. The models underestimate the observed mainly undisturbed wind speed from western and south-western directions.

Leeuwarden (ID270)

Similar to Jagel the measuring site in Leeuwarden is located on the site of an airport North-East of the city. The RCMs capture the observed wind speed in the direction of the runway, which is SW-NE. Due to continuous structures in the North and Northwest of the airport area the wind speed at the measuring site is reduced and therefore overestimated by the regional climate models.

De Bilt (ID260)

The RCMs overestimate the observed wind speeds at De Bilt. The station is located within a very urban area on the roof top of a building at a height of 20 m above the ground. For this investigation the wind speed has been interpolated to the constant height of 10 m, as described in Section 2.1. Anyway the measurement is slightly disturbed by a radar tower and turbulences due to the building and high trees, nearby. As for the other examples given before, the RCMs do not capture the very specific characteristics of the environment of the station.

General remarks

The results for the regime depending standard deviation and Perkins-Skill-Score analysis show the same reflection of the station's surrounding as the findings in the bias, and are, therefore, not shown.

5.6 Discussion and summary

In this study the performance of regional climate models in describing the surface wind speed at the German and Dutch coastal area in comparison to observations is evaluated. These observations have been provided by the German weather service (DWD) and the meteorological Service from the Netherlands (KNMI). The observed data is available hourly for mean wind speed and hourly or daily for maximum wind speed. The data was taken in different measuring heights and corrected to a reference height of 10 m above ground by applying a logarithmic approach. The investigated regional climate model ensemble was developed in the ENSEMBLES framework. Daily surface wind speed, daily maximum wind speed without gusts and, from a reduced number of models, also daily maximum wind speed including gusts is available for the time period of 1961 – 2000. (cf. Chapter 2) The mean wind conditions in the coastal area of the southern North Sea and the German Bight have been investigated based on the observation data. Mean annual values and the variability for daily wind speed, the seasonal cycle, but also the main wind directions in each month of the year and the influence of the NAO have been analysed.

Several measures and skill scores were applied to analyse the RCMs performance compared to the driving field and to evaluate accuracy gain by including higher spatial resolution of the models. Figure 5.26 summarises the findings for the RCM ensemble mean. The investigations show the ensemble mean being closer to the observed values than the individual RCMs. The results are categorised in three qualities – "good", "fair" and "poor" – based on the definitions made by the author presented in Table 5.5. The presentation of the results

Table 5.5: From results for different skill scores to qualities.

SKILL SCORES	QUALITIES		
	"good"	"fair"	"poor"
bias [%]	$< \pm 10 $	$\geq \pm 10 - \leq \pm 25 $	$> \pm 25 $
standard deviation[-]	0.75 – 1.25	0.5 – 0.75; 1.25 – 2	< 0.5 ; > 2
correlation [-]	> 0.8	0.7 – 0.8	< 0.7
Brier skill score [-]	> 0.25	-0.25 – 0.25	< -0.25
Perkins skill score [-]	> 0	-0.1 – 0	< -0.1
percentiles (mean) [m/s]	$< \pm 1 $	$\geq \pm 1 - \leq \pm 2.5 $	$> \pm 2.5 $

in one map should help to identify regions with similar results. It can be stated that the ensemble mean performs well concerning bias, standard deviation and correlation. Only for the station De Bilt (ID260) the bias is too large, which is related to the very urban area around the station, which is not included in the RCMs.

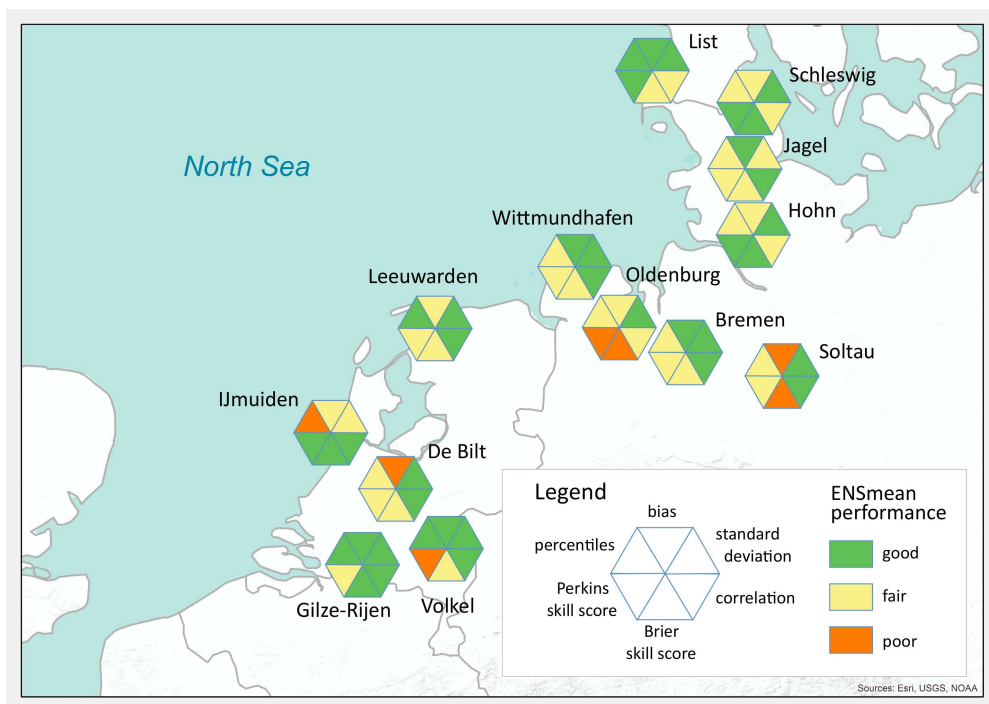


Figure 5.26: Qualitative assessment of the RCM ensemble mean performance (ENSmean) in the spatial resolution of 25 km for simulating daily mean wind speed concerning different skill scores at the 5 Dutch and 8 German locations analysed within the time period 1971 – 2000 (cf. Table 5.5). (black dots: all measuring sites of the individual network)

Station covering grid cell in RCMs vs neighbouring grid cell and interpolation

The wind speed from the observation covering grid cell in each RCM in the two spatial resolutions is used for evaluation, but also the 8 surrounding grid cells in the models have been taken into account. Winterfeldt and Weisse (2009) interpolated simulated wind speeds from the RCM from the four grid points surrounding the measurement location in a bilinear way. In this study no interpolation has been carried out. Especially for the stations List (ID1402) and IJmuiden (ID225), located close to the coastline, the covering and surrounding grid cells in the model often show different land-sea fraction (cf. Figure 5.27) and thus very different results for, e.g., bias assessment, shown in Figure 5.10. For List the covering grid cell for most of the models with 50 km is defined as land, while in the increased spatial resolution in all models the covering grid cell is defined as water. While in the coarse resolution the models underestimate the observed wind speed, the bias is very small and close to zero in the 25 km resolution. In general it can be stated, that the covering grid cell gives the best results compared to the observation. An interpolation would mix up wind speed values referring to very different surface roughness lengths.

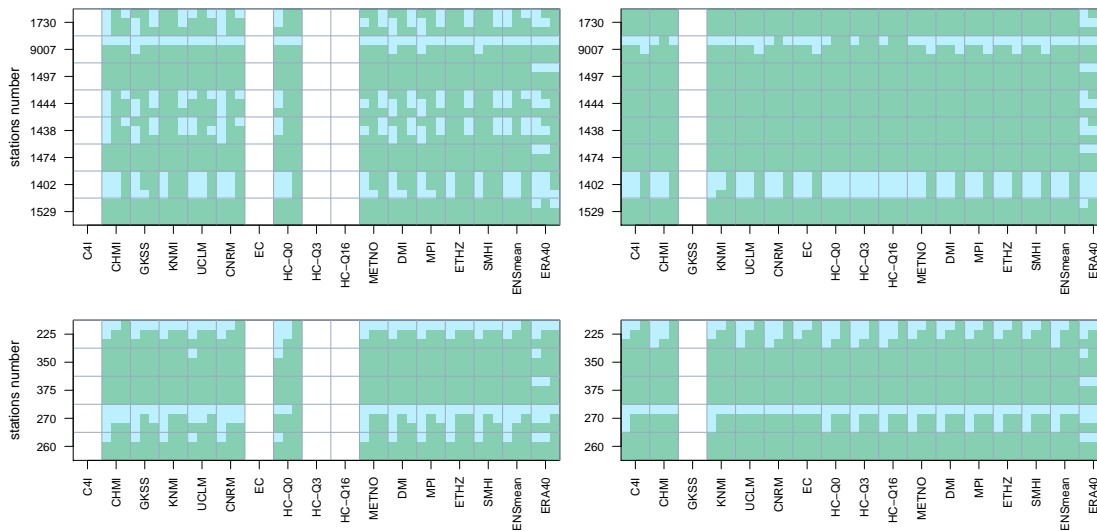


Figure 5.27: Land-Sea distribution at the covering and the 8 surrounding grid cells in each RCM according to the location of the observations in the DWD network (upper row) and KNMI network (lower row) for the two different spatial resolutions 50km (left column) and 25km (right column). blue: land-sea fraction < 0.5 , green: land-sea-fraction ≥ 0.5

Added value: RCM performance vs ERA40 forcing

As already stated before, wind speed assessment has been carried out for both, the RCM ensemble and the ERA40 forcing. An aim of this study is to investigate the value added by the RCM simulation instead of using wind speed information directly from ERA40. Therefore, all results for bias, standard deviation, correlation and percentiles have been

compared. The modified Brier skill score and the modified Perkins skill score indicate the added value directly (cf. Equations 5.3, 5.4, 5.5, 5.6, 5.7). All findings have been summarised in Figure 5.28. At the locations IJmuiden (ID225), List (ID1402), Schleswig (ID1438) and Hohn (ID1444) the RCM ensemble mean shows a clear added value for most of the skill scores compared to ERA40. Reasons could be:

- low frequency or no assimilation of observation data in the reanalysis ERA40, and
- higher spatial resolution of the RCMs and therefore a better representation of land-sea distribution and surface roughness.

The observed data at the locations Schleswig and IJmuiden have not been, or with very low temporal frequency, assimilated in the ERA40 simulation. Other observations, which is true for most of the German stations used in this study, have been assimilated not from the beginning of the analysed time period of 1971 – 2000, but constantly later in time.

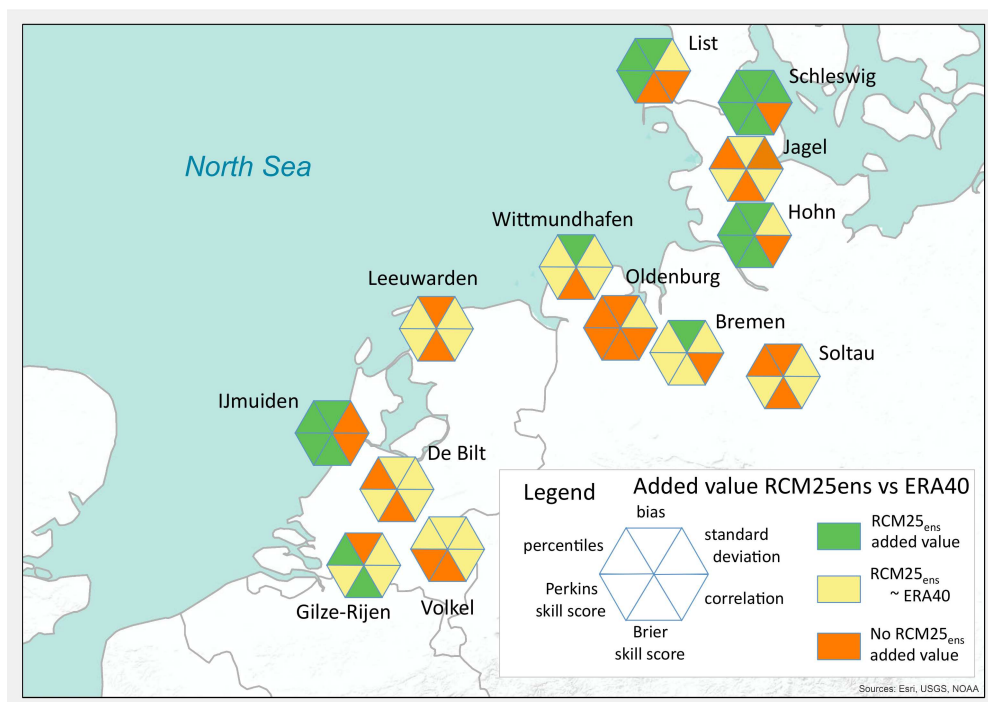


Figure 5.28: Qualitative assessment of the existence of value added by the RCM ensemble mean (ENSmean) in the spatial resolution of 25 km compared to the reanalysis ERA40 for daily mean wind speed concerning different skill scores at the 5 Dutch and 8 German locations analysed within the time period 1971 – 2000. (black dots: all measuring sites of the individual network)

Due to the high quality undisturbed data, the observation data of Jagel (ID1730) was assimilated with high temporal frequency. Therefore, ERA40 performs very well at this location and can hardly be beaten by the RCMs. Instead for Schleswig and IJmuiden the RCMs show a clear added value concerning most of the skill scores.

Additionally, at List and IJmuiden the RCMs add value due to the higher spatial resolution compared to the ERA40. The station covering grid cell in ERA40 has a spatial resolution of about 125 km by 125 km and is defined as water in both cases, but using a tile approach for describing the covered area. The higher resolution of the RCMs of 25 km can resolve the coastline much better and, therefore, add value for most of the analysed skill scores.

Added value: coarse vs high spatial resolution in the RCMs

From most of the RCMs results in two spatial resolutions are available. Although, often not the same model versions or underlying forcing data has been used, a clear advantage of the usage of the higher resolution can be observed in the wind speed analysis. The added value can be detected over all skill scores across the different locations. As stated before, for the comparison between ERA40 and the RCMs, the better resolved surface characteristic in the 25 km simulation is the reason for the better representation of the surface wind climate.

Added value: maximum wind speed

From the regional climate models daily wind speed and daily maximum wind speed without gusts are provided. Few models applied gust parameterisation and, additionally, include maximum wind speed including gusts. The simulated daily maximum wind speed with and without gusts have been compared to daily maximum wind speed from the observation. The distribution and percentiles derived from the RCMs daily maximum wind speed without gusts are not able to capture the values from the observations. Only the maximum wind speeds including gusts provided by the models applied at the institutions C4I, KNMI, MPI, ETHZ and the SMHI perform very well. Especially the percentiles at inland stations can be reproduced by the models and show very small differences up to the highest percentiles.

Regime dependent validation and local features

From the regional climate model ensemble and from ERA40 no daily prevailing wind direction was available. The directional component of the wind is given by a weather regime classification carried out for the North Sea (cf. Section 4.3). In a first step, bias, differences in the standard deviation and the Perkins skill score have been calculated for the simulated daily wind speed from the RCMs as well as from ERA40 in comparison to the observations and, additionally, depending on the leading regime. Some wind directions had to be blanked out from the analysis, as the number of days with certain regime has been too small for statistics. The results per location have been very diverse. For the

German stations southern and south-western wind directions seem to be overestimated by the models. Due to the size of the grid cells of minimum 25 km by 25 km, the orography is smooth and miss local differences in elevation. This can lead to a reduced roughness length. Furthermore, the wind from southern direction blows undisturbed over a long distance over land. This together with a smooth orography could be a reason for the higher wind speeds than observed. Although some models use tile approach for describing the grid cells surface, the models overestimate mostly the wind from the described directions. Concerning the standard deviation, a quite constant overestimation can be detected for the regime "C", the cyclonic type centered over the North Sea. During this regime the wind speed comes from different directions at the stations. In contrast, during the anticyclonic regime, with same location and same characteristics related to the wind speed, no outstanding features can be found in the results for this regime.

To increase the number of regime days available for further analysis and to include the blanked out regimes, three most promising simulations have been taken out of the regional climate model ensemble. The investigated skill scores have been calculated again for the reduced number of models. The results show certain regimes standing out from the others, but this had to be addressed to local effects of the station's environment.

Local features like land-sea circulation, "crash barrier effect", tunneling effect and inhomogenous surface lead to very individual wind conditions at the different locations, which can not be captured by the comparable coarsely resolved models.

6 Conclusion and Outlook

6.1 Conclusion

Based on results from the regional climate model simulations carried out in the ENSEMBLES framework, the present study aimed on two topics. One is the overestimation of summer air temperature in South-Eastern Europe, which goes together with a strong underestimation of precipitation in this season. This known issue is called "summer drying" problem of climate models. The other issue is the underestimation of higher wind speeds of the models over land. In previous investigations, it was shown that RCMs represent surface wind speeds over the ocean very well, but underestimate strong winds over the continent.

According to the research questions defined in Section 1.2 the major finding can be summarised as follows:

Is there an influence of the underlying soil type distribution on the results from a regional climate model?

Based on soil maps from Haase et al. (2007) and Stremme (1937), two simulations with the regional climate model CLM have been carried out, using either default sandy loam or silt loam over an area north of the Black Sea. Due to its higher porosity, silt loam assimilates more water during rainfalls than sandy loam. This leads to a 30 % to 75 % increase in soil moisture in the modified simulation (with silt loam) compared to the control simulation (with sandy loam). Changes in the soil moisture lead to changes in surface albedo and thus in net solar radiation. During summer the wetness of soil results in an increase of evaporation up to 60 %. This provides more humidity in the air and higher precipitation amounts during the summer months can be observed. As the energy is needed for the evaporation, the air temperature is reduced by up to 1.5 K.

Can the summer drying in Southeast Europe be reduced in the models?

In the present study the hypothesis has been investigated, that a positive bias in summer in Southeast Europe is related to a false representation of soil properties in this region. This theory is based on divergences between soil maps from Haase et al. (2007) and Stremme (1937) and the FAO soil data set, which is commonly used in the RCMs. Using silt loam distribution from the *International soil map of Europe* in combination with the FAO soil map leads to a reduction of the detected bias by up to 1.5 K and a better representation of the observed climate in a larger area around the region of interest. Nevertheless, the changes only affect a part of the region of the "summer drying", so it can not be removed

completely. Anyway, the study showed that the improvement of soil moisture has strong positive influence on the simulation of processes in the boundary layer.

What is a suitable weather regime classification to describe the wind climate in the North Sea?

Within the ENSEMBLES framework a weather regime classification based on a principle component analysis of daily 500 hPa geopotential height from ERA40 has been carried out by Sanchez-Gomez et al. (2009) for whole Europe. Four main regimes (BL, NAO+, AR, NAO-) have been transformed to each of the regional climate models within the RCM ensemble for two seasons in 1961 – 2000. In this study another classification has been carried out for all RCMs in the ensemble, based on MSLP following the method by Jenkinson and Collison (1977). This regime classification is centered over the North Sea and defines 27 regime classes, which have been reduced to a number of 11. For both classifications the mean occurrence and MSLP composites have been derived for each regime. Depending on the weather regime, composites of local wind observations have been calculated. With focus on the southern and eastern coastal area of the North Sea, composite wind roses for observations show no clear prevailing wind direction for the regimes provided by Sanchez-Gomez et al. (2009). In contrast, comparing the composite wind roses for the second weather classification, the regimes clearly reflect the local wind characteristics. In conclusion, the weather regime classification after Jenkinson and Collison (1977) centered over the North Sea, describes the local wind climate best and is used for further regime dependent evaluation of the regional climate model ensemble.

Are the regional climate models able to reproduce the observed large scale atmospheric pattern?

As already summarised in the answer of the previous question, two objective regime classifications have been investigated to be a sufficient diagnostic tool for present wind climate validation at the German and Dutch coastal area of the North Sea. One classification was carried out for Europe within the ENSEMBLES framework (Sanchez-Gomez et al. (2009)), the other was carried out for all RCMs and the ERA40 forcing with focus on the North Sea following the method from Jenkinson and Collison (1977). For both classifications the agreement between the regimes detected in the RCMs and the regimes defined in ERA40 as reference has been calculated. Independent from the regime classification method, the models are able to reproduce the observed large scale weather regime in different quality. While most of the regional climate models perform very well across the different weather regimes with a coverage between 80% and 99%, some models are not able to capture

more than 55 to 75 % of the observed regime days. Generally, it can be stated, that the agreement in winter is higher than in summer for almost all RCMs.

Is the RCM ensemble able to represent the temporal and statistical characteristics of the wind field at different locations over the German and Dutch coast of the North Sea?

The daily mean and daily maximum wind speed simulated by the regional climate model ensemble and, in case of mean wind speed, by ERA40 have been compared to observational data, provided by DWD and KNMI, in the coastal area of southern North Sea and the German Bight. Several skill scores have been applied to investigate the model's ability to simulate the present wind climate in the focused region. The analysis refer to two time periods, 1971 - 1983 and 1971 - 2000, predefined by the availability of observations, undisturbed by any changes during the measuring. The models show good or moderate results for bias and standard deviation. Remarkable is a strong negative bias at IJmuiden with values up to -50 %, which is, related to the high mean wind speed at this measuring site, within the range of the other stations (-50 up to +80 %). The models seem to overestimate the mean wind speed at inland stations. The differences between the simulated and observed standard deviations are small and in most of the cases the observed values can be reproduced by the models. For correlation assessment the results for the models are very diverse. Most of the RCMs are highly correlated with observations (0.6 - 0.9), but some models show a very low agreement of 0.3-0.4. Due to data assimilation the correlation for ERA40 and the observed values is between 0.75 and 0.95. Best performance for correlation, close to that one from ERA40, is given by a CLM simulation in 50 km spatial resolution applying spectral nudging, beside the common forcing at the lateral boundaries. The Brier skill score shows an added value for the RCMs compared to ERA40 only at Hohn, Schleswig and IJmuiden and for the CLM simulation mentioned before. The Perkins skill score, comparing similarity of observed and simulated wind speed distributions, identifies much more cases of RCMs added value as in the Brier skill score analysis. Again Hohn, Schleswig and IJmuiden stand out here. Wind speed percentiles, especially for higher values, are often underestimated by the model at coastal stations and overestimated at inland stations. A large spread of the percentile values can be observed among the models.

The simulated daily maximum wind speed distributions only agree with observations if models include a gust parameterisation. Here the models overestimate small and underestimate high percentile values at the near coastal stations e.g. List and IJmuiden, and almost perfectly fit the distribution for inland stations e.g. Soltau. This is supported by the percentiles analysis. In all skill scores seasonal cycles can be detected.

How do atmospheric patterns relate to the representation of the wind climate in the climate model simulations?

From the regional climate models as well as from ERA40 only daily wind speed but no daily prevailing wind direction has been available. With help of the directional component of the wind given by the weather regime classification, mentioned before, the wind performance of the models has been investigated. Bias, differences in standard deviation and the Perkins skill score have been calculated for each model, at the individual locations and depending on the leading regime. Only those days have been taken into account where all RCMs and ERA40 showed the same regime. For German stations the wind speed from southern and south-western wind directions seems to be overestimated by the models. The coarse resolution with 25 km minimum, the smoothed orography and thus reduced roughness length and the fact that the wind from southern directions blows undisturbed over long distances, could lead all together to the detected overestimation. Concerning the standard deviation, an overestimation can be detected for the regime "C", where the wind comes from all directions.

In a second step, some most promising simulations have been selected to increase the number of analysed days and thus increase the robustness of the results. The results showed regimes standing out from the others, but had to be addressed to local effects of the near environment of the measuring sites. The individual wind conditions with respect to the wind directions at the different locations can not be captured by the regional climate models.

What are the benefits and shortcomings of using regional climate models for wind speed analysis compared to the coarse resolution reanalysis fields?

The analysis is based on both, the wind speed from RCMs the same as from ERA40 forcing. An aim was to identify value added by the RCMs to the forcing global model. All skill scores like bias, standard deviation, correlation and percentiles, derived from the RCMs have been compared to the results from ERA40. Other skill scores like the Brier skill score and the Perkins skill score give by modification a direct information on an added value. For locations like IJmuiden, List, Schleswig and Hohn, the RCM ensemble mean shows an added value for most of the skill. The assimilation in general and the assimilation frequency of several observations in the ERA40 and the higher spatial resolution of the RCMs, and thus better resolved orography, seems to be important for the added value assessment. ERA40 performs very well at Jagel, high quality observation data assimilated in the reanalysis with high temporal frequency, whereas the RCMs show a clear added value for most of the skill at Schleswig and IJmuiden, which have been rarely or not at all assimilated.

Is there an added value of the regional climate model results for wind climate by increasing the spatial resolution from 50 km to 25 km?

From most participating institutions within the ENSEMBLES project the hindcast was provided in two spatial resolutions, 50 km and 25 km. For the present study, this gave the opportunity to investigate a possible added value in wind climate assessment from a coarse to higher spatial resolution. Although, the pairs of the RCM simulations have often not been carried out using the same model version or basic setup, a clear added value of the higher resolutions compared to the simulations with 50 km grid space can be observed. This added value can be detected over all investigated skill across the different locations.

6.2 Outlook

In the present study it could be shown, that the underlying soil type distribution is influencing the results from the RCMs. Despite a better representation of soil characteristics, the "summer drying" - problem can not be eliminated completely. However, the resulting positive temperature bias can at least be reduced and the precipitation amount can be increased. In the results from the recently published RCM hindcast simulations for Europe provided by the EURO-CORDEX initiative, the "summer drying" is still visible in six out of nine models (Kotlarski et al. (2014)). The same as in the ENSEMBLES simulations, most of the models use the soil type distribution from FAO. The European Commission Joint Research Center (JRC) released the "European Soil Database" (European Commission (2004)). Based on this data Guillod et al. (2013) investigated the impact on European climate simulations and found similar results as have been presented in this study. Especially with increasing spatial resolutions, the impact of soil characteristics is getting more and more important in RCMs, and thus should be implemented in more detail.

With focus on the area of the North Sea a weather regime classification has been carried out based on MSLP fields from the RCMs and ERA40. The models are able to reproduce the regimes well. The analysis could be repeated with the latest simulations from the CORDEX initiative, mentioned before. Similar to the ENSEMBLES-project two spatial resolutions are available, 50 km and 12 km. The question could be investigated, whether the representation of the regimes in the RCMs increased due to - compared to ENSEMBLES - latest model developments implemented and the higher resolution of the models. In this study only the past development of the regimes has been analysed. With respect to future climate change, possible regime shifts could be identified, based on future mean sea level fields from ENSEMBLES- and CORDEX-simulations.

From the ENSEMBLES simulations the mean wind speed has only been available on a daily basis and without the knowledge of the prevailing direction of the wind per day. The use of higher temporally resolved data, like hourly data, would allow an analysis of the daily cycle of the wind and the development of local circulations like, for example, the land-sea-breeze or the "crash-barrier" effect. Therefore also the spatial resolution should be increased. To investigate the added value due to higher spatial resolution of the models a set of simulations can be set up with systematically increased spatial resolution.

Atmospheric stability has a strong impact on local wind conditions (Kara et al. (2008), Chelton and Freilich (2005)). Therefore, in further evaluation of simulated wind climate, stable, unstable and neutral stability of the atmosphere should be considered.

The spatial resolution of RCMs is a limitation of the models to represent local wind climate depending on the wind direction. Even in very highly resolved regional climate simulation of up to 1km, local effects identified in Section 5.5 will not be captured by the meso-scale models. For the simulation of local wind characteristics due to observation's environment micro-scale models or statistical downscaling methods need to be applied. Another possibility would be to correct the wind observations for the near by obstacles before comparing to RCM results.

The investigations in this study refer to the time periods of 1971–1983 and 1971–2000. The shorter period covers a phase of low NAO activity, between a longer negative and following positive NAO stage. The 30-year time period covers both the phase change with low and diverse NAO activity and a long positive phase until the end of the investigated period (cf. Appendix C). It would be of interest, how the wind speed evaluation results change in the period of 1950 or earlier until today concentrating on short time periods but explicitly strong positive or strong negative NAO phases. As the time periods would be shorter than 30 years, the analysis reflects decadal variability.

Long time series from wind speed observations, which are less disturbed and largely homogenous over time are generally very rare. Additionally, the number of observations to be integrated in the analysis was limited by the availability of the model data. Due to the ERA40 forcing the simulation only covered the time period of 1961–2000. The hindcast simulations provided by the CORDEX initiative for Europe are available for the period of 1989–2009 as they are forced by the reanalysis data from ERAinterim (Dee et al. (2011)). For this period a more dense network of wind speed observations is available and a next investigation concerning wind speed evaluation in a multi model ensemble would face to more robust results.

With the integration of a higher number of measuring sites, a regionalisation based on the observation's characteristics is recommended, to be able to make assumptions for larger

areas. Thereby it should be noted, that only general features can be taken into account, as far as possible independent from local influences, e.g., mean wind speeds and prevailing wind direction. This regionalisation should be tested for validity over time and in different seasons.

List of Abbreviation

ALADIN	RCM developed at CNRM and CHMI
AR	"Atlantic Ridge" - weather regime
BATS	Biosphere-Atmosphere Transfer Scheme
BL	"Blocking"-weather regime
BSH	Bundesamt für Seeschifffahrt und Hydrographie
C4I	Met Eireann, Community Climate Change Consortium for Ireland
CHMI	Czech Hydrometeorological Institute
CLM	Climate Local Model (now called COSMO-CLM)
CNRM	Centre National de Recherche Meteorologiques
CORDEX	COordinated Regional climate Downscaling Experiment
CRCM	Canadian Regional Climate Model
CRU	Climate Research Unit
CTL	control simulation using sandy loam
DMI	Danish Meteorological Institute
DSMW	Digital Soil Map of the World
DWD	Deutscher Wetterdienst
EC	Environment Canada
ECHAM	General Circulation Model developed at MPI Hamburg
ECMWF	European Centre for Medium-Range Weather Forecasts
ENSEMBLES	EU-funded project within the FP6-framework
ERA	ECMWF Re-Analysis
ERAinterim	A continously updated ERA starting from 1979
ERA40	A 45-year ERA from September 1957 to August 2002
EU	European Union
ETHZ	Eidgenössische Technische Hochschule Zürich
FAO	Food and Agriculture Organization
GCM	General Circulation Models
GEM-LAM	Global Environment Multiscale - Limited Area Model
GKSS	GKSS Reseach Center (now HZG)
HC	UK Met Office, Hadley Centre for Climate Prediction and Research
HZG	Helmholtz-Zentrum Geesthacht

ICTP	The Abdus Salam International Centre for Theoretical Physics
JRC	European Commission Joint Research Center
HadRM	HadleyCenter Regional Model
HIRLAM	High Resolution Limited Area Model
INM	Instituto Nacional de Meteorologia
IPCC	Intergovernmental Panel on Climate Change
KNMI	The Royal Netherlands Meteorological Institute
METNO	The Norwegian Meteorological Institute
MOD	modified simulation using silt loam
MPI	Max Planck Institute for Meteorology
MSLP	Mean Sea Level Pattern
NAO	North Atlantic Oscillation
NAO+	"Zonal" - weather regime
NAO-	"Greenland Anticyclone" - weather regime
NCAR	National Center for Atmospheric Research
NCEP	National Centers for Environmental Prediction
OURANOS	Consortium on Regional Climatology and Adaptation to Climate Change
PROMES	Mesoscale Prognosis model
PRUDENCE	EU-funded project
REMO	RCM from MPI and climate Service Center 2.0
RCA	Rosby Centre Regional Climate Model Version
RCM	Regional Climate Model
RMSE	Root mean squared error
SMHI	Swedish Meteorological and Hydrological Institute
STD	standard deviation
UCLM	Universidad de Castilla La Mancha
UKMO	UK MetOffice
UQAM	Université du Québec à Montreal

References

- Akkermans T, Boehme T, Demuzere M, Crewell S, Selbach C, Reinhardt T, Seifert A, Ament F, van Lipzig NPM (2012) Regime-dependent evaluation of accumulated precipitation in COSMO. *Theoretical and Applied Climatology* 108(1-2):39–52, DOI 10.1007/s00704-011-0502-0
- Anders I, Rockel B (2009) The influence of prescribed soil type distribution on the representation of present climate in a regional climate model. *Climate Dynamics* 33(2-3):177–186
- Barthelmie RJ, Palutikof JP (1996) Coastal wind speed modelling for wind energy applications. *Journal of Wind Engineering and Industrial Aerodynamics* 62(2-3):213–236, DOI 10.1016/S0167-6105(96)00079-7
- Baur H (1948) Einführung in die Großwetterkunde. Tech. rep., Dieterichsche Verlagsbuchhandlung
- Baur H, Hess P, Nagel H (1943) Kalender der Großwetterlagen Europas 1881 - 1939. Tech. rep., Forschungsinstitut für langfristige Witterungsvorhersage
- Betts AK (2004) Understanding hydrometeorology using global models. *Bulletin Of The American Meteorological Society* 85(11):1673–1688, DOI 10.1175/BAMS-85-11-1673
- Betts AK, Ball JH, Beljaars ACM, Miller MJ, Viterbo PA (1996) The land surface-atmosphere interaction: A review based on observational and global modeling perspectives. *Journal of Geophysical Research* 101(D3):7209–7225
- Bissolli P, Dittmann E (2001) The objective weather type classification of the German Weather Service and its possibilities of application to environmental and meteorological investigations. *Meteorologische Zeitschrift* 10(4):253–260
- Block A (2007) Unsicherheiten in Oberflächen- und Bodenparametern und ihre Auswirkungen auf die Ergebnisse regionaler Klimasimulationen. PhD thesis, Brandenburgische Technische Universität Cottbus
- Böhm U, Kücken M, Ahrens W, Block A, Hauffe D, Keuler K, Rockel B, Will A (2006) CLM - the climate version of LM: Brief description and long-term applications. *COSMO Newsletter* 6:225–235
- Buchanan C, Beverland I, Heal M (2002) The influence of weather-type and long-range transport on air particle concentrations in Edinburgh, UK. *Atmospheric Environment* 36:5343–5354

- Buishand TA, Brandsma T (1997) Comparison of circulation classification schemes for predicting temperature and precipitation in the Netherlands. *International Journal of Climatology* 17(8):875–889, DOI 10.1002/(SICI)1097-0088(19970630)17:8<875
- Caussinus H, Lyazrhi F (1997) Choosing a linear model with a random number of change-points and outliers. *Annals of the Institute of Statistical Mathematics* 49(4):761–775
- Caussinus H, Mestre O (2004) Detection and correction of artificial shifts in climate series. *Journal of the Royal Statistical Society Series C-applied Statistics* 53:405–425
- Cavicchia L, Storch H, Gualdi S (2014) Mediterranean tropical-like cyclones in present and future climate. *Journal of Climate* 27:7493–7501, DOI 10.1175/JCLI-D-14-00339.1
- Caya D, Laprise R (1999) A semi-implicit semi-Lagrangian regional climate model: The Canadian RCM. *Monthly Weather Review* 127(3):341–362
- Caya D, Laprise R, Giguere M, Bergeron G, Blanchet JP, Stocks BJ, Boer GJ, Mcfarlane NA (1995) Description of the Canadian Regional Climate Model. *Water Air and Soil Pollution* 82(1-2):477–482
- Chelton DB, Freilich MH (2005) Scatterometer-Based Assessment of 10-m Wind Analyses from the Operational ECMWF and NCEP Numerical Weather Prediction Models. *Mon Wea Rev* 133(2):409–429, DOI 10.1175/MWR-2861.1, URL <http://dx.doi.org/10.1175/MWR-2861.1>
- Christensen J, Christensen O, Lopez P, van Meijgaard E, Botzet M (1996) The HIRHAM4 regional atmospheric climate models. *Scientific Report 96-4*, DMI
- Christensen JH, Christensen OB (2007) A summary of the PRUDENCE model projections of changes in European climate by the end of this century. *Clim Change* 81:7–30
- Christensen JH, Machenhauer B, Jones RG, Schär C, Ruti PM, Castro M, Visconti G (1997) Validation of present-day regional climate simulations over Europe: LAM simulations with observed boundary conditions. *Clim Dyn* 13(7-8):489–506
- Christensen JH, Carter TR, Rummukainen M, Amanatidis G (2007) Evaluating the performance and utility of regional climate models: the PRUDENCE project. *Clim Change* 81:1–6
- Collins M, Booth BBB, Harris GR, Murphy JM, Sexton DMH, Webb MJ (2006) Towards quantifying uncertainty in transient climate change. *Climate Dynamics* 27(2-3):127–147

- CPC (2000) Climate Prediction Center (CPC) Daily North Arctic Oscillation Index. URL <ftp://ftp.cpc.ncep.noaa.gov/cwlinks/norm.daily.nao.index.b500101.current.ascii>, (Last time checked 06.02.2015)
- D'Andrea F, Tibaldi S, Blackburn M, Boer G, Deque M, Dix MR, Dugas B, Ferranti L, Iwasaki T, Kitoh A, Pope V, Randall D, Roeckner E, Straus D, Stern W, Van den Dool H, Williamson D (1998) Northern Hemisphere atmospheric blocking as simulated by 15 atmospheric general circulation models in the period 1979-1988. *Climate Dynamics* 14(6):385–407
- Davies H (1976) A lateral boundary formulation for multi-level prediction models. *Quart J Roy Meteor Soc* 102:405–418
- Dee D, Uppala S, Simmons A, Berrisford P, Poli P, Kobayashi S, Andrae U, Balmaseda M, Balsamo G, Bauer P, et al. (2011) The ERA-Interim reanalysis: Configuration and performance of the data assimilation system. *Quart J Roy Meteor Soc* 137(656):553–597, URL <http://onlinelibrary.wiley.com/doi/10.1002/qj.828/full>
- Demuzere M, Werner M, van Lipzig N, Roeckner E (2009) An analysis of present and future ECHAM5 pressure fields using a classification of circulation patterns. *International Journal of Climatology* 29(12):1796–810, DOI 10.1002/joc.1821
- Dickinson R (1984) Modeling evaporation for three-dimensional global climate models. In: Hansen J, Takahashi T (eds) *Climate processes and climate sensitivity*, Geophysical Monograph, vol 29, American Geophysical Union, pp 58–72
- Dickinson R, Henderson-Sellers A, Kennedy P, Wilson M (1986) Biosphere-Atmosphere Transfer Scheme (BATS) forcing the NCAR Community Climate Models. NCAR Technical Note TN275+STR, NCAR
- Diercke C, Dehmel R (1966) *Diercke Weltatlas*, 129th edn. Georg Westermann Verlag
- Dittmann E, Barth S, Lang J, Müller-Westermeier G (1995) Objektive Wetterlagenklassifikation. *Berichte des Deutschen Wetterdienstes* 197, Deutscher Wetterdienst
- Doms G, Förstner J, Heise E, Herzog HJ, Raschendorfer M, Schrodin R, Reinhardt T, Vogel G (2002) A description of the Nonhydrostatic Regional Model LM, Part II: physical parametrization. Tech. rep., Deutscher Wetterdienst, Offenbach
- Donat MG, Leckebusch GC, Pinto JG, Ulbrich U (2010) European storminess and associated circulation weather types: future changes deduced from a multi-model ensemble of GCM simulations. *Climate Research* 42(1):27–43, DOI 10.3354/cr00853

- Donat MG, Renggli D, Wild S, Alexander LV, Leckebusch GC, Ulbrich U (2011) Reanalysis suggests long-term upward trends in European storminess since 1871. *Geophysical Research Letters* 38:L14,703, DOI 10.1029/2011GL047995
- Driessen P (1986) The water balance of soil. In: Van Keulen H, Wolf J (eds) *Modelling of agricultural production: weather, soils and crops*, Poduc, pp 76–116
- Eltahir EAB (1998) A soil moisture rainfall feedback mechanism 1. Theory and observations. *Water Resour Res* 34(4):765–776
- EuropeanCommission (2004) *The european soil database distribution – version 2.0*
- FAO (1996) *The digitized soil map of the World including derived soil properties*. Food and Agriculture Organization, Rom
- FAO/UNESCO (1974) *Soil Map of the World*. UNESCO
- Farda A, Stepanek P, Halenka T, Skalak P, Belda M (2007) Model ALADIN in climate mode forced with ERA40 reanalysis (coarse resolution experiment). *Meteorological Journal* 10:123–130
- Fennessy MJ, Shukla J (1999) Impact of initial soil wetness on seasonal atmospheric prediction. *Journal Of Climate* 12(11):3167–3180
- Ferranti L, Viterbo P (2006) The European summer of 2003: Sensitivity to soil water initial conditions. *Journal Of Climate* 19(15):3659–3680
- Feser F, von Storch H (2005) A spatial two-dimensional discrete filter for limited-area-model evaluation purposes. *Mon Weather Rev* 133(6):1774–1786
- Feser F, Rockel B, von Storch H, Winterfeldt J, Zahn M (2011) Regional Climate Models add Value to Global Model Data: A Review and selected Examples. *Bull Amer Meteor Soc* 92:1181–1192, DOI 10.1175/2011BAMS3061.1
- Findell KL, Eltahir EAB (2003a) Atmospheric controls on soil moisture-boundary layer interactions. Part I: Framework development. *Journal Of Hydrometeorology* 4(3):552–569
- Findell KL, Eltahir EAB (2003b) Atmospheric controls on soil moisture-boundary layer interactions. Part II: Feedbacks within the continental United States. *Journal Of Hydrometeorology* 4(3):570–583

- Fischer EM, Seneviratne SI, Lüthi D, Schär C (2007a) Contribution of land-atmosphere coupling to recent European summer heat waves. *Geophys Res Lett* 34(6), DOI 10.1029/2006GL029068
- Fischer EM, Seneviratne SI, Vidale PL, Lüthi D, Schär C (2007b) Soil moisture - Atmosphere interactions during the 2003 European summer heat wave. *J Clim* 20:5081–5099, DOI 10.1175/JCLI4288.1
- Fowler H, Kilsby C (2002) A weather-type approach to analyzing water resource drought in the Yorkshire region from 1881 to 1998. *Journal of Hydrology* 262:177–192
- Gerstengarbe FW, Werner P, Rüge U (1999) Katalog der Großwetterlagen Europas 1881–1998 nach P. Hess und H. Brezowsky. *Berichte des Deutschen Wetterdienstes Bd. 113* (5. Auflage), Deutscher Wetterdienst and Potsdam-Institut für Klimafolgenforschung
- Giorgi F, Mearns LO (1999) Introduction to special section: Regional climate modeling revisited. *Journal of Geophysical Research-atmospheres* 104(D6):6335–6352
- Guillod B, Davin E, Kündig C, Smiatek G, Seneviratne S (2013) Impact of soil map specifications for European climate simulations. *Climate Dynamics* 40:123–141
- Haase D, Fink J, Haase G, Ruske R, Pecs M, Richter H, Altermann M, Jäger KD (2007) Loess in Europe - its spatial distribution based on a European Loess Map, scale 1 : 2.500.000. *Quat Sci Rev* 26(9-10):1301–1312
- Hagemann S, Botzet M, Machenhauer B (2001) The summer drying problem over southeastern Europe: Sensitivity of the limited area model HIRHAM4 to improvements in physical parameterization and resolution. *Physics and Chemistry of the Earth, Part B* 26(5-6):391–396
- Hagemann S, Machenhauer B, Jones R, Christensen OB, Déqué M, Jacob D, Vidale PL (2004) Evaluation of water and energy budgets in regional climate models applied over Europe. *Clim Dyn* 23(5):547–567, DOI 10.1007/s00382-004-0444-7
- Haugen JE, Haakenstad H (2006) Validation of the HIRHAM version 2 with 50 km and 25 km Resolution. *RegClim General technical Report 9*, Norwegian Meteorological Institute, pp. 159- 180.
- Heikkilä U, Sandvik A, Sorteberg A (2011) Dynamical downscaling of ERA-40 in complex terrain using the WRF regional climate models. *Climate Dynamics* 37(7-8):1551–1564, DOI 10.1007/s00382-010-0928-6, URL <http://dx.doi.org/10.1007/s00382-010-0928-6>

- Herrmann M, Somot S, Calmanti S, Dubois C, Sevault F (2011) Representation of spatial and temporal variability of daily wind speed and of intense wind events over the Mediterranean Sea using dynamical downscaling: impact of the regional climate model configuration. *Natural Hazards and Earth System Sciences* 11(7):1983–2001, DOI 10.5194/nhess-11-1983-2011
- Hess P, Brezowsky H (1952) Katalog der Großwetterlagen Europas. *Berichte Des Deutschen Wetterdienstes in der US Zone 33*, Deutscher Wetterdienst
- Hurrell J (1995) Decadal trends in the North Atlantic Oscillation: regional temperatures and precipitation. *Science* 269:676–679
- Hurrell J, van Loon H (1997) Decadal variations in climate associated with the North Atlantic Oscillation. *Climatic Change* 36:301–326
- IPCC-SRES (2000) Special Report on Emissions Scenarios: A special report of Working Group III of the Intergovernmental Panel on Climate Change. Cambridge University Press
- Jacob D (2001) A note to the simulation of the annual and inter-annual variability of the water budget over the Baltic Sea drainage basin. *Meteorology and Atmospheric Physics* 77(1-4):61–73
- Jacob D, Barring L, Christensen OB, Christensen JH, de Castro M, Déqué M, Giorgi F, Hagemann S, Lenderink G, Rockel B, Sanchez E, Schär C, Seneviratne SI, Somot S, van Ulden A, van den Hurk B (2007) An inter-comparison of regional climate models for Europe: model performance in present-day climate. *Clim Change* 81:31–52
- Jaeger EB, Anders I, Lüthi D, Rockel B, Schär C, Seneviratne SI (2008) Analysis of ERA40-driven CLM simulations for Europe. *Meteorologische Zeitschrift* 17(4):19, DOI 10.1127/0941-2948/2008/0301
- Jenkinson A, Collison F (1977) An initial climatology of gales over the North Sea. *Synoptic Climatology Branch Memorandum 62:18pp*, UK Met Office
- Jones CG, Willén U, Ullerstig A, Hansson U (2004) The Rossby Centre regional atmospheric climate model part I: model climatology and performance for the present climate over Europe. *Ambio* 33:199–210
- Kalnay E, Kanamitsu M, Kistler R, Collins W, Deaven D, Gandin L, Iredell M, Saha S, White G, Woollen J, Zhu Y, Chelliah M, Ebisuzaki W, Higgins W, Janowiak J, Mo

- KC, Ropelewski C, Wang J, Leetmaa A, Reynolds R, Jenne R, Joseph D (1996) The NCEP/NCAR 40-year reanalysis project. *Bull Amer Meteorol Soc* 77(3):437–471
- Kara AB, Wallcraft AJ, Bourassa MA (2008) Air-sea stability effects on the 10 m winds over the global ocean: Evaluations of air-sea flux algorithms. *Journal of Geophysical Research: Oceans* 113(C4):1–14, DOI 10.1029/2007JC004324, URL <http://dx.doi.org/10.1029/2007JC004324>
- Kendall M (ed) (1975) *Rank Correlation Methods*, 4th edn. Charles Griffin, London
- Kiss P, Janosi IM (2008) Comprehensive empirical analysis of ERA-40 surface wind speed distribution over Europe. *Energy Conversion and Management* 49(8):2142–2151, DOI 10.1016/j.enconman.2008.02.003
- Kjellström E, Bärring L, Gollvik S, Hansson U, Jones C, Samuelsson P, Rummukainen M, Ullerstig A, Willen U, Wyser K (2005) A 140-year simulation of European climate with the new version of the Rossby Centre regional atmospheric climate model (RCA3). *SMHI Reports Meteorology and Climatology* 108, SMHI, SE-60176 Norrköping, Sweden
- Kjellström E, Boberg F, Castro M, Christensen J, Nikulin G, Sanchez E (2010) Daily and monthly temperature and precipitation statistics as performance indicators for regional climate models. *Climate Research* 44:135–150
- Koster RD, Suarez MJ (2001) Soil moisture memory in climate models. *Journal Of Hydrometeorology* 2(6):558–570
- Koster RD, Suarez MJ (2003) Impact of land surface initialization on seasonal precipitation and temperature prediction. *Journal Of Hydrometeorology* 4(2):408–423
- Koster RD, Dirmeyer PA, Guo ZC, Bonan G, Chan E, Cox P, Gordon CT, Kanae S, Kowalczyk E, Lawrence D, Liu P, Lu CH, Malyshev S, McAvaney B, Mitchell K, Mocko D, Oki T, Oleson K, Pitman A, Sud YC, Taylor CM, Verseghy D, Vasic R, Xue YK, Yamada T, Team G (2004) Regions of strong coupling between soil moisture and precipitation. *Science* 305(5687):1138–1140
- Koster RD, Guo ZC, Dirmeyer PA, Bonan G, Chan E, Cox P, Davies H, Gordon CT, Kanae S, Kowalczyk E, Lawrence D, Liu P, Lu CH, Malyshev S, McAvaney B, Mitchell K, Mocko D, Oki T, Oleson KW, Pitman A, Sud YC, Taylor CM, Verseghy D, Vasic R, Xue YK, Yamada T (2006) GLACE: The Global Land-Atmosphere Coupling Experiment. Part I: Overview. *J Hydrometeor* 7(4):590–610, DOI 10.1175/JHM511.1

- Kotlarski S, Keuler K, Christensen OB, Colette A, Déqué M, Gobiet A, Goergen K, Jacob D, Lüthi D, van Meijgaard E, Nikulin G, Schär C, Teichmann C, Vautard R, Warrach-Sagi K, Wulfmeyer V (2014) Regional climate modeling on European scales: a joint standard evaluation of the EURO-CORDEX RCM ensemble. *Geoscientific Model Development* 7(4):1297–1333, DOI 10.5194/gmd-7-1297-2014, URL <http://www.geoscientific-model-dev.net/7/1297/2014/>
- Krueger O, Storch H (2011) Evaluation of an air pressure based proxy for storm activity. *Journal of Climate* 24:2612–2619
- Krueger O, Schenk F, Feser F, Weisse R (2013) Inconsistencies between Long-Term Trends in Storminess Derived from the 20CR Reanalysis and Observations. *Journal of Climate* 26(3):868–874, DOI 10.1175/JCLI-D-12-00309.1
- Kunne B (2012) Evaluation of the Wind Field Distribution in the Rossby Center Regional Climate Model RVCA4 of the North Sea for 1979–2010. Tech. rep., Wageningen University
- Lamb H (1972) British Isles weather types and a register of the daily sequence of circulation patterns. *Geophysical Memoirs* 116
- Landberg L, Myllerup L, Rathmann O, Petersen EL, Jorgensen BH, Badger J, Mortensen NG (2003) Wind resource estimation - An overview. *Wind Energy* 6(3):261–271, DOI 10.1002/we.94
- Leckebusch G, Ulbrich U (2004) On the relationship between cyclones and extreme wind-storm events over Europe under climate changes. *Global and Planetary Change* 4:181–193
- Lenderik G, van der Hurk B, van Meijgaard E, van Ulden A, Cujipers H (2003) Simulation of present day climate in RACMO2: first results and model developments. technical report 252:24, KNMI
- Lindenberg J, Mengelkamp HT, Rosenhagen G (2012) Representativity of near surface wind measurements from coastal stations at the German Bight. *Meteorologische Zeitschrift* 21(1):99–106, DOI 10.1127/0941-2948/2012/0131
- Linderson ML (2001) Objective classification of atmospheric circulation over southern Scandinavia. *International Journal of Climatology* 21(2):155–169, DOI 10.1002/joc.604
- Loewe P (2005) Nordseezustand 2003. *Berichte des BSH* 38, BSH

- Loewe P (2009) System Nordsee. Berichte des BSH 44, Bundesamt für Seeschifffahrt und Hydrographie
- Loewe P (2013) System Nordsee. Berichte des BSH 49, Bundesamt für Seeschifffahrt und Hydrographie
- Machenhauer B, Windelband M, Botzet M, Christensen J, M D, Jones R, Ruti P, Visconti G (1998) Validation and analysis of regional present-day climate and climate change simulations over Europe. Report 275, Max-Planck-Institute for Meteorology
- Mann H (1945) Non-parametric tests against trend. *Econometrica* 13:163–171
- Marshall CH, Pielke RA, Steyaert LT, Willard DA (2004) The impact of anthropogenic land-cover change on the Florida peninsula sea breezes and warm season sensible weather. *Mon Weather Rev* 132(1):28–52
- Matulla C, Schöner W, Alexandersson H, Storch H, Wang X (2008) European storminess: Late nineteenth century to present. *Climate Dynamics* 31:125–130, DOI 10.1007/s00382-007-0333-y
- MetOffice (2011) Met Office Northern Hemisphere Mean Sea Level Pressure (MSLP) fields (1873-2005) Data. (01.03.2015). <http://catalogue.ceda.ac.uk/uuid/a2ce888a0a8a8238b1621447e65d5a88>
- Mitchell TD, Jones PD (2005) An improved method of constructing a database of monthly climate observations and associated high-resolution grids. *Int J Climatol* 25(6):693–712, DOI 10.1002/joc.1181
- Moberg A, Jones PD (2004) Regional climate model simulations of daily maximum and minimum near-surface temperatures across Europe compared with observed station data 1961-1990. *Clim Dyn* 23(7-8):695–715
- Moccia J, Arapogianni A, Wilkes J, Kjaer C, Gruet R (2011) Pure power – wind energy targets for 2020 and 2030. European wind energy association report, EWEA
- Najac J, Boe J, Terray L (2009) A multi-model ensemble approach for assessment of climate change impact on surface winds in France. *Climate Dynamics* 32(5):615–634, DOI 10.1007/s00382-008-0440-4
- Noguer M, Jones R, Murphy J (1998) Sources of systematic errors in the climatology of a regional climate model over Europe. *Clim Dyn* 14(10):691–712

- Pan ZT, Arritt RW, Gutowski WJ, Takle ES (2001) Soil moisture in a regional climate model: simulation and projection. *Geophys Res Lett* 28(15):2947–2950
- Pearson K (1895) Notes on regression and inheritance in the case of two parents. *Proceedings of the Royal Society of London* 58:240–242
- Perkins SE, Pitman AJ, Holbrook NJ, McAneney J (2007) Evaluation of the AR4 climate models' simulated daily maximum temperature, minimum temperature, and precipitation over Australia using probability density functions. *Journal of Climate* 20(17):4356–4376, DOI 10.1175/JCLI4253.1
- Picard F, Robin S, Lavielle M, Vaisse C, Daudin JJ (2005) A statistical approach for array CGH data analysis. *Bmc Bioinformatics* 6, DOI 10.1186/1471-2105-6-27
- Pielke RA (2001) Influence of the spatial distribution of vegetation and soils on the prediction of cumulus convective rainfall. *Rev Geophys* 39(2):151–177
- Pielke RA, Walko RL, Steyaert LT, Vidale PL, Liston GE, Lyons WA, Chase TN (1999) The influence of anthropogenic landscape changes on weather in south Florida. *Mon Weather Rev* 127(7):1663–1673
- Plummer DA, Caya D, Frigon A, Cote H, Giguere M, Paquin D, Biner S, Harvey R, De Elia R (2006) Climate and climate change over North America as simulated by the Canadian RCM. *Journal of Climate* 19(13):3112–3132
- Post P, Truija V, Tuulik J (2002) Circulation weather types and their influence on temperature and precipitation in Estonia. *Boreal Environment Research* 7(3):281–289
- Prein AF, Gobiet A, Suklitsch M, Truhetz H, Awan NK, Keuler K, Georgievski G (2013) Added value of convection permitting seasonal simulations. *Climate Dynamics* 41(9–10):2655–2677, DOI 10.1007/s00382-013-1744-6
- Prömmel K, Geyer B, Jones JM, Widmann M (2010) Evaluation of the skill and added value of a reanalysis-driven regional simulation for Alpine temperatures. *International Journal of Climatology* 30(5):760–773, DOI 10.1002/joc.1916
- Pryor SC, Schoof JT (2010) Importance of the SRES in projections of climate change impacts on near-surface wind regimes. *Meteorologische Zeitschrift* 19(3):267–274, DOI 10.1127/0941-2948/2010/0454
- Pryor SC, Barthelmie RJ, Kjellstrom E (2005a) Potential climate change impact on wind energy resources in northern Europe: analyses using a regional climate models. *Climate Dynamics* 25(7–8):815–835, DOI 10.1007/s00382-005-0072-x

- Pryor SC, Schoof JT, Barthelmie RJ (2005b) Climate change impacts on wind speeds and wind energy density in northern Europe: empirical downscaling of multiple AOGCMs. *Climate Research* 29(3):183–198, DOI 10.3354/cr029183
- Pryor SC, Barthelmie RJ, Clausen NE, Drews M, MacKellar N, Kjellstroem E (2012) Analyses of possible changes in intense and extreme wind speeds over northern Europe under climate change scenarios. *Climate Dynamics* 38(1-2):189–208, DOI 10.1007/s00382-010-0955-3
- Radu R, Deque M, Somot S (2008) Spectral nudging in a spectral regional climate model. *Tellus Series A-dynamic Meteorology and Oceanography* 60(5):898–910
- Räisänen J, Hansson U, Ullerstig A, Doscher R, Graham LP, Jones C, Meier HEM, Samuelsson P, Willen U (2004) European climate in the late twenty-first century: regional simulations with two driving global models and two forcing scenarios. *Clim Dyn* 22(1):13–31
- Rockel B, Woth K (2007) Extremes of near-surface wind speed over Europe and their future changes as estimated from an ensemble of RCM simulations. *Clim Change* 81:267–280
- Rowell DP, Jones RG (2006) Causes and uncertainty of future summer drying over Europe. *Clim Dyn* 27(2-3):281–299
- Sanchez E, Gallardo C, Gaertner MA, Arribas A, Castro M (2004) Future climate extreme events in the Mediterranean simulated by a regional climate model: a first approach. *Global and Planetary Change* 44(1-4):163–180
- Sánchez E, Gaertner MA, Gallardo C, Padorno E, Arribas A, Castro M (2007) Impacts of a change in vegetation description on simulated European summer present-day and future climates. *Clim Dyn* 29(2-3):319–332
- Sanchez-Gomez E, Somot S, Deque M (2009) Ability of an ensemble of regional climate models to reproduce weather regimes over Europe-Atlantic during the period 1961-2000. *Climate Dynamics* 33(5):723–736, DOI 10.1007/s00382-008-0502-7
- Schär C, Lüthi D, Beyerle U, Heise E (1999) The soil-precipitation feedback: Area process study with a regional climate model. *J Clim* 12(3):722–741
- Schrodin R, Heise E (2001) The Multi-Layer Version of the DWD Soil Model TERRA-LM. COSMO Technical Report 2, Deutscher Wetterdienst
- Seneviratne SI, Koster R, Guo Z, Dirmeyer A, Kowalczyk E, Lawrence D, Liu P, Lu CH, Mocko D, Oleson K, Verseghy D (2006a) Soil moisture memory in AGCM simulations:

- Analysis of Global Land-Atmosphere Coupling Experiment (GLACE) data. *Journal of Hydrometeorology* 7:1090–1112
- Seneviratne SI, Lüthi D, Litschi M, Schär C (2006b) Land-atmosphere coupling and climate change in Europe. *Nature* 443(7108):205–209, DOI 10.1038/nature05095
- von Storch H, Langenberg H, Feser F (2000) A spectral nudging technique for dynamical downscaling purposes. *Monthly Weather Review* 128(10):3664–3673
- Stremme H (1937) *International Soil Map of Europe*, 1:2500000. Gea Verlag, Berlin
- Suselj K, Sood A, Heinemann D (2010) North Sea near-surface wind climate and its relation to the large-scale circulation patterns. *Theoretical and Applied Climatology* 99(3-4):403–419, DOI 10.1007/s00704-009-0149-2
- Taylor KE (2001) Summarizing multiple aspects of model performance in a single diagram. *Journal of Geophysical Research* 106 (D7):7183–7192
- Tebaldi C, Knutti R (2007) The use of the multi-model ensemble in probabilistic climate projections. *Philosophical Transactions of the Royal Society of London A: Mathematical, Physical and Engineering Sciences* 365(1857):2053–2075, DOI 10.1098/rsta.2007.2076
- Teuling A, Seneviratne SI (2008) Contrasting spectral changes limit albedo impact on land-atmosphere coupling during the 2003 European heat waves. *Geophys Res Lett* 35:L03,401, DOI 10.1029/2007GL032778
- Trigo RM, DaCamara CC (2000) Circulation weather types and their influence on the precipitation regime in Portugal. *International Journal of Climatology* 20(13):1559–1581, DOI 10.1002/1097-0088(20001115)20:13<1559
- Uppala SM, Kallberg PW, Simmons AJ, Andrae U, Bechtold VD, Fiorino M, Gibson JK, Haseler J, Hernandez A, Kelly GA, Li X, Onogi K, Saarinen S, Sokka N, Allan RP, Andersson E, Arpe K, Balmaseda MA, Beljaars ACM, Van De Berg L, Bidlot J, Bormann N, Caires S, Chevallier F, Dethof A, Dragosavac M, Fisher M, Fuentes M, Hagemann S, Holm E, Hoskins BJ, Isaksen I, Janssen PAEM, Jenne R, McNally AP, Mahfouf JF, Morcrette JJ, Rayner NA, Saunders RW, Simon P, Sterl A, Trenberth KE, Untch A, Vasiljevic D, Viterbo P, Woollen J (2005) The ERA-40 re-analysis. *Quarterly Journal of the Royal Meteorological Society* 131(612):2961–3012, DOI 10.1256/qj.04.176
- Vidale PL, Lüthi D, Frei C, Seneviratne SI, Schär C (2003) Predictability and uncertainty in a regional climate model. *J Geophys Res* 108(D18):4586

- Wanner H, Brönnimann S, Casty C, Gyalistras D, Luterbacher J, Schmutz C, Stephenson D, Xoplaki E (2001) North Atlantic Oscillation - concepts and studies. *Surveys in Geophysics* 22:321–328
- Winterfeldt J, Weisse R (2009) Assessment of Value Added for Surface Marine Wind Speed Obtained from Two Regional Climate Models. *Monthly Weather Review* 137(9):2955–2965, DOI 10.1175/2009MWR2704.1
- Winterfeldt J, Geyer B, Weisse R (2011) Using QuikSCAT in the added value assessment of dynamically downscaled wind speeds. *International Journal of Climatology* 31(7):1028–1039, DOI 10.1002/joc.2105
- Wu WR, Dickinson RE (2004) Time scales of layered soil moisture memory in the context of land-atmosphere interaction. *Journal Of Climate* 17(14):2752–2764
- Yue S, Pilon PJ, Phinney B, Cavadias G (2002) The influence of autocorrelation on the ability to detect trend in hydrological series. *Hydrological Processes* 16(16):1807–1829
- Zaitchik BF, Evans JP, Geerken RA, Smith RB (2007) Climate and vegetation in the Middle East: Interannual variability and drought feedbacks. *Journal Of Climate* 20(15):3924–3941, DOI 10.1175/JCLI4223.1

A RCMs in the Multi Model Ensemble

Model	RCA3	Aladin	Aladin- RM4.5	HIRHAM	CLM	CLM	HadRM	RegCM3
Institution	C4I	CHMI	CNRM	DMI	ETHZ	GKSS	HC	ICTP
Country	Ireland	Czech Rep.	France	Danmark	Switzerland	Germany	Great Britain	Italy
Grid	rot	lc	lc	rot	rot	rot	rot	
grid dimensions								
- 50 km	–	84x95	93x101	90x95	91x97	85x95	118x115	86x98
- 25 km	190x190	167x189	213x213	174x190	193x201	–	220x214	174x200
number of atm. layers	31	27	31		32	32	19	34
sftls tile appr.	yes	no	no	no	no	no	yes	-

Table A.1: Part 1: Summary of grid configurations for all RCMs.

Model	RCA3	RACMO2	HIRHAM	REMO	RCA3	PROMES	CRCM
Institution	INM	KNMI	METNO	MPI	SMHI	UCLM	EC
Country	Spain	Netherlands	Norway	Germany	Sweden	Spain	Canada
Grid	rot	rot	rot	rot	rot	rot	rot
grid dimensions							
- 50 km	198x100	85x95	85x95	85x95	91x91	85x95	104x94
- 25 km	230x141	170x190	170x190	170x190	170x190	170x190	221x209
number of atm. layers	31	40	31	27	24	28	29
sftls tile appr.	yes	yes	no	–	yes	yes	–

Table A.2: Part 2: Summary of grid configurations for all RCMs.

B Statistical values for the German and Dutch observations

ID	Name	\bar{x}_0	σ_0	$\bar{x}_0^{Oct-Mar}$	$\sigma_0^{Oct-Mar}$	$\bar{x}_0^{Apr-Sep}$	$\sigma_0^{Apr-Sep}$
1529	Soltau	2.94	1.35	3.12	1.4	2.76	1.24
1402	List	6.97	2.81	7.03	2.8	6.89	2.77
1468	Bremerhaven	5.18	2.38	5.32	2.4	5.03	2.27
1474	Bremen	4.33	1.96	4.64	2.04	4.02	1.78
1040	Helgoland	6.71	2.88	6.87	2.84	6.55	2.86
1438	Schleswig	3.88	1.67	4.11	1.81	3.66	1.45
1444	Hohn	4.19	2.14	4.55	2.3	3.82	1.84
1497	Oldenburg	3.77	1.71	4.09	1.8	3.45	1.51
1132	Lingen	3.16	1.31	3.36	1.37	2.95	1.18
9007	Wittmundhafen	4.94	2.41	5.39	2.59	4.48	2.09
1730	Jagel	4.83	2.31	5.15	2.49	4.5	2.03
260	De Bilt	3.21	1.5	3.54	1.61	2.88	1.28
270	Leeuwarden	5.22	2.25	5.63	2.4	4.82	1.98
280	Eelde	4.58	2.16	4.9	2.28	4.24	1.9
370	Eindhoven	4.53	1.99	4.86	2.09	4.19	1.81
375	Volkel	4.18	2.01	4.57	2.06	3.78	1.86
380	Beek	4.29	1.96	4.61	2.03	3.95	1.79
344	Zestienhoven	5	2.39	5.33	2.46	4.64	2.21
290	Twenthe	3.5	1.55	3.73	1.63	3.26	1.41
350	Gilze-Rijen	4.3	1.9	4.61	2.03	3.97	1.67
225	IJmuiden	7.29	3.05	7.44	3.08	7.09	3.02

Table B.1: Statistical values for the German and Dutch observations for daily mean wind speed covering the time period t1: 1971 to 1983.

ID	Name	\bar{x}_{0max}	σ_{0max}	$\bar{x}_{0max}^{Oct-Mar}$	$\sigma_{0max}^{Oct-Mar}$	$\bar{x}_{0max}^{Apr-Sep}$	$\sigma_{0max}^{Apr-Sep}$
1529	Soltau	8.95	3.84	9.24	4.07	8.65	3.66
1402	List	15.1	5.22	15.34	5.66	14.87	5.49
1468	Bremerhaven	12.08	4.56	12.34	4.87	11.79	4.49
1474	Bremen	10.9	4.34	11.23	4.6	10.54	4.16
1040	Helgoland	13.84	4.5	14.11	4.91	13.53	4.97
1438	Schleswig	10.88	4.33	11.21	4.65	10.53	4.09
1444	Hohn	10.56	3.99	10.91	4.28	10.2	3.7
1497	Oldenburg	10.5	4.45	10.93	4.76	10.06	4.13
1132	Lingen	9.48	3.87	9.79	4.13	9.15	3.68
9007	Wittmundhafen	11.9	4.59	12.41	4.99	11.38	4.39
1730	Jagel	11.73	4.85	11.99	5.27	11.44	4.52
260	De Bilt	9.92	3.93	10.49	4.19	9.34	3.58
270	Leeuwarden	11.7	4.32	12.15	4.67	11.23	4.08
280	Eelde	11.3	4.15	11.66	4.53	10.92	3.95
370	Eindhoven	11.12	3.92	11.47	4.14	10.77	3.68
375	Volkel	10.1	3.81	10.52	4.03	9.67	3.63
380	Beek	10.27	4.07	10.72	4.38	9.8	3.97
344	Zestienhoven	11.6	4.27	12.05	4.58	11.12	4.1
290	Twenthe	9.86	3.59	10.2	3.84	9.49	3.32
350	Gilze-Rijen	10.89	4.01	11.24	4.24	10.53	3.73
225	IJmuiden	13.86	5.12	14.09	5.44	13.56	5.05

Table B.2: Statistical values for the German and Dutch observations for daily maximum wind speed covering the time period t1: 1971 to 1983.

C The North Atlantic Oscillation (NAO) and the NAO-index

The atmospheres and oceans variability in the North Atlantic and Europe is strongly dominated by the North Atlantic Oscillation (NAO). In the 18th century, where instrumental observation was limited, the scientific discussion on the NAO as the climate see-saw started. Later in the 19th and 20th century the NAO was linked to surface pressure fields and extensive statistical analysis have been carried out to understand the underlying processes (Hurrell (1995), Hurrell and van Loon (1997), Wanner et al. (2001)).

The NAO describes the variability in the difference of atmospheric pressure at sea level between the Icelandic Low and the Azores High. During the positive phase of the NAO the pressure gradient between the two locations is stronger than normal. This enhances westerly winds across the North Atlantic. In consequence this leads to northerly tracks of cyclones, which results in wind to a warm and moist air transport to Central and North Europe. In contrast South Europe is left out from cyclone tracks and thus leads to drier conditions than normal. The negative NAO phase the pressure difference the Icelandic Low and the Azores High is weaker compared to the mean state, followed by also weaker westerly winds. Cyclone tracks pass more in the South, which causes wet conditions in the Mediterranean region and wet and dry conditions in the north of Europe.

The NAO is most pronounced in winter. The temporal variations is indicated by an index. There are different methods to derive the NAO-index. The station-based index of the NAO is based on the difference of normalized sea level pressure (SLP) between Lisbon, Portugal and Stykkisholmur/Reykjavik, Iceland since 1864. As the Icelandic Low and the Azores High are not stationary, another method to calculate the NAO-state is a principal component (PC)-based approach. The PC-based indices of the NAO are the time series of the leading Empirical Orthogonal Function (EOF) of SLP anomalies over the Atlantic sector, 20°N-80°N, 90°W-40°E. Advantages of this method are more optimal representations of the full spatial patterns of the NAO.

In the present study the PC-based NAO-index was used CPC (2000). Figure C.1 shows mean annual NAO-index per year for different seasons.

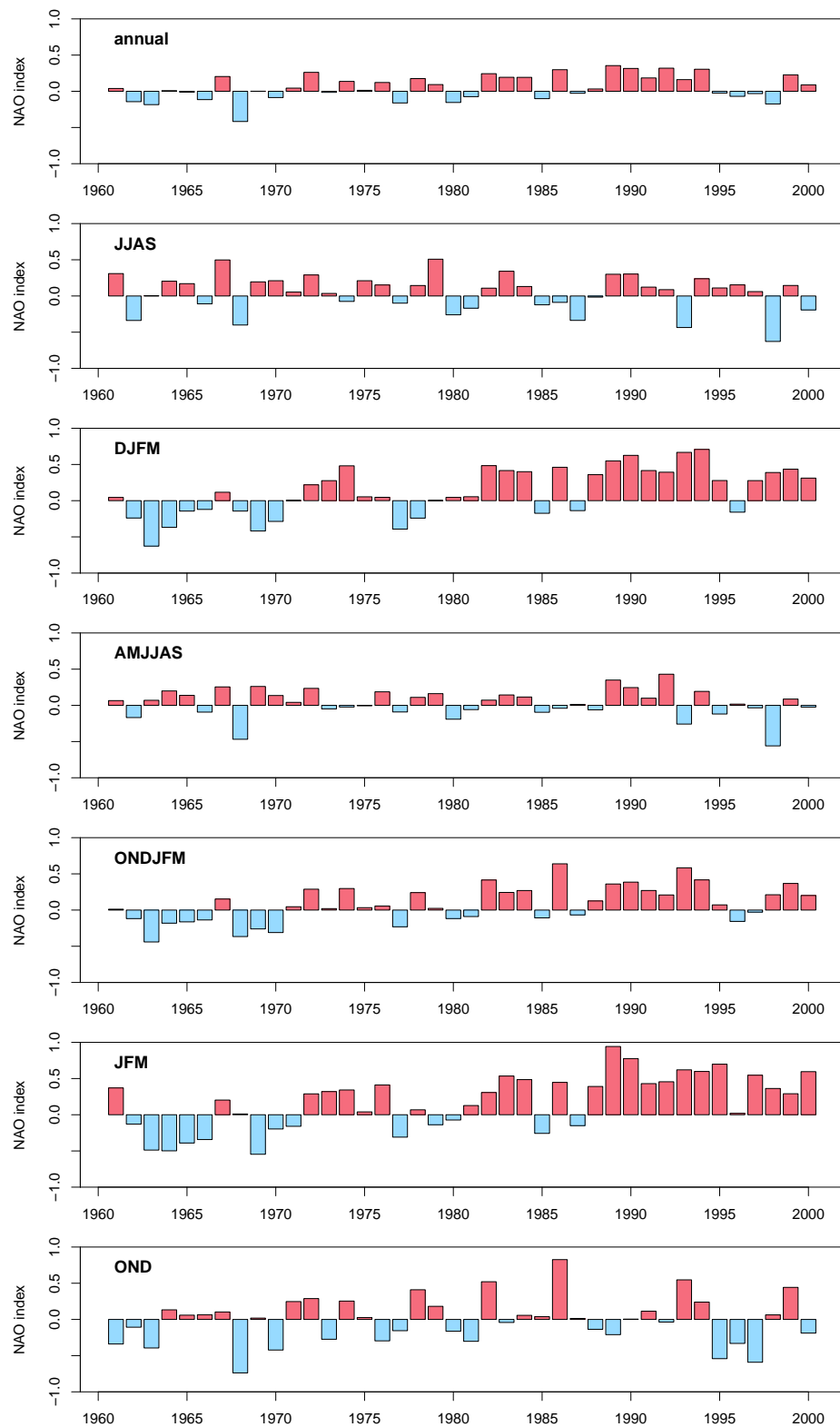


Figure C.1: Annual mean NAO-Index for different seasons in the time period of 1961 to 2000.

D Weather regime classification

The objective method to classify the circulation weather types at surface has been developed by Jenkinson and Collison (1977). The distribution of the mean sea level air

pressure is used to derive indices for wind and vorticity. Via empirical relations between these indices a circulation type but also storm events can be identified.

Wind

The horizontal equation of motion is reduced by a geostrophic approximation to a diagnostic equilibrium between the Coriolis acceleration and the pressure gradient:

$$\begin{aligned} -fu &= -2\Omega \sin\varphi u = \rho^{-1} \frac{\delta p}{\delta y} = \rho^{-1} \frac{\delta p}{R\delta\varphi} \approx \rho^{-1} \frac{\Delta_\varphi p}{R\Delta\varphi} \\ fv &= 2\Omega \sin\varphi v = \rho^{-1} \frac{\delta p}{\delta x} = \rho^{-1} \frac{\delta p}{R\cos\varphi\delta\lambda} \approx \rho^{-1} \frac{\Delta_\lambda p}{R\cos\varphi\Delta\lambda} \end{aligned} \quad (\text{D.1})$$

where x and y are the arc length across the parallel φ and the meridian λ within the spherical coordinate system with R as the Earth's radius. The orientation of the axes is Eastward and Northward and vertical positive in the upward direction. In this case $u > 0$ and $v = 0$ ($u=0, v>0$) represent a pure wind from the West (from the South).

Furthermore ρ and p are air density and air pressure at the mean sea level, $\Omega (= 2\pi/24h)$ the angular velocity of the Earth's rotation and $f (= 2\Omega \sin\varphi)$ the Coriolis parameter dependent on the latitude. The Coriolis acceleration leads to a deflection to the right of the wind along the strongest pressure gradients. In the geostrophical balance is the wind direction tangential to the isobars and wind speed is proportional to the pressure gradient.

The following constant values

$$\begin{aligned} \rho &= 1.225 \text{ kg/m}^3 \\ \Omega &= 2\pi/86400 \text{ s} = 0.7272 * 10^{-4} (\text{radian}) \text{ s}^{-1} \\ f(55^\circ N) &= 1.1914 * 10^{-4} (\text{radian}) \text{ s}^{-1} \\ R &= R_e = 6\,366\,707 \text{ m} \\ \Delta\lambda &= \Delta\varphi = 10^\circ = 0.17453283 (\text{radian}) \\ R\Delta\varphi &= 600' * 1852 \text{ m} = 600 \text{ sm} \end{aligned} \quad (\text{D.2})$$

have been used for the definition of the proportionality

$$c_w = \frac{100}{\rho f R \Delta\varphi} = 0.62 \text{ m}^2 \text{ s/kg} \quad (\text{D.3})$$

and the simplification of the Equations D.1

$$\begin{aligned} u(m/s) &= c_w \Delta_\varphi p = 0.62 u^* \\ v(m/s) &= \frac{c_w \Delta_\lambda p}{\cos \varphi} = 0.62 v^*. \end{aligned} \quad (\text{D.4})$$

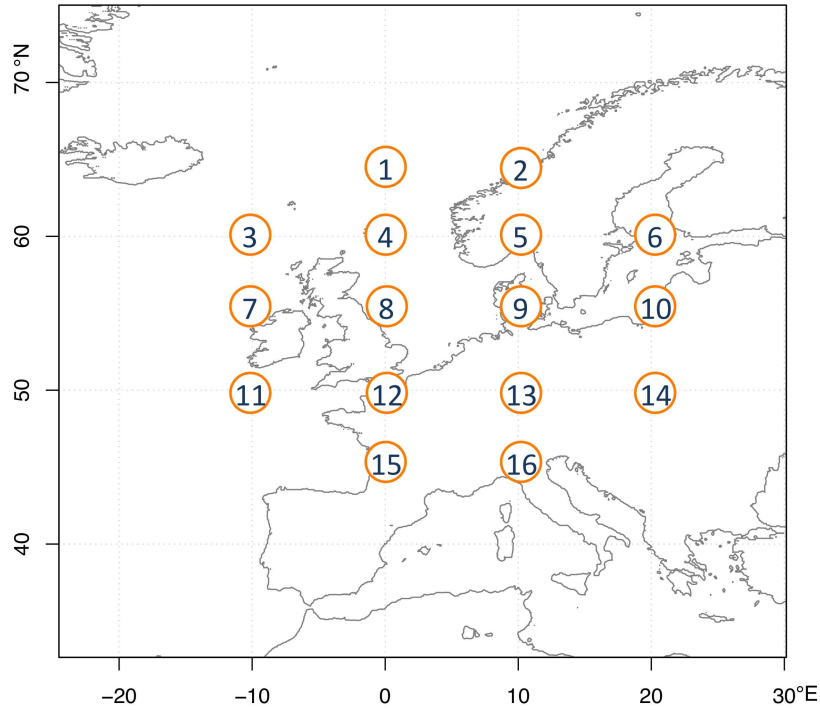


Figure D.1: Positions for weather regime classification.

Finally, the approximation of the wind (and vorticity) is based on the pattern of mean sea level pressure. The method is a combination from discrete differentiation and weighted (binomial) mean from pressure values at the 16 locations signed in Figure D.1 and results in speed indices given in hPa :

$$\begin{aligned} u^* (hPa) &= -\{p(\lambda_0, \varphi_0 + \Delta\varphi/2) - p(\lambda_0, \varphi_0 - \Delta\varphi/2)\} \\ &= \frac{1}{2}(p_{12} + p_{13}) - \frac{1}{2}(p_4 + p_5) \end{aligned} \quad (\text{D.5})$$

$$\begin{aligned} v^* (hPa) &= \frac{1}{\cos \varphi_0} \{p(\lambda_0 + \Delta\lambda/2, \varphi_0) - p(\lambda_0 - \Delta\lambda/2, \varphi_0)\} \\ &= \frac{1}{\cos 55^\circ} \left\{ \frac{1}{4}(p_5 + 2p_9 + p_{13}) - \frac{1}{4}(p_4 + 2p_8 + p_{12}) \right\} \end{aligned} \quad (\text{D.6})$$

The locations taken into account are centered over the North Sea at $(\lambda_0, \varphi_0) = (5^\circ \text{ E}, 55^\circ \text{ N})$, and are representative for the area $0^\circ - 10^\circ \text{ E}$ and $50^\circ - 60^\circ \text{ N}$.

The resulting wind vector V^* and the wind direction ϑ is calculated by

$$V^* = \sqrt{u^{*2} + v^{*2}} \quad (\text{D.7})$$

and

$$\vartheta = \frac{180^\circ}{\pi} \text{atan}(v^*/u^*) \quad (\text{D.8})$$

Vorticity

The relative vorticity is defined as the vertical component of the rotation the wind field and, under geostrophic conditions, proportional to the divergence of the pressure gradient

$$\zeta = \frac{\delta v}{\delta x} - \frac{\delta u}{\delta y} \approx \frac{1}{\rho f} \left\{ \frac{\delta^2 p}{\delta x^2} + \frac{\delta^2 p}{\delta y^2} \right\}, \quad (\text{D.9})$$

if the first derivative of the Coriolis parameter f is suppressed. The same as before $R \cos \varphi \delta \lambda$ and $R \Delta \varphi$ are described as dx and dy . Due to $\Delta \varphi = \Delta \lambda$, the proportional value

$$c_\zeta = \frac{c_w}{R \Delta \varphi} = 0.55 \times 10^{-6} \text{ ms/kg} \quad (\text{D.10})$$

is introduced and the speed shear in Equation D.9 is transformed in the discrete form:

$$\zeta(s^{-1}) = c_\zeta \left\{ \frac{\Delta \lambda V^*}{2 \cos \varphi} - \Delta \varphi k_f u^* \right\} = c_\zeta \{ \zeta_v^* + \zeta_u^* \} = 0.55 \times 10^{-6} \zeta^* \quad (\text{D.11})$$

The western and southern shear vorticity index is calculated by a linear combination of air pressure (hPa).

$$\begin{aligned}
\zeta_u^* &= \left\{ \frac{\sin\varphi_0}{\sin(\varphi_0 + \Delta\varphi/2)} u^*(\lambda_0, \varphi_1 + \Delta\varphi/2) - \frac{\sin\varphi_0}{\sin(\varphi_0 + \Delta\varphi/2)} u^*(\lambda_0, \varphi_1 + \Delta\varphi/2) \right\} \\
&= \frac{\sin 55^\circ}{\sin 50^\circ} \left\{ \frac{1}{2} [(p_{15} + p_{16}) - (p_8 + p_9)] \right\} \\
&\quad - \frac{\sin 55^\circ}{\sin 60^\circ} \left\{ \frac{1}{2} [(p_8 + p_9) - (p_1 + p_2)] \right\}
\end{aligned} \tag{D.12}$$

$$\begin{aligned}
\zeta_v^* &= \frac{1}{2\cos\varphi_0} \{v^*(\lambda_0 + \Delta\lambda, \varphi_0) - v^*(\lambda_0 + \Delta\lambda, \varphi_0)\} \\
&= \frac{1}{2\cos^2 55^\circ} \left\{ \frac{1}{4} [(p_6 + 2p_{10} + p_{14}) - (p_5 + 2p_9 + p_{13})] - \frac{1}{4} [(p_4 + 2p_8 + p_{12}) - (p_3 + 2p_7 + p_{11})] \right\}
\end{aligned} \tag{D.13}$$

Criteria for weather classification

(In Section 4.3 the method of the classification from wind- and vorticity-index has been already described, but for the sake of completeness, listed again at this point.)

The classification basically uses empirical relations between the wind-index V^* and the vorticity-index ζ^* as listed in Table D.1.

Table D.1: Relations between wind-index V^* and the vorticity-index ζ^* to derive the weather classes

condition	flow	type
$ \zeta^* < V^*$	directional	e.g. NW, wind direction
$ \zeta^* > 2V^*$	rotational	C (if $\zeta^* > 0$), cyclonic A (if $\zeta^* < 0$), anticyclonic
$V^* \leq \zeta^* \leq 2V^*$	hybrid	e.g. CW
$V^* \leq 6hPa \leq \zeta^* $	diffuse	UNC, unclassified

In this way 27 different weather types can be distinguished: beside the predefined 8 prevailed wind directions and the two possibilities on cyclonic or anticyclonic turbulences, 2x8 hybrid weather types can be defined. Additionally there is an unclassifiable type (UNC), which mainly occurs in combination with weak pressure gradients.

Beside the weather types also storm events can be identified and quantified. The storm

index G^* is calculated from the wind- and vorticity-indices.

$$G^{*2} = \sqrt{V^{*2} + \zeta^{*2}/4} \quad (\text{D.14})$$

Table D.2: Reanalysis data set dependent thresholds for storm-index G^* to define storm categories

G^* (hPa) <			severity	type
UKMO	NCEP I	ERA40		
30	28.3	29.0	gale	G
40	36.6	37.9	severe gale	SG
50	44.6	45.2	very severe gale	VSG

E Additional Material

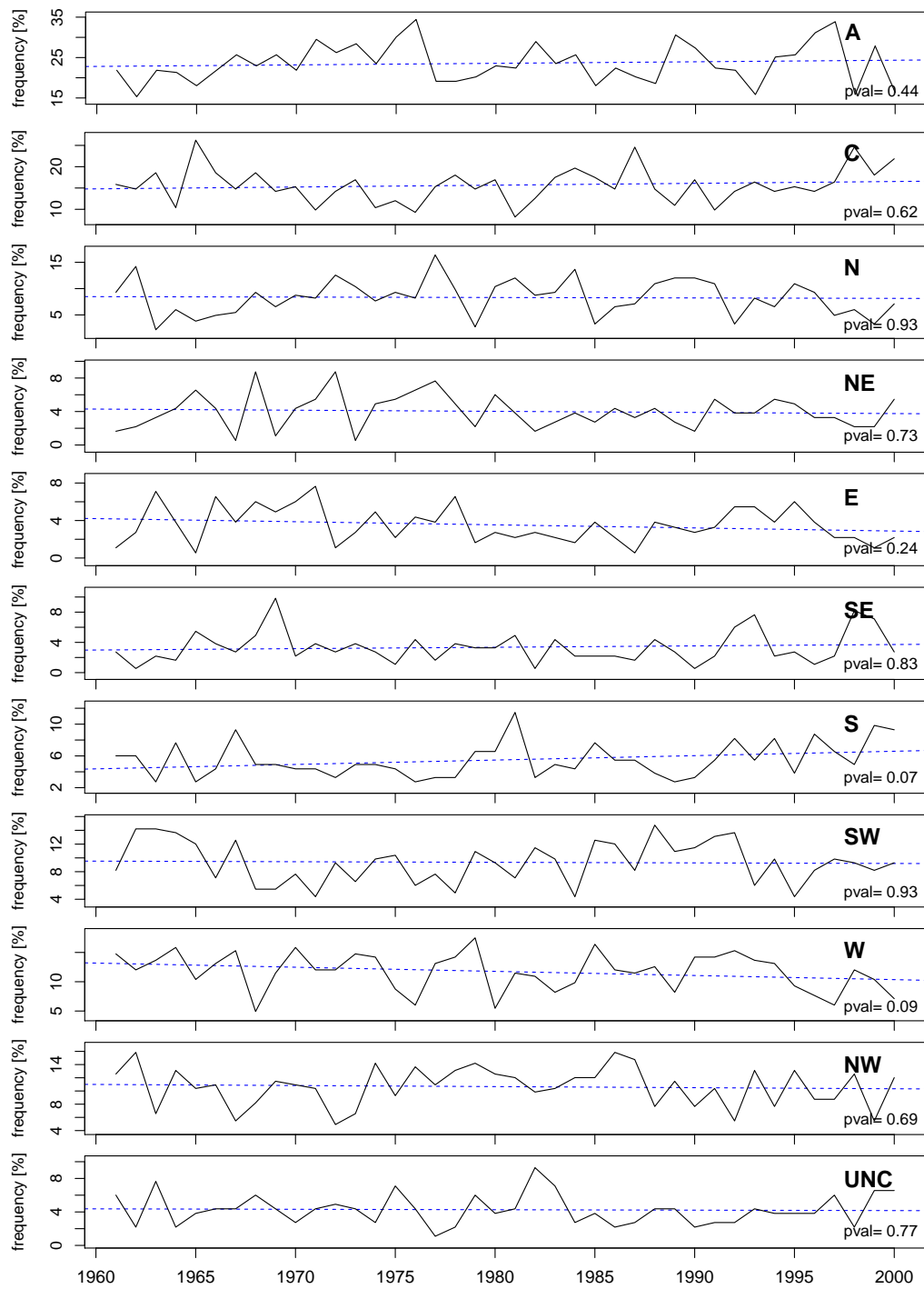


Figure E.1: Annual occurrence of each regime from April to September in the time period of 1961- 2000 (black) and linear trend (blue dashed line and in case of significance blue solid line).

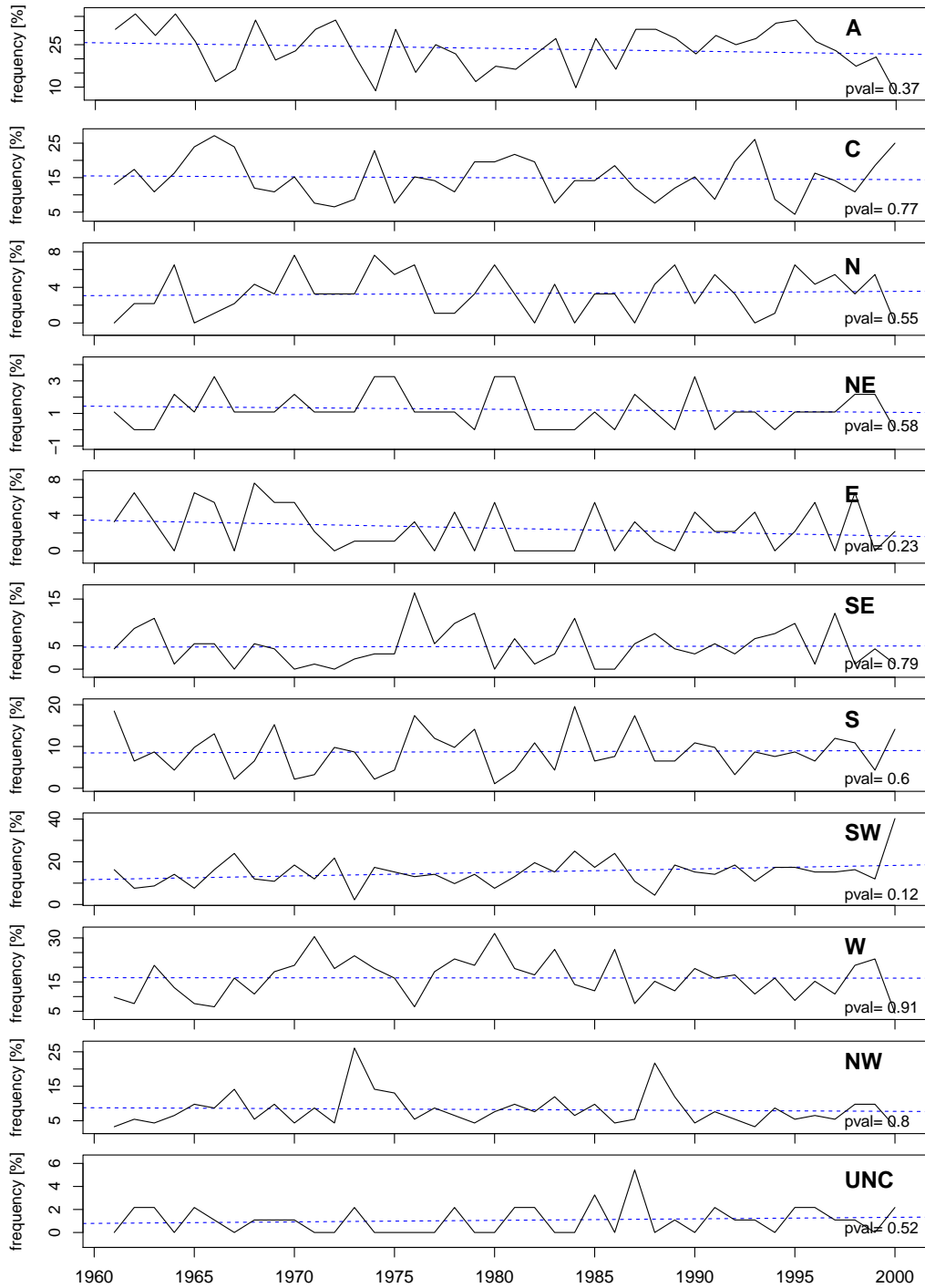


Figure E.2: Annual occurrence of each regime from October to December in the time period of 1961- 2000 (black) and linear trend (blue dashed line and in case of significance blue solid line).

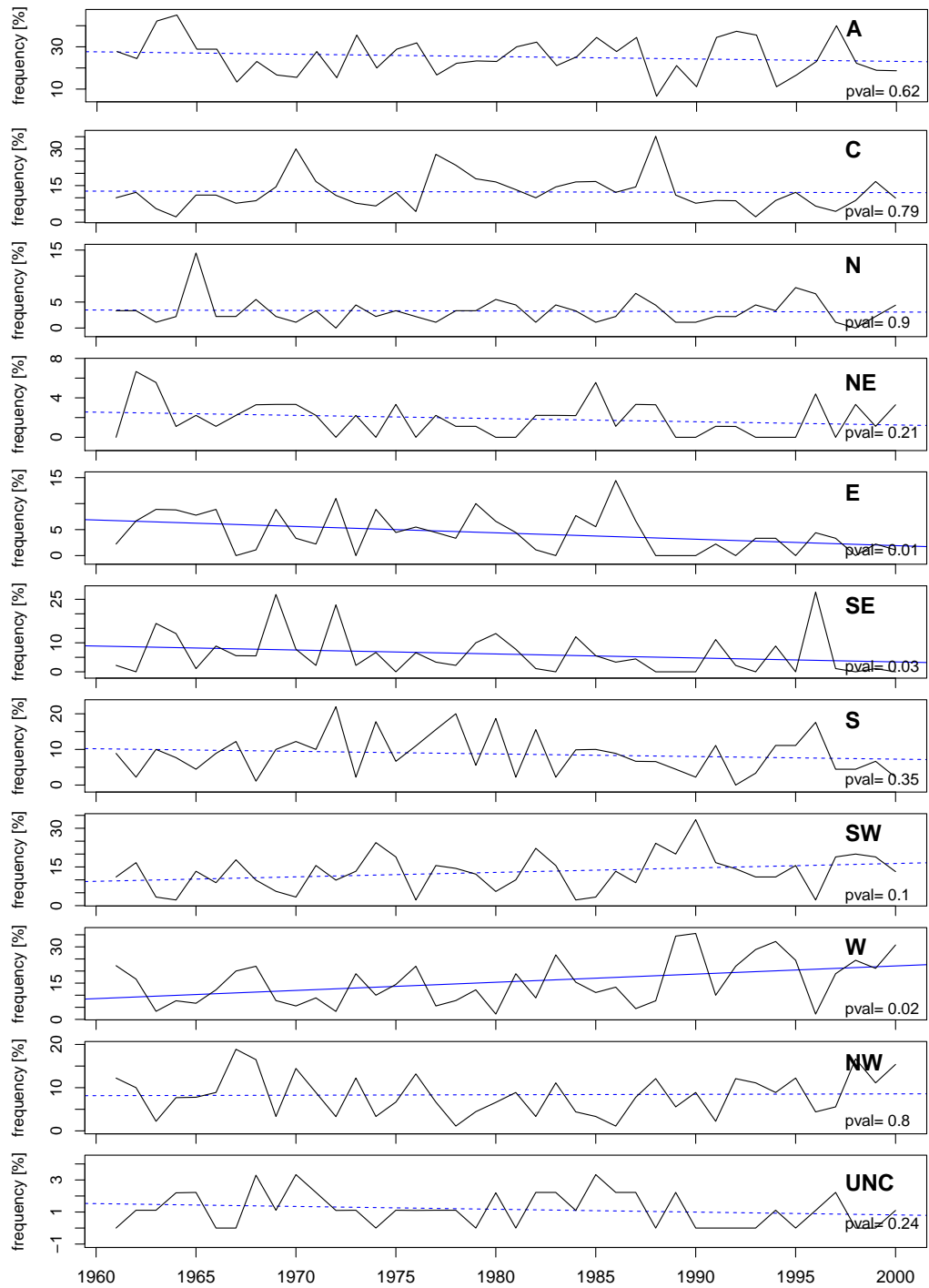


Figure E.3: Annual occurrence of each regime from January to March in the time period of 1961- 2000 (black) and linear trend (blue dashed line and in case of significance blue solid line).

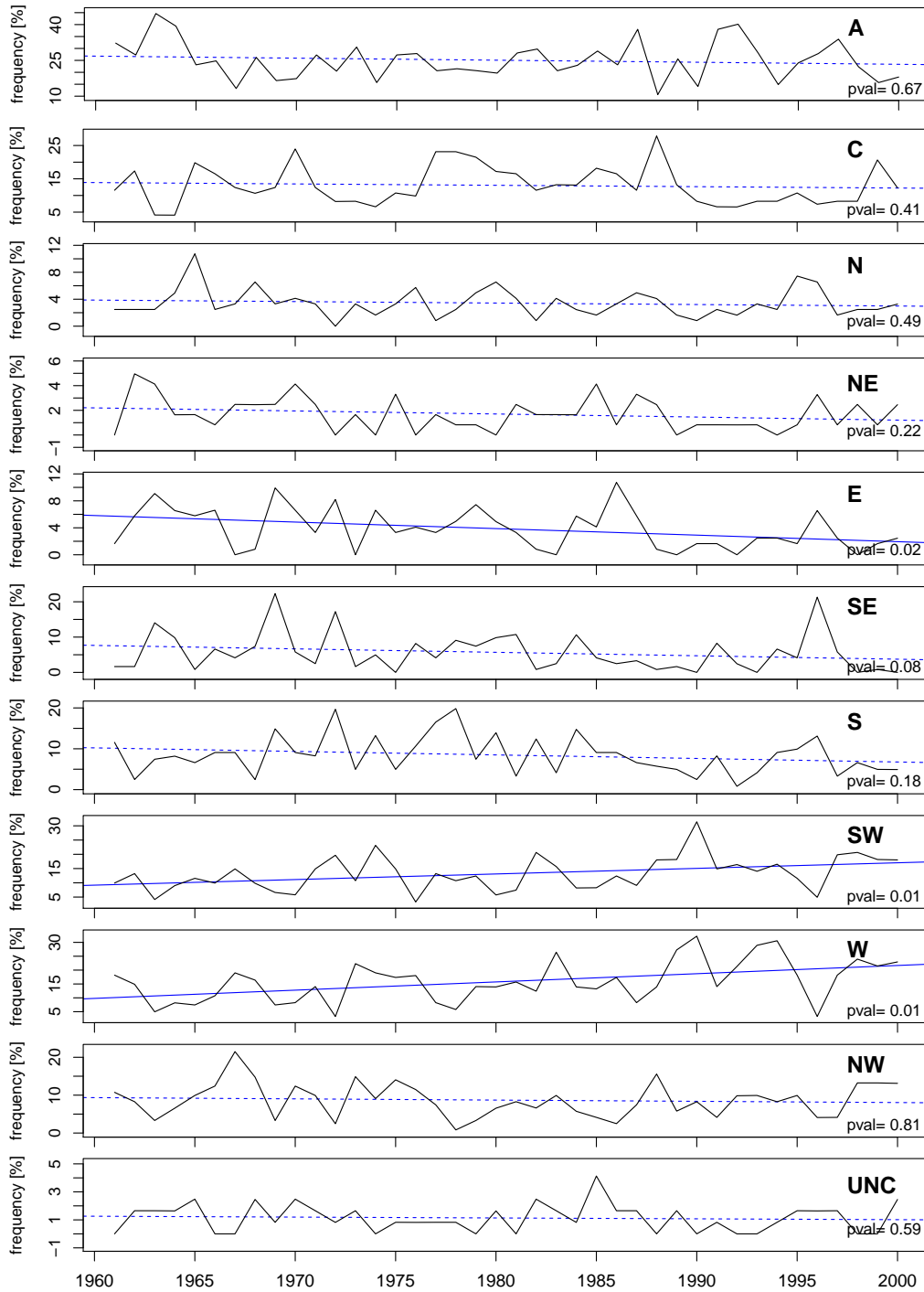


Figure E.4: Annual occurrence of each regime from December to March in the time period of 1961- 2000 (black) and linear trend (blue dashed line and in case of significance blue solid line).

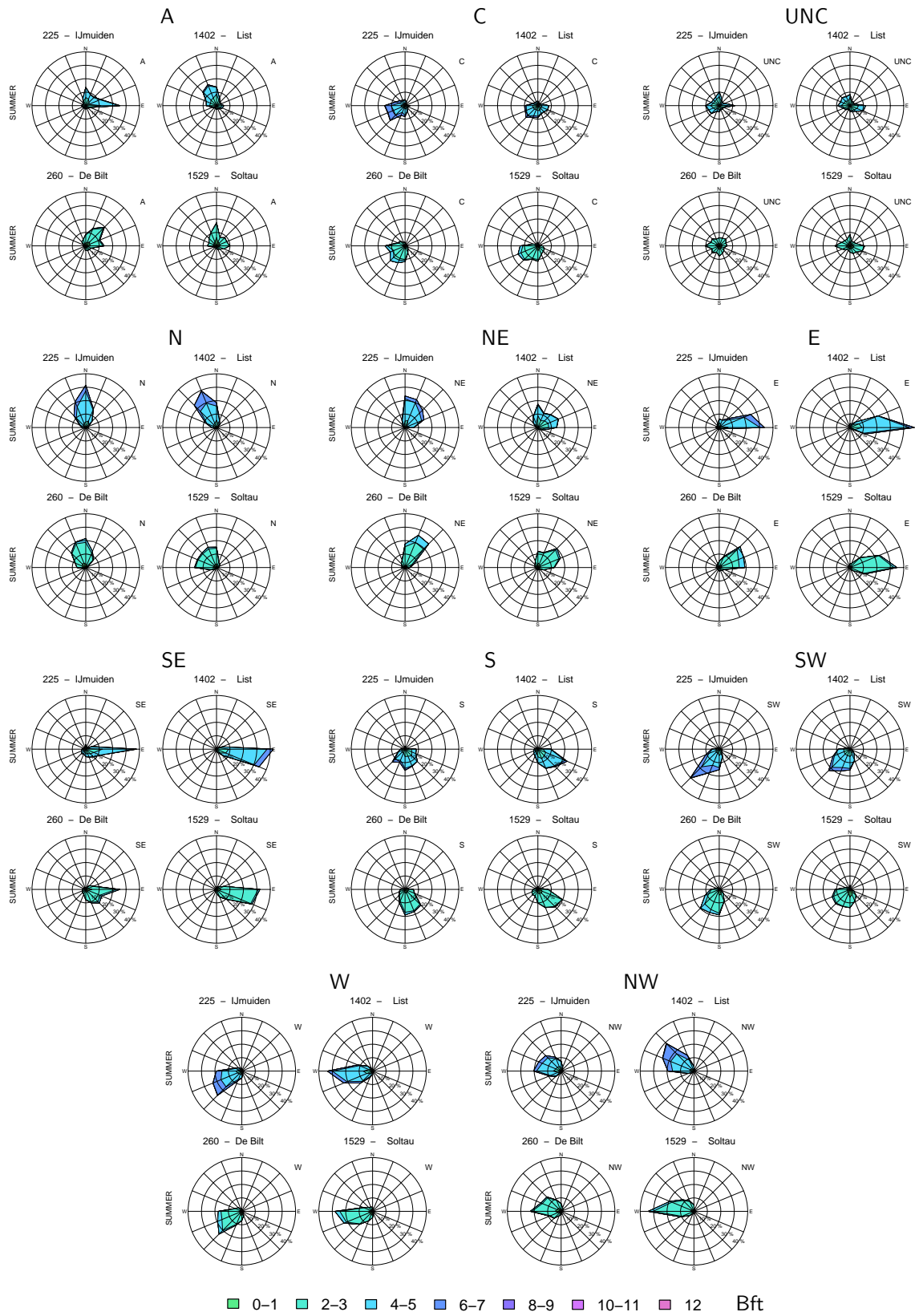


Figure E.5: Wind characteristics at four stations during the 11 weather regimes for the summer half year (Mai-Sep) in 1971 to 2000.

Acknowledgements

First of all, I would like to thank Prof. Dr. Hans von Storch for giving me the opportunity to accomplish this thesis at the Institute for Coastal Research at the Helmholtz Centre Geesthacht former GKSS Research Centre Geesthacht and for the appraisal of this work. Furthermore, I would like to express my gratitude to my day-to-day advisors Dr. Burkhardt Rockel and my colleagues for numerous fruitful scientific discussions strengthening my work. Special thanks is to the ZAMG giving me the opportunity to take some time off the work to finish my PhD.

A part of this work has been realised within the EU framework 6 project ENSEMBLES and I wish to thank all partners of the project for an interesting, interdisciplinary and detailed view on climate and climate change in Europe. I thank the DWD and the KNMI, especially Dr. Gudrun Rosenhagen (DWD) and Dr. Henk van der Brink (KNMI) for providing station data and for their assistance with these data. The simulations have been performed at the German High Performance Computing Centre for Climate- and Earth System Research (DKRZ).

I am grateful to Dr. Kerstin Prömmel, Dr. Maja Zuvela-Aloise, Dr. Beate Geyer and Dr. Andrea Lammert-Stockschläder for proof reading, Mag. Stefanie Obmann for cartographic support and Mag. Roland Koch for great scientific discussions. My special thanks is to my best friends for their support and for being there, and to Patrick the starfish. I also would like to thank my family for their constant support.